Hypoplastic models for fine-grained soils

A dissertation submitted for the Degree of Doctor of Philosophy

David Mašín

September 2006

Charles University, Prague
Institute of Hydrogeology, Engineering Geology and Applied Geophysics

Contents

List of Tables

List of Figures

Acknowledgements

The thesis would not have been written in this form without Prof. Ivo Herle and Dr. Jan Boháč. Ivo introduced me into numerical modelling in geomechanics and through our numerous discussions guided my research activities, Jan originated my interest in soil mechanics and, particularly, managed to create perfect conditions for research at Charles University.

Although the research presented in the thesis was basically done in the period 2003 – 2006, it was initiated during my stay at City University. I would like to express my gratitude to the staff of the Geotechnical engineering research centre, especially to Dr. S. E. Stallebrass and Prof. J. H. Atkinson.

I was lucky to work with many wise people who all left their traces in my research presented in the thesis. Particularly I would like to thank to Prof. D. Kolymbas from the University of Innsbruck, Prof. C. Viggiani, Prof. C. Tamagnini, Prof. J. Desrues and Prof. R. Chambon, whom I met during my stay in Grenoble and Prof. G. Gudehus from the University of Karlsruhe.

I thank to Dr. Luigi Callisto who provided data on Pisa clay, and to Prof. Mahdia Hattab for making available the experimental results on Kaolin clay.

Finally, many thanks are due to all my other colleagues who contributed to my work, and to all my friends.

Abstract

Hypoplasticity has been shown to be a promising approach to constitutive modelling of geomaterials. An extensive research at universities in Karlsruhe and Grenoble led to the development of comprehensive constitutive models for granular materials. Much less effort, however, was put into the research on hypoplastic models for fine-grained soils. A new hypoplastic model suitable for description of clay behaviour is proposed in this dissertation.

The primary task was to develop a model suitable for practical applications – it should require minimum number of parameters, which can be evaluated using standard laboratory procedures. The proposed model requires only five parameters, equivalent to the parameters of the well-established Modified Cam clay model. In principle, only two experiments are required for their evaluation – an isotropic loading and unloading test and a triaxial shear test. Void ratio is considered as a state variable and therefore, at least theoretically, a single set of material parameters may be used to predict the behaviour of soils with different degrees of overconsolidation.

Tensorial analysis of the proposed model reveals that it predicts the state boundary surface, which is a natural ingredient of elasto-plastic models, but only a consequence of the mathematical formulation of hypoplastic models. A possibility to derive an analytical expression of the state boundary surface is important for further developments of the model.

The thesis further brings an extensive evaluation of the proposed model. Two main aspects are studied – predictions of the response to experiments with stress paths pointing in different directions in the stress space and predictions of the behaviour of soils with different degrees of overconsolidation. The proposed model was in both cases compared with different advanced constitutive models, both elasto-plastic and hypoplastic. Although quantitative comparison of the quality of different models is a relatively complex task, predictions by the proposed model were always at least comparable to predictions by the other advanced models tested.

Finally, a possibility for further development of the model is demonstrated by means of incorporating the effects of structure in natural clays. An additional state variable – sensitivity – is a measure of the ratio of sizes of the state boundary surfaces of the reconstituted and natural soil. A suitable evolution equation of it allows us to predict progressive changes in structure caused by degradation of cementation bonds.

Chapter 1

Introduction

Theory of hypoplasticity is a relatively recent approach to constitutive modelling of geomaterials, developed independently during the last two decades at universities in Karlsruhe (e.g., [77]) and Grenoble [26, 29]. Initially, the research of both the schools focused on the development of constitutive models for granular materials, the progress of hypoplastic models suitable for description of fine-grained soils has been delayed until recent years.

The hypoplastic models for fine-grained soils available when the present research started [105, 106, 61, 54] suffered from several shortcomings outlined in Chapter 2. The first aim of the present work was to develop a hypoplastic constitutive model for fine-grained soils that would be applicable in geotechnical practice, i.e. it should predict the behaviour of fine-grained soils with reasonable accuracy while requiring only minimum number of material parameters. A further task was a study of some mathematical properties of the proposed model and its thorough evaluation with respect to experimental data. Finally, a possibility to extend the basic formulation to describe the behaviour of materials with more complex structure was studied.

The thesis consists of six main chapters, which are formed by research articles that appeared in different international journals and in conference proceedings.

The development of the new constitutive model is described step-by-step in *Chapter 2*. The reference constitutive model by Herle and Kolymbas [61] is modified taking into account principles set by Niemunis [106]. An evaluation of the proposed constitutive model with respect to experimental data on London clay [86, 98, 126] is also presented (more detailed evaluation is given in Chapters 4 and 5). Chapter 2 was published as a research article in the *International Journal for Numerical and Analytical Methods in Geomechanics* [87].

Some consequences of the mathematical structure of the new model are studied in *Chapter 3*. Tensorial analysis reveals that the model predicts existence of the so-called state boundary surface, defined as a boundary of all admissible states in the stress-void ratio space. Conclusions from Chapter 3 are important not only from the theoretical point of view, but also for further development of the model (as demonstrated, e.g., in Chapter 6). Chapter 3, written by D. Mašín and I. Herle, was published in *Computers and Geotechnics*

[97], a similar topic (together with the analysis of the hypoplastic model by von Wolffersdorff [141]) was discussed by the same authors in Reference [96].

Chapter 4 presents an evaluation of predictive capabilities of the proposed model in comparison with different advanced constitutive models, both elasto-plastic and hypoplastic. D. Mašín, C. Tamagnini, G. Viggiani and D. Costanzo studied directional response of the models (response to probes in different directions in the stress space from a common initial state) and compared them with experimental results by Costanzo et al. [31]. Chapter 4 was published in the *International Journal for Numerical and Analytical Methods in Geomechanics* [99], some selected results, together with description of the experimental evidence, can be found in Reference [130].

Further evaluation of the proposed model and comparison of its predictions with different models is presented in *Chapter 5* (V. Hájek and D. Mašín, proceedings of the 6^{th} *European Conference on Numerical Methods in Geomechanics* [56]). Laboratory experiments (Hattab and Hicher [58]) were in this case characterised by identical stress paths directions (p' constant tests), but started at different overconsolidation ratios. A range of overconsolidation ratios for which a single set of material parameters can be used was studied.

Chapter 6 presents further development of the proposed model. Conclusions from Chapter 3 and an existing framework for the mechanical behaviour of structured clays [34] are used to enhance the basic hypoplastic model by additional state variable, *sensitivity*. A suitable evolution equation for sensitivity then allows us to predict the behaviour of clays with metastable structure. Chapter 6 has been accepted for publication in *Canadian Geotechnical Journal* [88].

Predictions by the enhanced hypoplastic model are compared with its elasto-plastic 'equivalent' (from the point of view of required material parameters) in *Chapter 7*. Advantage of the non-linear hypoplastic formulation is revealed. Chapter 7 is about to be published in proceedings of the *International Workshop on Constitutive Modelling - Development, Implementation, Evaluation, and Application* [90].

The last two chapters present a summary of the research and an outlook, where the possibilities for further developments within hypoplastic framework are discussed.

Chapter 2

A hypoplastic constitutive model for clays

2.1 Introduction

In the past years many constitutive models based on the theory of hypoplasticity [77] have been developed for granular materials. This research, traced in Sec. 2.2.1, has led to constitutive equations that can take into account the nonlinearity of the soil behaviour, the influence of barotropy and pyknotropy and also the behaviour at small to very small strains with the influence of the recent history of deformation [108].

The research into hypoplasticity, based at the University of Karlsruhe, was mainly focused on the development of constitutive models for granular materials, such as sands or gravels. An important example is the model by von Wolffersdorff [141] (referred to in the following text "VW model"), which can be considered as a synthesis of the research work carried out in Karlsruhe[1] on this subject. Only a few attempts however have been made to apply hypoplastic principles to fine grained soils. A notable example are the visco–hypoplastic models by Niemunis [105, 109, 106]. These models assume logarithmic compression law [18] and, in line with the critical state soil mechanics [122], the lower limit for the void ratio e is equal to 0. Their formulation however concentrates on prediction of viscous effects and, since they arise from the model by von Wolffersdorff [141], it is not possible to specify the shear stiffness independently of the bulk stiffness and, as discussed by Herle and Kolymbas [61], the shear stiffness is significantly underpredicted.

A modification of the VW model, which allows for an independent calibration of the shear and bulk stiffnesses, was proposed by Herle and Kolymbas [61] (referred to in the following as the "HK model"). In the HK model, Herle and Kolymbas modified the hypoelastic tensor $\boldsymbol{\mathcal{L}}$ (Sec. 2.2.1), which was responsible for the too low shear stiffness predicted by the VW model for soils with low friction angles, and introduced an additional model parameter

[1] There is also the second school of thought in the research on incrementally nonlinear models, Grenoble (e.g., [29]). This article however focuses on the developments of the German school.

r controlling the ratio of shear and bulk moduli. This model however assumes the influence of the barotropy and pyknotropy identical to the VW model, which is not suitable for clays. Moreover, the modification of the tensor $\boldsymbol{\mathcal{L}}$ must vanish as the stress approaches the limit state, which leads to incorrect predictions of the shear stiffness for anisotropic stress states (for further discussion see Sec. 2.3). The lack of a suitable hypoplastic formulation for fine grained soils led to the development of the model proposed in this paper.

In the following, the usual sign convention of solid mechanics (compression negative) is adopted throughout, except Roscoe's variables p, q, ϵ_v and ϵ_s (e.g. [104]), which are defined positive in compression. In line with the Terzaghi principle of effective stress, all stresses are *effective* stresses. Second–order tensors are denoted with bold letters (e.g., $\mathbf{T}$, $\mathbf{m}$) and fourth–order tensors with calligraphic bold letters (e.g., $\boldsymbol{\mathcal{L}}$). Different types of tensorial multiplication are used: $\mathbf{T} \otimes \mathbf{D} = \mathrm{T}_{ij}\mathrm{D}_{kl}$, $\mathbf{T} : \mathbf{D} = \mathrm{T}_{ij}\mathrm{D}_{ij}$, $\boldsymbol{\mathcal{L}} : \mathbf{D} = \mathcal{L}_{ijkl}\mathrm{D}_{kl}$, $\mathbf{T} \cdot \mathbf{D} = \mathrm{T}_{ij}\mathrm{D}_{jk}$. The quantity $\|\mathbf{X}\| = \sqrt{\mathbf{X} : \mathbf{X}}$ denotes the Euclidean norm of $\mathbf{X}$, the operator arrow is defined as $\vec{\mathbf{X}} = \mathbf{X}/\|\mathbf{X}\|$ and trace by $\mathrm{tr}\mathbf{X} = \mathbf{X} : \mathbf{1}$. $\mathbf{1}$ is a second–order unity tensor and $\boldsymbol{\mathcal{I}}$ is a fourth order unity tensor with components $\mathcal{I}_{ijkl} = \frac{1}{2}(1_{ik}1_{jl} + 1_{il}1_{jk})$.

2.2 Hypoplasticity

2.2.1 General aspects

The hypoplastic constitutive equations are usually described by a simple non–linear tensorial equation that relates the objective (Jaumann) stress rate $\mathring{\mathbf{T}}$ with the Euler's stretching tensor $\mathbf{D}$.

The early hypoplastic models were developed by trial and error, by choosing suitable candidate functions (Kolymbas [75]) from the most general form of isotropic tensor–valued functions of two tensorial arguments (representation theorem due to Wang [142]). The suitable candidate functions were combined automatically using a computer program that tested the capability of the constitutive model to predict the most important aspects of the soil behaviour [76]. The research led to a practically useful equation with four parameters proposed by Wu [149] and Wu and Bauer [151].

As proven in [80], the hypoplastic equation may be written in its general form as

$$\mathring{\mathbf{T}} = \boldsymbol{\mathcal{L}} : \mathbf{D} + \mathbf{N}\|\mathbf{D}\|, \tag{2.1}$$

where $\boldsymbol{\mathcal{L}}$ and $\mathbf{N}$ are fourth and second–order constitutive tensors respectively that are functions of the Cauchy stress $\mathbf{T}$ only in the case of early hypoplastic models.

An important step forward in developing the hypoplastic model was the implementation of the critical state concept. Gudehus [53] proposed a modification of Eq. (2.1) to include the influence of the stress level (barotropy) and the influence of density (pyknotropy). The modified equation reads

$$\mathring{\mathbf{T}} = f_s\boldsymbol{\mathcal{L}} : \mathbf{D} + f_s f_d\mathbf{N}\|\mathbf{D}\|. \tag{2.2}$$

Here f_s and f_d are scalar factors expressing the influence of barotropy and pyknotropy. The model [53] was later refined by von Wolffersdorff [141] to incorporate Matsuoka–Nakai critical state stress condition.

A successful modification of the VW model is not straightforward due to the fact that the constitutive tensors $\boldsymbol{\mathcal{L}}$ and $\mathbf{N}$ are interrelated – they act together as a hypoplastic flow rule and limit stress condition. To overcome this problem, it is convenient to introduce the tensorial function

$$\mathbf{B} = \boldsymbol{\mathcal{L}}^{-1} : \mathbf{N}, \tag{2.3}$$

which has been already used in the development of both Karlsruhe hypoplastic models [76] and CLoE hypoplastic models [29]. The Eq. (2.2) may be re–written,

$$\mathring{\mathbf{T}} = f_s \boldsymbol{\mathcal{L}} : (\mathbf{D} + f_d \mathbf{B} \|\mathbf{D}\|) . \tag{2.4}$$

The critical state condition can be found by substituting $\mathring{\mathbf{T}} = \mathbf{0}$ and $f_d = 1$ into (2.4). It follows that $\mathring{\mathbf{T}} = \mathbf{0}$ is satisfied trivially by $\mathbf{D} = \mathbf{0}$ and for $\mathbf{D} \neq \mathbf{0}$ by

$$\vec{\mathbf{D}} = -\mathbf{B}. \tag{2.5}$$

Eq. (2.5) imposes a condition on stress, which can be revealed by elimination of $\vec{\mathbf{D}}$ from (2.5). Taking the norm of both sides of (2.5) we obtain for the critical state

$$f = \|\mathbf{B}\| - 1 = 0. \tag{2.6}$$

The stress function f may be seen as a counterpart of the critical state stress criterion in elasto–plasticity [75]. A hypoplastic flow rule is then given by Eq. (2.5).

Using these transformations, Niemunis [106] proposed a simple rearrangement of the basic hypoplastic equation (2.2), which allows definition of the flow rule, critical state stress condition and tensor $\boldsymbol{\mathcal{L}}$ independently. Such a rearrangement is useful for model development and will also be used in this work.

The second–order tensor $\mathbf{N}$ is now calculated by

$$\mathbf{N} = \boldsymbol{\mathcal{L}} : \left(-Y \frac{\mathbf{m}}{\|\mathbf{m}\|} \right) . \tag{2.7}$$

Here the scalar quantity $Y = f + 1$ (named the *degree of nonlinearity* [106]) stands for a limit stress condition, $\mathbf{m}$ is a second–order tensor denoted hypoplastic flow rule and $\boldsymbol{\mathcal{L}}$ is a fourth–order hypoelastic tensor from Eq. (2.2).

Eqs. (2.2) and (2.7) can be combined to get

$$\mathring{\mathbf{T}} = f_s \boldsymbol{\mathcal{L}} : \left(\mathbf{D} - f_d Y \frac{\mathbf{m}}{\|\mathbf{m}\|} \|\mathbf{D}\| \right) . \tag{2.8}$$

Eqs. (2.2) and (2.7), or Eq. (2.8), define the general stress–strain relationship of the model proposed. Following [106], this formulation is named “generalised hypoplasticity”.

2.2.2 Reference constitutive model

The HK model, introduced in Sec. 2.1, is taken as a reference model for the present research and its mathematical formulation is summarised in Appendix A. The tensor $\boldsymbol{\mathcal{L}}$ of the VW model is modified by introducing two scalar factors c_1 and c_2,

$$\boldsymbol{\mathcal{L}} = \frac{1}{\hat{\mathbf{T}} : \hat{\mathbf{T}}} \left(c_1 F^2 \boldsymbol{\mathcal{I}} + c_2 a^2 \hat{\mathbf{T}} \otimes \hat{\mathbf{T}} \right), \tag{2.9}$$

where quantities $\hat{\mathbf{T}}$, F and a are defined in Appendix A. The expression for the factor c_1 is derived in order to ensure that the additional model parameter r specifies the ratio of the bulk and shear moduli at isotropic stress state (details are given in Sec. 2.4.6) and factor c_2 follows from the requirement that the isotropic formulations of both the HK and VW models merge,

$$c_1 = \left(\frac{1 + \frac{1}{3}a^2 - \frac{1}{\sqrt{3}}a}{1.5r} \right)^{\xi}, \qquad c_2 = 1 + (1 - c_1)\,\frac{3}{a^2}. \tag{2.10}$$

Because the HK model does not make use of the generalised hypoplasticity formulation (Sec. 2.2.1), the influence of fators c_1 and c_2 must vanish as the stress approaches Matsuoka–Nakai critical state stress criterion. For this reason, a scalar factor ξ is introduced in the formulation of the factor c_1 (Eq. (2.10)), which reads

$$\xi = \left\langle \frac{\sin\varphi_c - \sin\varphi_{mob}}{\sin\varphi_c} \right\rangle, \qquad \text{where} \qquad \sin\varphi_{mob} = \frac{T_1 - T_3}{T_1 + T_3}. \tag{2.11}$$

T_1 and T_3 are the maximal and minimal principal stresses, φ_{mob} is a mobilized friction angle and $\langle\rangle$ are Macauley brackets: $\langle x \rangle = (x + |x|)/2$.

2.2.3 Intergranular strain concept

The hypoplastic models discussed in previous sections are capable of predicting the soil behavior upon monotonic loading at medium to large strain levels. In order to prevent excessive ratcheting upon cyclic loading and to improve model performance in the small–strain range, the mathematical formulation has been enhanced by the intergranular strain concept [108].

The rate formulation of the enhanced model is given by

$$\mathring{\mathbf{T}} = \boldsymbol{\mathcal{M}} : \mathbf{D}, \tag{2.12}$$

where $\boldsymbol{\mathcal{M}}$ is the fourth–order tangent stiffness tensor of the material. The formulation introduces the additional state variable $\boldsymbol{\delta}$, which is a symmetric second order tensor called *intergranular strain*.

In the formulation described above, the total strain can be thought of as the sum of a component related to the deformation of interface layers at integranular contacts, quantified

by $\boldsymbol{\delta}$, and a component related to the rearrangement of the soil skeleton. For reverse loading conditions ($\hat{\boldsymbol{\delta}} : \mathbf{D} < 0$, where $\hat{\boldsymbol{\delta}}$ is defined in Appendix B) and neutral loading conditions ($\hat{\boldsymbol{\delta}} : \mathbf{D} = 0$), the observed overall strain is related only to the deformation of the intergranular interface layer and the soil behaviour is hypoelastic, whereas in continuous loading conditions ($\hat{\boldsymbol{\delta}} : \mathbf{D} > 0$) the observed overall response is also affected by particle rearrangement in the soil skeleton. From the mathematical standpoint, the response of the model is determined by interpolating between the following three special cases:

$$\begin{array}{lll} \mathring{\mathbf{T}} = m_R f_s \boldsymbol{\mathcal{L}} : \mathbf{D}, & \text{for} & \hat{\boldsymbol{\delta}} : \mathbf{D} = -1 \text{ and } \boldsymbol{\delta} = \mathbf{0}; \\ \mathring{\mathbf{T}} = m_T f_s \boldsymbol{\mathcal{L}} : \mathbf{D}, & \text{for} & \hat{\boldsymbol{\delta}} : \mathbf{D} = 0; \\ \mathring{\mathbf{T}} = f_s \boldsymbol{\mathcal{L}} : \mathbf{D} + f_s f_d \mathbf{N} \|\mathbf{D}\|, & \text{for} & \hat{\boldsymbol{\delta}} : \mathbf{D} = 1. \end{array} \tag{2.13}$$

Full details of the mathematical structure of the model are provided in Appendix B. The model, which incorporates the intergranular strain concept is in the paper denoted as "enhanced", the model without this modification as "basic".

2.3 Limitations of the reference model

As pointed out in the introduction, although the HK model improved predictions of the clay behaviour significantly, several shortcomings may still be identified. The most important are:

- Measurements of the shear stiffness at very small strains (G_0), by means of propagation of shear waves, allows investigation of the dependence of G_0 on the stress level. For clays such studies were performed for example in [139, 69, 135, 22]. It was shown that for stresses inside the limit state surface G_0 depends on the mean stress p but the influence of the deviatoric stress q is not significant (both for triaxial compression and extension). The HK model with intergranular strains however predicts significant decrease of the hypoelastic shear modulus G_0 with the ratio $\eta = q/p$, as discussed in Sec. 2.5 (Figs. 2.3 and 2.4).

- The HK model assumes a non–zero, pressure–dependent lower limit of void ratio, e_d. While this approach is suitable for granular materials, for clays it is reasonable to consider the lower limit of void ratio of $e = 0$, according to the critical state soil mechanics [122], supported by experimental studies on the shape of the state boundary surface of fine–grained soils (e.g., [32, 33, 34]). Taking the pyknotropy factor f_d a function of relative density r_e calculated by

$$r_e = \frac{e - e_d}{e_c - e_d}, \tag{2.14}$$

  with e_c being void ratio at the critical state line at current mean stress, leads to incorrect predictions of the stress–dilatancy behaviour by the HK model (for details see Sec. 2.5, Fig. 2.6), also for the case when lower limit of void ratio $e = 0$ is prescribed ($e_{d0} = 0$).

- The HK model adopts exponential expressions for the isotropic normal compression and critical state lines [10]. Compared to the logarithmic expression, the exponential expression has the advantage of having limits for $p \to 0$ and $p \to \infty$. For clays however the logarithmic expression is more accurate in the stress range applicable in geotechnical engineering [18], with the further advantage of having one material parameter less.
- Taking into account the desired simplicity of the calibration of the proposed model, the parameter defining the position of the critical state line in the $e : p$ plane (e_{c0}) may be regarded as superfluous. For clays the position of the critical state line calculated using the state boundary surface of the Modified Cam clay model [117] is sufficiently accurate, as shown recently for different clays in [32, 33, 34].
- The HK model does not allow specifying directly the swelling index, κ^*. The slope of the isotropic unloading line is governed by two parameters, α and β. Direct evaluation of these parameters from isotropic unloading test is complicated and the calibration is usually performed by means of a parametric study.

The proposed hypoplastic model for clays aims at overcoming the outlined shortcomings of the HK model and achieving maximal simplicity of the calibration of the new model, which is desired in practical applications.

2.4 Proposed constitutive model

2.4.1 Tensor $\mathcal{L}$

The tensor $\mathcal{L}$ (Eq. (2.9)) determines, in the model enhanced by the intergranular strain concept (Sec. 2.2.3), the initial hypoelastic stiffness and causes the HK model to predict a decrease of the initial shear modulus G_0 with the stress ratio η, which is not in agreement with experiment (see Sec. 2.3). The influence of η on G_0 is caused by the factor $1/(\hat{\mathbf{T}} : \hat{\mathbf{T}})$ (where $\hat{\mathbf{T}} = \mathbf{T}/\mathrm{tr}\mathbf{T}$), the decrease of the scalar quantity ξ as the stress approaches limit state and the factor F, which increases the compressibility for Lode angles different than $\pi/6$.

The influence of the first two factors is studied using the concept of incremental response envelopes [134]. This concept follows directly from the concept of rate response envelope [50], with rates replaced by finite–size increments with *constant* direction of stretching $\vec{\mathbf{D}}$ (for brevity, incremental response envelopes are referred to as response envelopes in this work). Response envelopes are plotted for $\Delta t\|\mathbf{D}\| = 0.0015$, where t is pseudo–time used for time integration of the model response. The HK model enhanced by the intergranular strain concept is used in the simulations, modified by either keeping $1/(\hat{\mathbf{T}} : \hat{\mathbf{T}}) = \text{const.} = 3$ or $\eta = \text{const.} = 1$ (Fig. 2.1). The initial value of the intergranular strain tensor $\boldsymbol{\delta}$ is equal to $\mathbf{0}$.

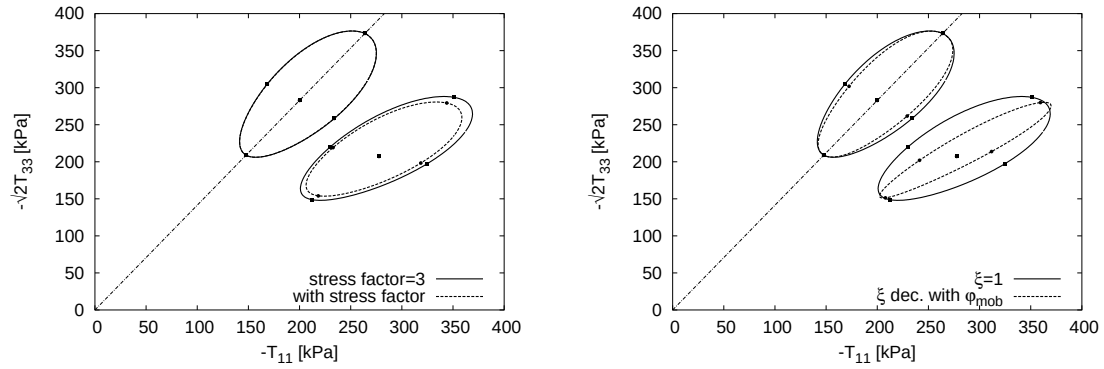

Figure 2.1: The influence of the stress factor $1/(\hat{\mathbf{T}} : \hat{\mathbf{T}})$ (left) and the scalar quantity ξ (right) in the expression for $\boldsymbol{\mathcal{L}}$ on the size and shape of response envelopes.

It may be seen From Fig. 2.1 (left) that the influence of the stress quantity $1/(\hat{\mathbf{T}} : \hat{\mathbf{T}})$ is not significant. In the VW model this quantity was introduced in order to emphasize that the overall compressibility of sand is larger at higher stress ratios. For clays it is well known that the normal compression lines are approximately parallel for different radial stress paths (as isotropic and K_0 normal compression lines and critical state line). Following Niemunis [106], the factor $1/(\hat{\mathbf{T}} : \hat{\mathbf{T}})$ may be disregarded and in the present model it is replaced by its isotropic value equal to 3.

Fig. 2.1 (right) shows that the influence of the factor ξ, which in the HK model must decrease with φ_{mob} in order to ensure that the model predicts correctly the critical state (Sec. 2.2.2), is very significant. The response envelopes become narrower as the stress approaches the critical state and the initial shear modulus G_0 decreases significantly. The proposed model therefore does not make use of the quantity ξ and so constant values of scalar factors c_1 and c_2 (Sec. 2.2.2) are assumed. This modification is enabled by adopting the generalised hypoplastic formulation (Sec. 2.2.1).

In the VW model the factor F had to enter the expression for $\boldsymbol{\mathcal{L}}$ to ensure that the function $\mathbf{B}$ conforms with the Matsuoka–Nakai failure criterion. As quoted in Sec. 2.3, according to experiments on fine–grained soils, G_0 is independent of η in both triaxial compression and extension [139]. Therefore, the factor F should be in the expression for $\boldsymbol{\mathcal{L}}$ omitted.

We assume the following formulation of the hypoelastic tensor $\boldsymbol{\mathcal{L}}$:

$$\boldsymbol{\mathcal{L}} = 3\left(c_1\boldsymbol{\mathcal{I}} + c_2 a^2 \hat{\mathbf{T}} \otimes \hat{\mathbf{T}}\right). \tag{2.15}$$

The calculation of scalar factors c_1 and c_2, which follows [61], is described in Sec. 2.4.6. The scalar factor a is a function of material parameter φ_c and follows from VW model,

$$a = \frac{\sqrt{3}\,(3 - \sin\varphi_c)}{2\sqrt{2}\sin\varphi_c}. \tag{2.16}$$

2.4.2 Limit stress condition Y

As shown, for example, in [73, 20, 114] the Drucker–Prager critical state stress criterion, which is assumed also by the Modified Cam clay model, is not suitable for clays. The actual critical state stress criterion circumscribes the Mohr–Coulomb criterion with approximately equal friction angles in triaxial compression and extension.

Therefore, the Matsuoka–Nakai [85] criterion assumed by the VW hypoplastic model is applicable also for clays. It is described by the equation

$$f = -\frac{I_1 I_2}{I_3} - \frac{9 - \sin^2\varphi_c}{1 - \sin^2\varphi_c} \leq 0, \tag{2.17}$$

with the stress invariants

$$I_1 = \mathrm{tr}\mathbf{T}, \qquad I_2 = \frac{1}{2}\left[\mathbf{T} : \mathbf{T} - (I_1)^2\right], \qquad I_3 = \det\mathbf{T}. \tag{2.18}$$

As pointed out by Niemunis [106], the quantity Y should have a minimum value at the isotropic axis (maximum $Y = 1$ at the critical state stress criterion). Direct linear interpolation between the isotropic value $Y = Y_i$ and limit state value $Y = 1$ is assumed in the proposed model, following [106].

Using the fact that $I_1 I_2 / I_3 = -9$ at the hydrostatic stress state, the linear interpolation reads

$$Y = (1 - Y_i)\left[\frac{-\dfrac{I_1 I_2}{I_3} - 9}{\dfrac{9 - \sin^2\varphi_c}{1 - \sin^2\varphi_c} - 9}\right] + Y_i, \tag{2.19}$$

with Y_i being equal to the isotropic value of the function $\|\mathbf{B}\|$ of the VW (HK) model,

$$Y_i = \frac{\sqrt{3}a}{3 + a^2}. \tag{2.20}$$

2.4.3 Hypoplastic flow rule (tensorial quantity m)

$\vec{\mathbf{m}} = \mathbf{m}/\|\mathbf{m}\|$ is a tensorial function that should have purely volumetric direction at isotropic stress state and purely deviatoric direction (tr $\mathbf{m} = 0$) at Matsuoka–Nakai states,

$$\begin{cases} \vec{\mathbf{m}} = -\hat{\mathbf{T}}^*/\|\hat{\mathbf{T}}^*\|, & \text{for} \quad Y = 1; \\ \vec{\mathbf{m}} = -\frac{1}{\sqrt{3}}\mathbf{1}, & \text{for} \quad Y = Y_i, \end{cases} \tag{2.21}$$

where the stress quantity $\hat{\mathbf{T}}^*$ is defined as $\hat{\mathbf{T}}^* = \hat{\mathbf{T}} - \mathbf{1}/3$. A suitable candidate is the function $-\mathbf{B}$ of the VW hypoplastic model [141],

$$\mathbf{m} = -\frac{a}{F}\left[\hat{\mathbf{T}} + \hat{\mathbf{T}}^* - \frac{\hat{\mathbf{T}}}{3}\left(\frac{6\ \hat{\mathbf{T}} : \hat{\mathbf{T}} - 1}{(F/a)^2 + \hat{\mathbf{T}} : \hat{\mathbf{T}}}\right)\right], \tag{2.22}$$

with factor F defined by

$$F = \sqrt{\frac{1}{8}\tan^2\psi + \frac{2-\tan^2\psi}{2+\sqrt{2}\tan\psi\cos 3\theta}} - \frac{1}{2\sqrt{2}}\tan\psi, \tag{2.23}$$

where

$$\tan\psi = \sqrt{3}\|\hat{\mathbf{T}}^*\|, \qquad \cos 3\theta = -\sqrt{6}\frac{\mathrm{tr}\left(\hat{\mathbf{T}}^*\cdot\hat{\mathbf{T}}^*\cdot\hat{\mathbf{T}}^*\right)}{\left[\hat{\mathbf{T}}^* : \hat{\mathbf{T}}^*\right]^{3/2}}. \tag{2.24}$$

Note that the adopted formulation of the function $\mathbf{m}$ implies radial strain increments in octahedral plane at the critical state. For fine–grained soils this choice is supported by the experimental evidence given by Kirkgard and Lade [73].

2.4.4 Barotropy factor f_s

The aim of the barotropy factor f_s is to incorporate the influence of the mean stress $p = -\mathrm{tr}\mathbf{T}/3$. The calculation of the factor f_s is based on the formulation of the pre–defined isotropic normal compression line.

The proposed model assumes isotropic normal compression line linear in the $\ln(1+e) : \ln p$ space, which is suitable for clays [18]. Its position is governed by the parameter N and its slope by the parameter λ^*,

$$\ln(1+e) = N - \lambda^* \ln p. \tag{2.25}$$

Time differentiation of (2.25) results in

$$\frac{\dot{e}}{1+e} = -\frac{\lambda^*}{p}\dot{p}. \tag{2.26}$$

The already defined quantities $\boldsymbol{\mathcal{L}}$, $\mathbf{m}$ and Y, together with the yet unknown values of pyknotropy factor f_d at the isotropic normally compressed state (f_{di}) and the factors c_1 and c_2, may be used to derive the form of the Eq. (2.7) for isotropic stress state. With the use of

$$\dot{p} = -\frac{1}{3}\mathrm{tr}\mathring{\mathbf{T}}, \quad \mathbf{D} = \frac{\dot{e}}{3\,(1+e)}\mathbf{1}, \quad \text{and} \quad \|\mathbf{D}\| = \frac{|\dot{e}|}{3\,(1+e)}\sqrt{3}, \tag{2.27}$$

we find

$$\dot{p} = -\frac{f_s}{3\,(1+e)}\left(3c_1 + a^2c_2\right)\left[\dot{e} + f_{di}\frac{a\sqrt{3}}{3+a^2}|\dot{e}|\right]. \tag{2.28}$$

As discussed in Sec. 2.2.2, calculation of the scalar factor c_2, introduced in [61], ensures that the modification of the tensor $\boldsymbol{\mathcal{L}}$ does not influence the isotropic formulation of the model. Therefore it follows from (2.28) that

$$3c_1 + a^2c_2 = 3 + a^2. \tag{2.29}$$

Eq. (2.28) may be therefore simplified to

$$\dot{p} = -\frac{1}{3\,(1+e)} f_s \left[\left(3 + a^2\right) \dot{e} + f_{di} a \sqrt{3} |\dot{e}| \right], \tag{2.30}$$

and for isotropic compression with $\dot{e} < 0$

$$\dot{p} = -\left[\frac{1}{3\,(1+e)} f_s \left(3 + a^2 - f_{di} a \sqrt{3}\right) \right] \dot{e}. \tag{2.31}$$

Comparing (2.26) with (2.31) we derive the expression for the barotropy factor f_s,

$$f_s = -\frac{\mathrm{tr}\mathbf{T}}{\lambda^*} \left(3 + a^2 - f_{di} a \sqrt{3}\right)^{-1}. \tag{2.32}$$

2.4.5 Pyknotropy factor f_d

The pyknotropy factor f_d was introduced in [53] in order to incorporate the influence of density (overconsolidation ratio) on the soil behaviour. If we assume, following discussion in Sec. 2.3, that the lower limit of void ratio is $e = 0$ for clays, the pyknotropy factor f_d has the following properties:

- $f_d = 0$ for $p = 0$;
- $f_d = 1$ at the critical state;
- $f_d = \text{const.} > 1$ at isotropic normally compressed states.

Moreover, the pyknotropy factor f_d should have constant value along any other normal compression line (reasons for this choice are demonstrated in [95]). Taking into account the outlined properties of the factor f_d, we propose a simple expression

$$f_d = \left(\frac{p}{p_{cr}} \right)^{\alpha}, \tag{2.33}$$

where p_{cr} is the mean stress at the critical state line at the current void ratio (Fig. 2.2).

As discussed in Section 2.3, the position of the critical state line in $\ln(1+e) : \ln p$ space does not need to be controlled by an additional parameter, since for clays this position is sufficiently accurately defined by the state boundary surface of the Modified Cam clay model. The expression for the critical state line reads

$$\ln(1+e) = N - \lambda^* \ln 2 \frac{p_{cr}}{p_r}, \tag{2.34}$$

where p_r is the reference stress 1 kPa. Therefore,

$$f_d = \left[-\frac{2\mathrm{tr}\mathbf{T}}{3p_r} \exp\left(\frac{\ln(1+e) - N}{\lambda^*} \right) \right]^{\alpha}. \tag{2.35}$$

The scalar quantity α is calculated to allow for a direct calibration of the swelling index κ^*, defined as the slope of the isotropic unloading line in the $\ln(1+e) : \ln p$ space. This line has the expression

$$\ln(1+e) = \text{const.} - \kappa^* \ln p, \tag{2.36}$$

which leads after time differentiation to

$$\frac{\dot{e}}{1+e} = -\frac{\kappa^*}{p}\dot{p}. \tag{2.37}$$

For isotropic unloading from the isotropic *normally compressed* state the proposed model has the form (from Eq. (2.30))

$$\dot{p} = -\left[\frac{1}{3\,(1+e)} f_s \left(3 + a^2 + f_{di} a\sqrt{3}\right)\right] \dot{e}. \tag{2.38}$$

Having defined the barotropy factor f_s (2.32) and the pyknotropy factor for the isotropic normally compressed state f_{di} (from Eqs. (2.35) and (2.25)),

$$f_{di} = 2^{\alpha}, \tag{2.39}$$

we may rewrite Eq. (2.38) to get

$$\dot{p} = -\left[\frac{p}{\lambda^*\,(1+e)} \left(\frac{3 + a^2 + 2^{\alpha} a\sqrt{3}}{3 + a^2 - 2^{\alpha} a\sqrt{3}}\right)\right] \dot{e}. \tag{2.40}$$

Comparing (2.40) with (2.37) we derive the expression for the scalar quantity α,

$$\alpha = \frac{1}{\ln 2} \ln\left[\frac{\lambda^* - \kappa^*}{\lambda^* + \kappa^*} \left(\frac{3 + a^2}{a\sqrt{3}}\right)\right]. \tag{2.41}$$

The meaning of the model parameters N, λ^* and κ^* is demonstrated in Fig. 2.2.

2.4.6 Scalar factors c_1 and c_2

Calculation of the factor c_2 is based on Eq. (2.29) and follows [61],

$$c_2 = 1 + (1 - c_1)\frac{3}{a^2}. \tag{2.42}$$

For the calculation of the factor c_1, we define the constitutive parameter r as the ratio of the bulk modulus in isotropic compression (K_i) and the shear modulus in undrained shear (G_i) for tests starting from the isotropic normally compressed state. Manipulation with the proposed model leads to expressions for K_i and G_i,

$$K_i = \frac{f_s}{3}\left(3 + a^2 - 2^{\alpha} a\sqrt{3}\right), \tag{2.43}$$

$$G_i = \frac{3}{2} f_s c_1. \tag{2.44}$$

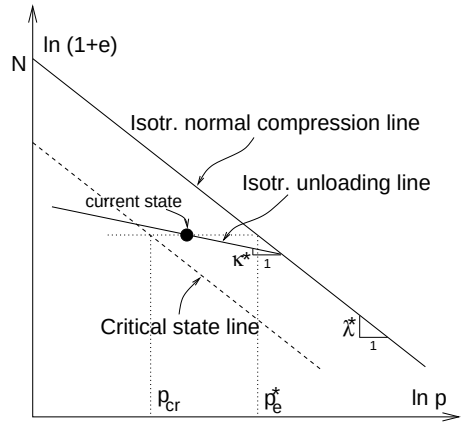

Figure 2.2: Definition of parameters N, λ^* and κ^* and quantities p_{cr} and p_e^* (from Sec. 2.5).

Because $r = K_i/G_i$, we find

$$c_1 = \frac{2\left(3 + a^2 - 2^\alpha a\sqrt{3}\right)}{9r}. \tag{2.45}$$

Having obtained factors c_1 and c_2, the mathematical formulation of the proposed model is complete. It is summarized in Appendix C. The model requires five constitutive parameters: φ_c, λ^*, κ^*, N and r.

2.5 Inspection into properties of the model

2.5.1 Shear moduli

A significant shortcoming of the HK model is the underprediction of the initial shear stiffness G_0 for tests starting from anisotropic stress states. This deficiency is very important for practical applications, since the stress state in the field is often anisotropic.

Using the intergranular strain concept (Sec. 2.2.3), the quasi–elastic behaviour is controlled by the equation

$$\mathring{\mathbf{T}} = m_R f_s \boldsymbol{\mathcal{L}} : \mathbf{D}. \tag{2.46}$$

In the following, we restrict our attention only to axisymmetric conditions, as we want to examine possibility of calibration of model parameters, not to provide a full analysis of model performance. We may define the shear modulus G^* using Roscoe's variables p, q, ϵ_v and ϵ_s (e.g., [104]) as follows [47]:

$$\begin{bmatrix} \dot{p} \\ \dot{q} \end{bmatrix} = \begin{bmatrix} K^* & J \\ J & 3G^* \end{bmatrix} \begin{bmatrix} \dot{\epsilon_v} \\ \dot{\epsilon_s} \end{bmatrix}. \tag{2.47}$$

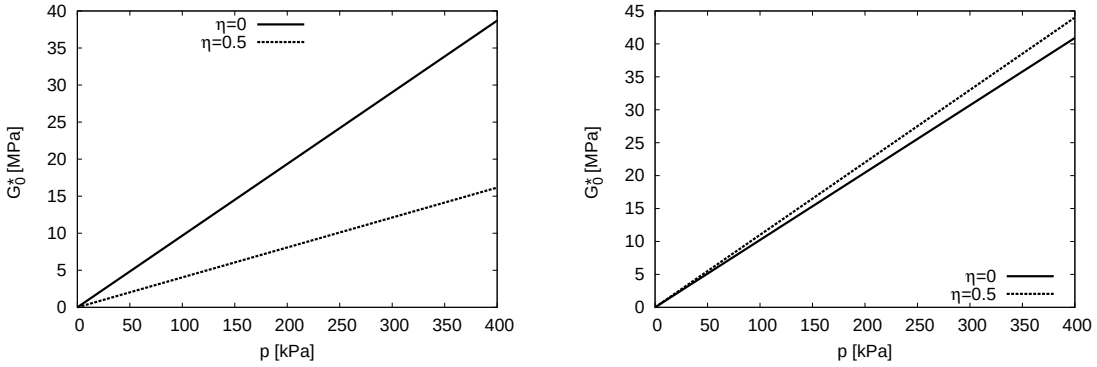

Figure 2.3: Influence of the stress ratio η on the hypoelastic shear modulus G_0^* calculated by the HK (left) and proposed (right) models with intergranular strains.

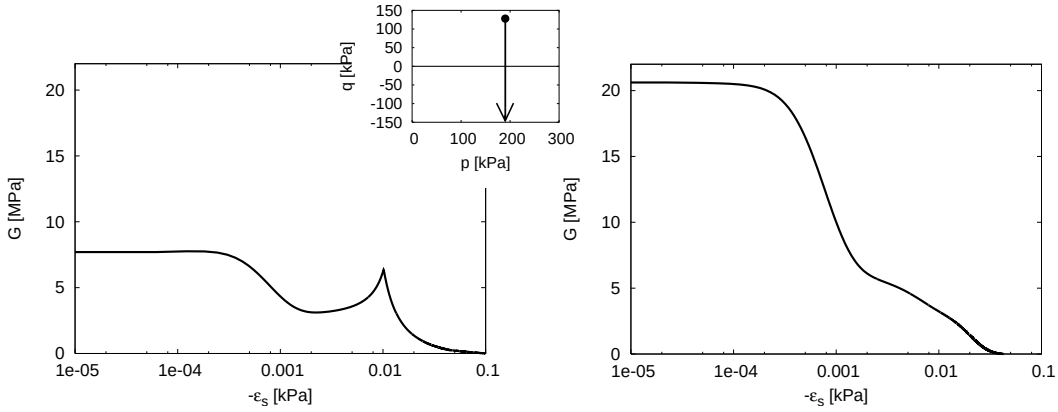

Figure 2.4: Erroneous increase of the shear stiffness calculated by the HK model enhanced by the intergranular strain concept for the stress path passing isotropic stress state (left) and corresponding predictions by the proposed model with intergranular strains (right).

Because the hypoelastic stiffness tensor $\boldsymbol{\mathcal{L}}$ is not isotropic, G^* is equal to the equivalent shear modulus defined by $G = \dot{q}/(3\dot{\epsilon_s})$ only for undrained conditions.

Combining (2.46) and (2.47) we find that

$$G_0^* = \frac{m_R f_s}{3}\left[\mathcal{L}_{1111} - 2\mathcal{L}_{2211} + \frac{1}{2}\left(\mathcal{L}_{2222} + \mathcal{L}_{2233}\right)\right]. \tag{2.48}$$

Substituting expressions for $\boldsymbol{\mathcal{L}}$ (2.15) and f_s (2.32) we get

$$G_0^* = \frac{m_R p}{3\lambda^*\left(3 + a^2 - 2^\alpha a\sqrt{3}\right)}\left[\frac{27}{2}c_1 + \frac{c_2 a^2}{p^2}\left(T_{11}^2 - 2T_{22}T_{11} + \frac{1}{2}T_{22}^2 + \frac{1}{2}T_{22}T_{33}\right)\right], \tag{2.49}$$

and therefore

$$G_0^* = \frac{m_R p}{3\lambda^*\left(3 + a^2 - 2^\alpha a\sqrt{3}\right)}\left(\frac{27}{2}c_1 + c_2 a^2 \eta^2\right). \tag{2.50}$$

Eq. (2.50) shows that the modulus G_0^* predicted by the proposed model depends both on the mean stress p and stress ratio η. The second term in parenthesis in (2.50) is however significantly smaller, than the first term (for parameters derived in Sec. 2.6 and $\eta = 0.5$ the first term is 13.2 times larger). Therefore, contrary to the HK model, the influence of η on G_0^* is not significant. This observation is shown in Fig. 2.3 (right), with predictions by the HK model in Fig. 2.3 (left) for comparison. This drawback of the formulation of HK model is also demonstrated in Fig. 2.4 (left). The initial stiffness for the stress path, which starts at anisotropic stress state and passes isotropic stress state, is underpredicted and the model predicts unrealistic increase of the tangent stiffness at isotropic conditions. The improved prediction by the proposed model is in Fig. 2.4 (right).

As follows from Fig. 2.3 (right), for stress states with lower stress ratios η we can neglect the second term in (2.50) and write

$$G_0^* \simeq \frac{9 m_R c_1}{2\lambda^*\left(3 + a^2 - 2^\alpha a\sqrt{3}\right)} p, \tag{2.51}$$

and after substituting the expression for c_1 (2.45) we get the final simple form

$$G_0^* \simeq \frac{m_R}{r\lambda^*} p. \tag{2.52}$$

The shear modulus G_0^* may be measured by means of an undrained shear test[2] in a triaxial apparatus equipped with high–accuracy local strain transducers (e.g., LVDT transducers [35]). However, because accurate quasi–static measurements of the shear stiffness are problematic, it is useful to derive an expression for the *out–of–axis* shear modulus G_0^{vh} [133, 78, 27, 80] (upper index v stands for *vertical* and h for *horizontal* direction), which can be measured by dynamic stiffness measurements (e.g., bender element tests [68]). Because

$$G_0^{vh} = \frac{m_R f_s}{2}\mathcal{L}_{1212}, \tag{2.53}$$

[2]In the context of this paper, the term "shear tests" is used for various types of axisymmetric loading tests performed in a triaxial cell, not in simple or torsional shear apparatuses.

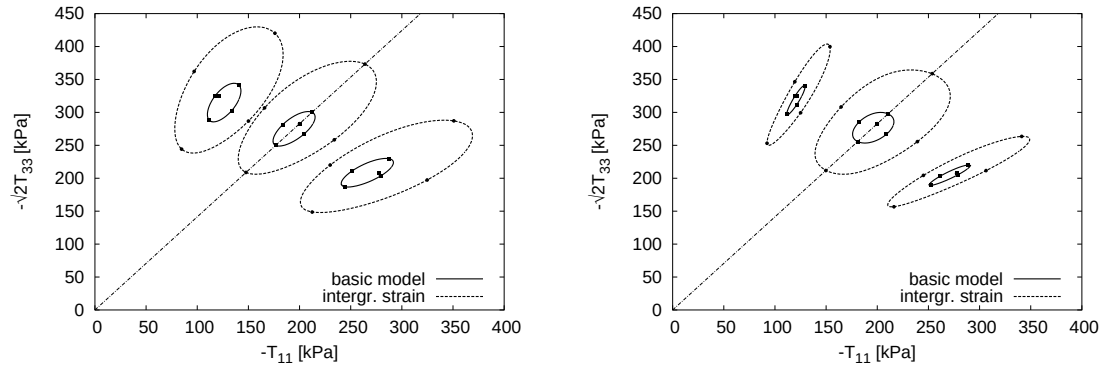

Figure 2.5: Response envelopes of the proposed model (left) and HK model (right) with and without intergranular strains for isotropic stress states and for $\varphi_{mob} = 18^\circ$ (with $\varphi_c = 22.6^\circ$) in triaxial compression and extension.

we find, after substituting expressions for $\boldsymbol{\mathcal{L}}$ (2.15), f_s (2.32) and c_1 (2.45), that

$$G_0^{vh} = \frac{m_R}{r\lambda^*} p. \tag{2.54}$$

Therefore, at axisymmetric conditions the proposed model predicts a linear dependency of the initial shear modulus G_0^{vh} on the mean stress p, which is approximately correct (e.g. [148, 139]). Eq. (2.54) is valuable for the calibration of the parameter m_R, as discussed in Sec. 2.6.

In the previous paragraph we demonstrated that the initial shear stiffness in the "quasi–elastic" range of the proposed model is practically independent of the stress ratio η. Nevertheless, the shear stiffness for *intergranular swept–out–memory* states [108] (and the shear stiffness of the basic model without intergranular strain concept) must vanish as the stress approaches Matsuoka–Nakai states. This property of the proposed model can be studied using response envelopes (Fig. 2.5 (left)). It is evident that the response envelopes of the model with intergranular strain are centered about the reference stress point. On the other hand, for larger φ_{mob} the response envelopes of the basic model are significantly translated (ultimately, at Matsuoka–Nakai limit state they touch the reference stress point). It is also worth noting that the response envelopes do not change their shape substantially as the stress approaches the critical state. This is not the case for the HK model (Fig. 2.5 (right)), where the response envelopes for larger φ_{mob} become narrower. Note that also the VW hypoplastic model for granular materials retains similar shapes[3] of response envelopes for different φ_{mob}.

[3]Only the size of response envelopes decreases slightly, due to the factor $1/(\hat{\mathbf{T}} : \hat{\mathbf{T}})$ in the expression for $\boldsymbol{\mathcal{L}}$ (Sec. 2.4.1).

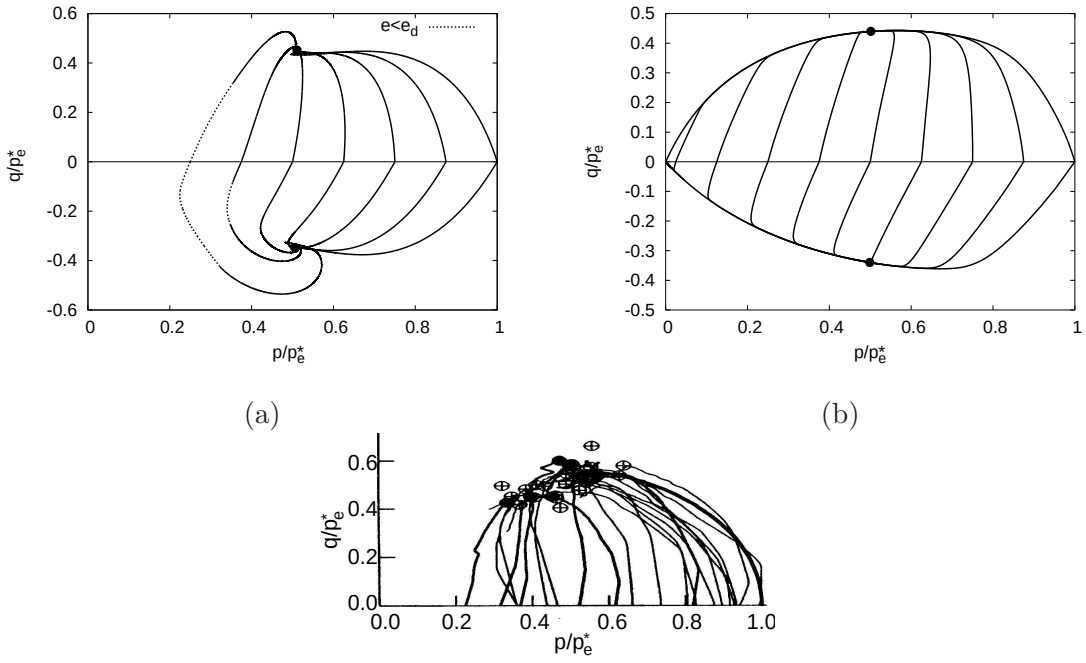

Figure 2.6: Normalized stress paths of drained shear tests calculated by the HK (a) and proposed (b) models, with critical states indicated by points. Experimental results by Rampello and Callisto [114] on natural Pisa clay for qualitative comparison (c). Simulations were performed with $e = \text{const.}$, $q = 0$ kPa and varying p.

2.5.2 Stress–dilatancy behaviour

In this section we will study the influence of the novel expression for the pyknotropy factor f_d. Since a detailed study on the shape of the state boundary surface of the proposed constitutive model, defined as a boundary of all admissible states in the stress–porosity space, is presented in a forthcoming paper [95], we will restrict our attention to the shape of stress paths normalized by the equivalent pressure at the isotropic normal compression line p_e^* [64] (Fig. 2.2), defined by

$$p_e^* = \exp\left\{\frac{N - \ln(1+e)}{\lambda^*}\right\}. \tag{2.55}$$

They are shown for drained triaxial tests in Fig. 2.6 (b), experimental results on natural Pisa clay [114] are given in Fig. 2.6 (c) for qualitative comparison. The proposed model predicts correctly dilatant/contractant behaviour for a wide range of overconsolidation ratios, down to $p = 0$. The increase in the peak friction angle for states *dry of critical* (defined by $p < p_{cr}$ or $p/p_e^* < 0.5$) is also evident.

Predictions by the HK model are shown for comparison in Fig. 2.6 (a). This figure reveals another shortcoming of the HK (VW) model, discussed by Niemunis et al. [110]. This

model allows the lower limit of void ratio e_d to be surpassed. The parts of the stress paths, which pass inadmissible state $e < e_d$, are plotted using dotted lines in Fig. 2.6 (a)[4]. It is clear that unlike the proposed model the HK model is not suitable for modelling clays with higher overconsolidation ratios.

2.5.3 Limitations of the proposed model

After sumarising the main advantages of the proposed model, let us now point out its limitations.

A particular form of barotropy and pyknotropy factors f_s and f_d prescribe constant shape and size of the state boundary surface (see [95] for detailed explanation). Therefore, the model is suitable for modeling reconstituted clays and natural clays with "stable" structure (constant sensitivity, in a sense defined in [34]). Its application to soft natural clays requires further development.

The aim of the work is to provide a practical engineering model with a minimal number of parameters, which may be evaluated on the basis of standard laboratory experiments. This fact certainly restricts freedom for calibration, which may be found to be limiting for certain non–standard geotechnical applications. In such a case, the proposed model may be used as a basis for further modifications.

2.6 Determination of parameters

The model is evaluated on the basis of laboratory tests on reconstituted London clay (Mašín [86, 98]). These were performed in computer controlled triaxial apparatuses. In addition to the standard equipment, three local submersible LVDT transducers RDP D5/200 [35] and a pair of bender elements [68] were used in order to study also the behaviour in the small strain range.

Parameters N, λ^* and κ^*: These parameters were calibrated on the basis of a single isotropic loading/unloading test (Fig. 2.7 left). Isotropic loading must exceed preconsolidation pressure in order to find the position and the slope of the normal compression line. Parameter κ^* should be calibrated from the slope of the isotropic unloading line close to the normally compressed state[5].

Parameter φ_c: The critical state friction angle was found using a linear regression through the critical state points of all shear tests available.

[4]Note that the factor f_d of the HK model is a complex number for $e < e_d$. In order to perform analyses, $f_d = 0$ for $e < e_d$ was prescribed, so predictions were for these states hypoelastic.

[5]Note that the proposed model is formulated in such a way that the slope of the predicted isotropic unloading line in $\ln(1+e) : \ln p$ space is exactly equal to parameter κ^* only for unloading from normally compressed state.

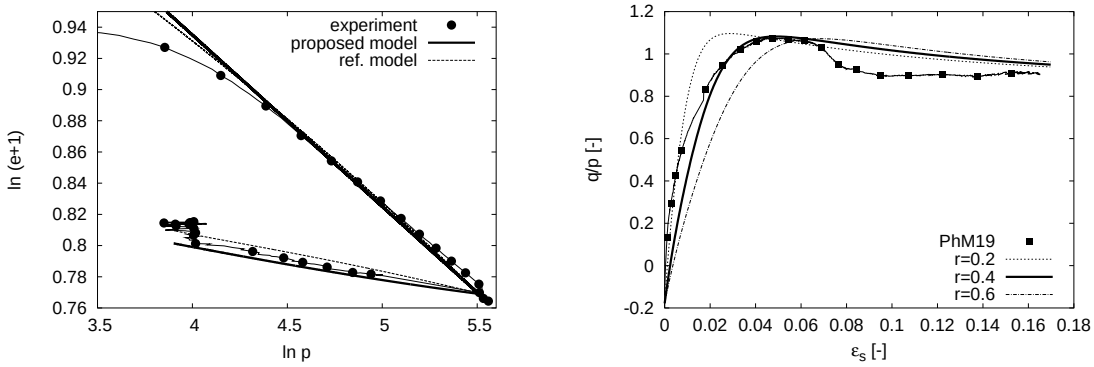

Figure 2.7: Calibration of parameters N, λ^* and κ^* on the basis of isotropic loading and unloading test. Unlike the experiment, simulation started from normally compressed state (left). Calibration of parameter r using a parametric study (right).

Table 2.1: Summary of parameters of the basic version of the proposed model (left) and of the intergranular strain extension (right) for London clay. Standard values may be assumed for parameters in parenthesis

φ_c [°]	λ^*	κ^*	N	r
22.6	0.11	0.016	1.375	0.4

m_R	(m_T)	(R)	(β_r)	(χ)
4.5	(4.5)	(10^{-4})	(0.2)	(6)

Parameter r: Parameter r may be evaluated directly, using the definition (Sec. 2.4.6), as a ratio of the bulk and shear moduli for tests starting from isotropic normally compressed stress state. However, since the model predicts gradual degradation of the shear stiffness, it is advisable to find an appropriate value of the parameter r by a parametric study. This approach is acceptable because there is no interrelation with other model parameters, which would require parametric study for calibration.

The parameter r was calibrated on the basis of the stress–strain curve of the shear test with constant mean pressure on K_0 overconsolidated specimen (PhM19), Fig. 2.7 (right).

Parameters for the small strain range (intergranular strain concept): Intergranular strain concept (Sec. 2.2.3) requires five additional model parameters. Their calibration is described in the original paper [108]. Experience however shows that three of these parameters have similar values for a broad range of different soils and without suitable laboratory experiments we can assume "standard" values: $R = 10^{-4}$, $\beta_r = 0.2$ and $\chi = 6$. Due to the lack of suitable laboratory experiments we also assume $m_T = m_R$.

The parameter m_R may be conveniently calibrated on the basis of the shear stiffness measurements with bender elements using Eq. (2.54). Knowing the values of parameters λ^* and r we use a linear regression in $G_0^{vh} : p$ space and from the slope calculate the value of parameter m_R, as shown in Figure 2.8.

Derived parameters of the proposed model for London clay are given in Table 2.1.

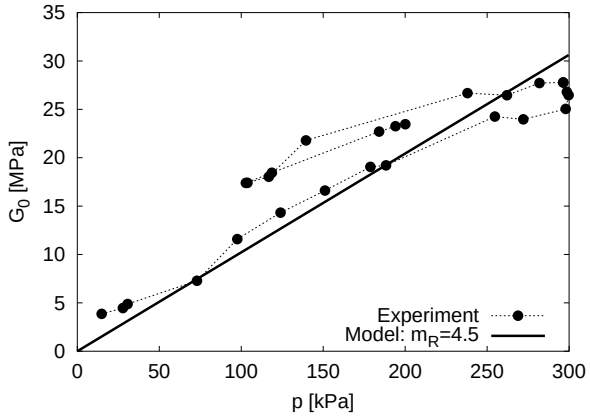

Figure 2.8: Calibration of parameter m_R using linear regression on results from bender element tests.

2.6.1 Calibration of the HK model

The HK model was calibrated on the basis of the same laboratory tests as the proposed model to compare their predictions. Parameters h_s, n and e_{i0}, which define the position and the shape of the isotropic normal compression line, were calibrated using isotropic compression test depicted in Fig. 2.7 (left). An isotropic unloading test was used to calibrate parameters α and β. Because a direct calibration is difficult, parameters α and β were derived by means of a parametric study. It may be seen from Fig. 2.7 (left) that correctly chosen parameters allow similar predictions of the isotropic test by both the HK and the proposed model (in the chosen stress range). The advantage of the proposed model is the smaller number of parameters, which all have a well defined physical meaning.

The parameter e_{c0} was calibrated by fitting the position of the critical state line in $p : e$ space. The calculation of the parameter e_{d0} from the water content at the plastic limit, as suggested in [61], leads to incorrect predictions of dilatant/contractant behaviour of overconsolidated specimens. The calibration of e_{d0} was therefore based on the correct predictions of dilatant behaviour of an overconsolidated specimen (PhM19). Finally, the parameter r was evaluated using a parametric study on a stress–strain curve of the test PhM19. The numerical value of the parameter r is different compared to the proposed model, due to slightly different expressions for scalar factor c_1, see Appendixes A and C[6]. The HK model does not allow direct evaluation of the parameter m_R using $G_0 : p$ curve. Small strain parameters of the proposed model were therefore assumed also for the HK model. Parameters of the HK model are summarized in Table 2.2.

[6]In the formulation of the HK model, the expression for f_{di} is omitted in the calculation of the scalar factor c_1

Table 2.2: Summary of parameters of the basic version of the HK model for London clay.

ϕ_c [°]	h_s [kPa]	n	e_{d0}	e_{c0}	e_{i0}	α	β	r
22.6	659	0.214	2.6	2.8	3.23	0.45	2	0.6

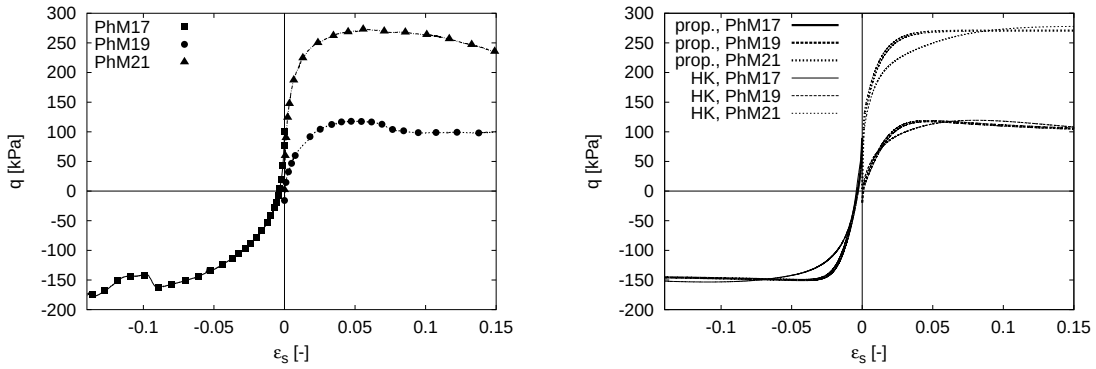

Figure 2.9: Stress–strain curves of three different compression tests. Experimental (left) and simulated (right). Simulation by the basic versions of the HK and proposed model.

2.7 Model predictions

An extensive evaluation of the predictions by the proposed model, compared with different elasto–plastic and hypoplastic models, is presented in a forthcoming paper [99]. In this work, we simulate laboratory experiments, which were not used to calibrate the constitutive model[7], in order to demonstrate the capability of the model to predict different aspects of the clay behaviour. The basic version of the model is mostly used, the intergranular strain concept is adopted only when the behaviour at small strains is important.

Two other shear tests in addition to the test PhM19 were simulated. An undrained compression test on a nearly normally compressed specimen (PhM21) and a constant p' extension test on a K_0 overconsolidated specimen (PhM17). The experimental and simulated stress–strain curves are shown in Fig. 2.9. To assess volumetric changes in drained tests and development of pore pressures in undrained tests, it is useful to study the shape of stress paths normalized with respect to the equivalent pressure p_e^*, shown in Fig. 2.10.

Comparisons of predictions by the HK and proposed model in Figs. 2.9 and 2.10 indicate that for soils with medium overconsolidation ratios the predictions of the shear behaviour at large strains are similar. In this case the proposed model has the advantage of a simpler calibration. For higher overconsolidation ratios however, large–strain predictions by both models differ significantly due to the different formulation of the pyknotropy factor f_d (Fig. 2.6).

Since stiffness at small strains was measured by means of local LVDT transducers, we can

[7]Except for parameter φ_c

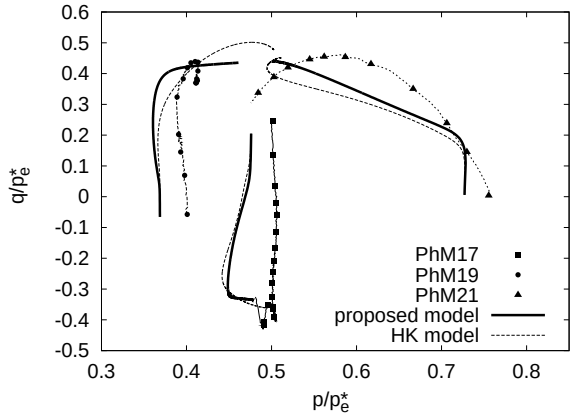

Figure 2.10: Normalised stress paths of three shear tests. Simulation by the HK and proposed models, both extended with the intergranular strain concept.

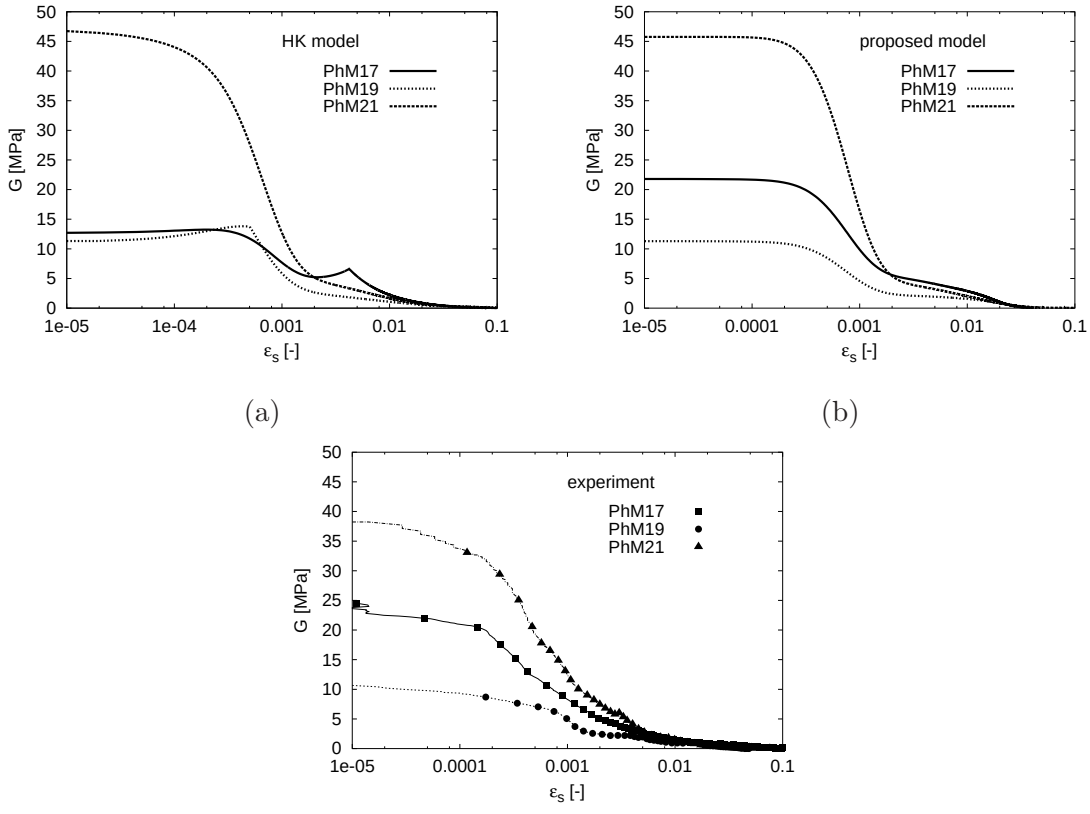

Figure 2.11: Degradation of the tangent shear stiffness at small strains. Simulation by the HK (a) and proposed (b) model, both enhanced by the intergranular strain concept, and experimental results (c).

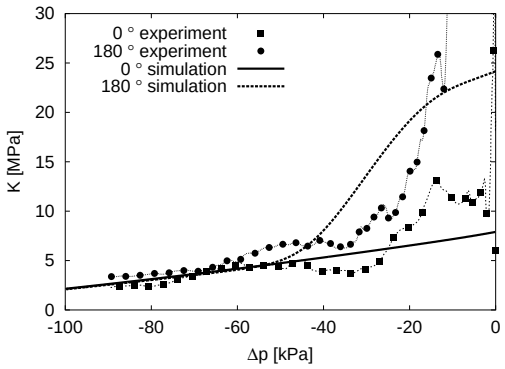

Figure 2.12: Variation of bulk modulus in the isotropic unloading test with different degrees of strain path rotation. Experiment and simulation by the proposed model with intergranular strains.

study also the capability of the models to predict degradation of the shear stiffness in the small strain range, Fig. 2.11. The proposed model (Fig. 2.11 (b)) predicts correctly initial shear modulus and degradation of stiffness for tests PhM17 and PhM19, although the test PhM17 started from an anisotropic stress state (Fig. 2.10). The initial stiffness of the test PhM21 is slightly overpredicted. This comes from the fact that the test PhM21 was performed at a larger mean stress (450 kPa) than the stress range used for calibration of the parameter m_R (Fig. 2.8). Predictions by the HK model (Fig. 2.11 (a)) are comparable with predictions by the proposed model only for the test PhM21, which started from the nearly isotropic stress state. The initial stiffness of the test PhM17, with the anisotropic initial stress state, is significantly underpredicted and the HK model simulates an incorrect increase of the shear stiffness at larger shear strains.

One isotropic loading/unloading test was performed with two different degrees of strain path rotation (0° and 180°) starting from the same mean stress and overconsolidation ratio. Experimental variation of the bulk moduli and simulations by the proposed model are shown in Fig. 2.12. The experimental data show a marked scatter and the model predicts correctly the trend. Satisfactory predictions were achieved although the parameter m_R was calibrated only on the basis of dynamic measurements of the *shear* stiffness.

2.8 Conclusions

This paper has presented a new hypoplastic constitutive model for clays. The model uses a formulation of the generalised hypoplasticity [106], which allows independent treatment of different aspects of soil behaviour. In this way it was possible to develop a model particularly suitable for fine–grained soils.

The proposed model combines hypoplasticity principles with the traditional critical state soil mechanics. Parameters required by the model correspond to the parameters of the

Modified Cam clay model and are simple to calibrate on the basis of standard laboratory tests, which makes the model particularly suitable for practical applications.

The model has been developed to predict soil behaviour at larger strains. However, it may be enhanced simply by the intergranular strain concept [108] to allow predictions to also be made at small to very small strains. The calibration of additional parameters, which are related to the parameters of the basic model, have also been discussed briefly in the paper.

The model is evaluated on the basis of high quality laboratory measurements on reconstituted specimens of London clay. It is demonstrated that with a minimal number of parameters the model is capable of predicting a wide range of aspects of fine grained soils behaviour. Apart from the advantage of simpler calibration, the proposed model significantly improves predictions of the HK model [61] for clays with higher overconsolidation ratios and predictions of the behaviour in the small–strain range at anisotropic stress states.

Appendix A

This appendix summarizes mathematical formulation of a hypoplastic model for soils with low friction angles by Herle and Kolymbas [61].

The model assumes the following stress–strain relation:

$$\mathring{\mathbf{T}} = f_s \boldsymbol{\mathcal{L}} : \mathbf{D} + f_s f_d \mathbf{N} \|\mathbf{D}\|, \tag{2.56}$$

with

$$\boldsymbol{\mathcal{L}} = \frac{1}{\hat{\mathbf{T}} : \hat{\mathbf{T}}} \left(c_1 F^2 \boldsymbol{\mathcal{I}} + c_2 a^2 \hat{\mathbf{T}} \otimes \hat{\mathbf{T}} \right), \tag{2.57}$$

$$\mathbf{N} = \frac{Fa}{\hat{\mathbf{T}} : \hat{\mathbf{T}}} \left(\hat{\mathbf{T}} + \hat{\mathbf{T}}^* \right), \tag{2.58}$$

where $\mathbf{1}$ is a second–order unity tensor, $\mathcal{I}_{ijkl} = \frac{1}{2}\left(1_{ik}1_{jl} + 1_{il}1_{jk}\right)$ is a fourth-order unity tensor and

$$\mathrm{tr}\mathbf{T} = \mathbf{T} : \mathbf{1}, \qquad \hat{\mathbf{T}} = \mathbf{T}/\mathrm{tr}\mathbf{T}, \qquad \hat{\mathbf{T}}^* = \hat{\mathbf{T}} - \mathbf{1}/3, \tag{2.59}$$

$$a = \frac{\sqrt{3}\left(3 - \sin\varphi_c\right)}{2\sqrt{2}\sin\varphi_c}, \qquad F = \sqrt{\frac{1}{8}\tan^2\psi + \frac{2 - \tan^2\psi}{2 + \sqrt{2}\tan\psi\cos 3\theta}} - \frac{1}{2\sqrt{2}}\tan\psi, \tag{2.60}$$

with

$$\tan\psi = \sqrt{3}\|\hat{\mathbf{T}}^*\|, \qquad \cos 3\theta = -\sqrt{6}, \frac{\mathrm{tr}\left(\hat{\mathbf{T}}^* \cdot \hat{\mathbf{T}}^* \cdot \hat{\mathbf{T}}^*\right)}{\left[\hat{\mathbf{T}}^* : \hat{\mathbf{T}}^*\right]^{3/2}}. \tag{2.61}$$

The scalar factors f_s and f_d take into account the influence of mean pressure and density,

$$f_s = \frac{h_s}{n}\left(\frac{e_i}{e}\right)^{\beta}\frac{1+e_i}{e}\left(\frac{-\mathrm{tr}\mathbf{T}}{h_s}\right)^{1-n}\left[3c_1 + a^2 c_2 - a\sqrt{3}\left(\frac{e_{i0}-e_{d0}}{e_{c0}-e_{d0}}\right)^{\alpha}\right]^{-1}, \tag{2.62}$$

$$f_d = \left(\frac{e-e_d}{e_c-e_d}\right)^{\alpha}. \tag{2.63}$$

The characteristic void ratios – e_i, e_c and e_d decrease with the mean pressure according to the relation

$$\frac{e_i}{e_{i0}} = \frac{e_c}{e_{c0}} = \frac{e_d}{e_{d0}} = \exp\left[-\left(\frac{-\mathrm{tr}\mathbf{T}}{h_s}\right)^{n}\right]. \tag{2.64}$$

The scalar factors c_1 and c_2 are calculated using

$$c_1 = \left(\frac{1+\frac{1}{3}a^2 - \frac{1}{\sqrt{3}}a}{1.5r}\right)^{\xi}, \tag{2.65}$$

$$c_2 = 1 + (1-c_1)\,\frac{3}{a^2}, \tag{2.66}$$

$$\xi = \left\langle \frac{\sin\varphi_c - \sin\varphi_{mob}}{\sin\varphi_c}\right\rangle, \qquad \text{where} \qquad \sin\varphi_{mob} = \frac{T_1 - T_3}{T_1 + T_3}. \tag{2.67}$$

T_1 and T_3 are the maximal and minimal principal stresses, φ_{mob} is a mobilized friction angle and $\langle\rangle$ are Macauley brackets: $\langle x\rangle = (x + |x|)/2$.

The model requires 9 parameters: ϕ_c, h_s, n, e_{d0}, e_{c0}, e_{i0}, α, β and r.

Appendix B

To capture correctly behaviour in the small to very small strain range the hypoplastic model must be enhanced by the intergranular strain concept [108].

In the extended hypoplastic model the strain is considered as a result of deformation of the intergranular interface layer and of rearrangement of the skeleton. The interface deformation is called *intergranular strain* $\boldsymbol{\delta}$ and is considered as a new tensorial state variable ($\boldsymbol{\delta}$ is a symmetric second–order tensor). It is convenient to denote the normalized magnitude of $\boldsymbol{\delta}$ as

$$\rho = \frac{\|\boldsymbol{\delta}\|}{R}, \tag{2.68}$$

and the direction $\hat{\boldsymbol{\delta}}$ of the intergranular strain as

$$\hat{\boldsymbol{\delta}} = \begin{cases} \boldsymbol{\delta}/\|\boldsymbol{\delta}\|, & \text{for } \boldsymbol{\delta} \neq \mathbf{0}; \\ \mathbf{0}, & \text{for } \boldsymbol{\delta} = \mathbf{0}. \end{cases} \tag{2.69}$$

The general stress–strain relation is now written as

$$\mathring{\mathbf{T}} = \boldsymbol{\mathcal{M}} : \mathbf{D}. \tag{2.70}$$

The fourth-order tensor $\boldsymbol{\mathcal{M}}$ represents stiffness and is calculated from the hypoplastic tensors $\boldsymbol{\mathcal{L}}$ and $\mathbf{N}$ and a function of the intergranular strain using the following interpolation:

$$\boldsymbol{\mathcal{M}} = \left[\rho^{\chi} m_T + (1-\rho^{\chi})\, m_R\right] f_s \boldsymbol{\mathcal{L}} + \begin{cases} \rho^{\chi}\,(1-m_T)\, f_s \boldsymbol{\mathcal{L}} : \hat{\boldsymbol{\delta}} \otimes \hat{\boldsymbol{\delta}} + \rho^{\chi} f_s f_d \mathbf{N}\hat{\boldsymbol{\delta}}, & \text{for } \hat{\boldsymbol{\delta}} : \mathbf{D} > 0; \\ \rho^{\chi}\,(m_R - m_T)\, f_s \boldsymbol{\mathcal{L}} : \hat{\boldsymbol{\delta}} \otimes \hat{\boldsymbol{\delta}}, & \text{for } \hat{\boldsymbol{\delta}} : \mathbf{D} \le 0. \end{cases} \tag{2.71}$$

The evolution equation for the intergranular strain tensor $\boldsymbol{\delta}$ is governed by

$$\mathring{\boldsymbol{\delta}} = \begin{cases} \left(\boldsymbol{\mathcal{I}} - \hat{\boldsymbol{\delta}} \otimes \hat{\boldsymbol{\delta}} \rho^{\beta_r}\right) : \mathbf{D}, & \text{for } \hat{\boldsymbol{\delta}} : \mathbf{D} > 0; \\ \mathbf{D}, & \text{for } \hat{\boldsymbol{\delta}} : \mathbf{D} \le 0. \end{cases} \tag{2.72}$$

where $\mathring{\boldsymbol{\delta}}$ is the objective rate of intergranular strain. The hypoplastic model with intergranular strains requires five additional model parameters: R, m_R, m_T, β_r and χ.

Appendix C

Mathematical formulation of the proposed hypoplastic constitutive model for clays:

The general stress–strain relation reads

$$\mathring{\mathbf{T}} = f_s \boldsymbol{\mathcal{L}} : \mathbf{D} + f_s f_d \mathbf{N} \|\mathbf{D}\|, \tag{2.73}$$

with

$$\mathbf{N} = \boldsymbol{\mathcal{L}} : \left(-Y \frac{\mathbf{m}}{\|\mathbf{m}\|}\right). \tag{2.74}$$

The hypoelastic tensor $\boldsymbol{\mathcal{L}}$ is

$$\boldsymbol{\mathcal{L}} = 3\left(c_1 \boldsymbol{\mathcal{I}} + c_2 a^2 \hat{\mathbf{T}} \otimes \hat{\mathbf{T}}\right), \tag{2.75}$$

where $\mathbf{1}$ is a second–order unity tensor, $\mathcal{I}_{ijkl} = \frac{1}{2}\left(1_{ik}1_{jl} + 1_{il}1_{jk}\right)$ is a fourth-order unity tensor and

$$\mathrm{tr}\mathbf{T} = \mathbf{T} : \mathbf{1}, \qquad \hat{\mathbf{T}} = \mathbf{T}/\mathrm{tr}\mathbf{T}, \qquad \hat{\mathbf{T}}^{*} = \hat{\mathbf{T}} - \mathbf{1}/3, \tag{2.76}$$

$$a = \frac{\sqrt{3}\,(3 - \sin\varphi_c)}{2\sqrt{2}\sin\varphi_c}. \tag{2.77}$$

The degree of nonlinearity Y, with the limit value $Y = 1$ at Matsuoka–Nakai failure surface, is calculated by

$$Y = \left(\frac{\sqrt{3}a}{3+a^2} - 1\right) \frac{(I_1 I_2 + 9I_3)\left(1 - \sin^2\varphi_c\right)}{8 I_3 \sin^2\varphi_c} + \frac{\sqrt{3}a}{3+a^2}, \tag{2.78}$$

with stress invariants I_1, I_2 and I_3,

$$I_1 = \mathrm{tr}\mathbf{T}, \qquad I_2 = \frac{1}{2}\left[\mathbf{T}:\mathbf{T} - (I_1)^2\right], \qquad I_3 = \det\mathbf{T}. \tag{2.79}$$

The tensorial quantity $\mathbf{m}$ defining the hypoplastic flow rule has the following formulation:

$$\mathbf{m} = -\frac{a}{F}\left[\hat{\mathbf{T}} + \hat{\mathbf{T}}^* - \frac{\hat{\mathbf{T}}}{3}\left(\frac{6\ \hat{\mathbf{T}}:\hat{\mathbf{T}} - 1}{(F/a)^2 + \hat{\mathbf{T}}:\hat{\mathbf{T}}}\right)\right], \tag{2.80}$$

with factor F given by

$$F = \sqrt{\frac{1}{8}\tan^2\psi + \frac{2 - \tan^2\psi}{2 + \sqrt{2}\tan\psi\cos 3\theta}} - \frac{1}{2\sqrt{2}}\tan\psi, \tag{2.81}$$

where

$$\tan\psi = \sqrt{3}\|\hat{\mathbf{T}}^*\|, \qquad \cos 3\theta = -\sqrt{6}\frac{\mathrm{tr}\left(\hat{\mathbf{T}}^*\cdot\hat{\mathbf{T}}^*\cdot\hat{\mathbf{T}}^*\right)}{\left[\hat{\mathbf{T}}^*:\hat{\mathbf{T}}^*\right]^{3/2}}. \tag{2.82}$$

Barotropy and pyknotropy factors f_s and f_d read

$$f_s = -\frac{\mathrm{tr}\mathbf{T}}{\lambda^*}\left(3 + a^2 - 2^\alpha a\sqrt{3}\right)^{-1}, \qquad f_d = \left[-\frac{2\mathrm{tr}\mathbf{T}}{3p_r}\exp\left(\frac{\ln(1+e) - N}{\lambda^*}\right)\right]^\alpha, \tag{2.83}$$

where p_r is the reference stress 1 kPa and the scalar quantity α is calculated by

$$\alpha = \frac{1}{\ln 2}\ln\left[\frac{\lambda^* - \kappa^*}{\lambda^* + \kappa^*}\left(\frac{3 + a^2}{a\sqrt{3}}\right)\right]. \tag{2.84}$$

Finally, factors c_1 and c_2 are calculated as follows:

$$c_1 = \frac{2\left(3 + a^2 - 2^\alpha a\sqrt{3}\right)}{9r}, \qquad c_2 = 1 + (1 - c_1)\frac{3}{a^2}. \tag{2.85}$$

The model requires five constitutive parameters: φ_c, λ^*, κ^*, N and r.

Chapter 3

State boundary surface of a hypoplastic model for clays

3.1 Introduction

Hypoplastic constitutive models have been developed since 1980's and since then they have established a solid base for an alternative description of the soil behaviour, without an explicit definition of yield and potential surfaces – see for example the review [133]. Recent hypoplastic models [53, 141] include the concept of critical states and have been successfully used in many computations of boundary value problems within coarse-grained soils, e.g. [136, 112, 70, 100, 36]. The progress of hypoplastic models suitable for the description of fine-grained soils has been delayed. Rate-dependent [105, 54] and rate-independent [61, 87] hypoplastic models for clays promise to follow the success of the development for sand. Nevertheless, a thorough testing of various constitutive aspects is required in order to ensure a correct performance in general conditions of boundary value problems.

One of the key characteristics of the behaviour of fine-grained soils, incorporated in different ways in most of the currently available elasto-plastic constitutive models for fine-grained soils, is a surface in the stress-void ratio space which bounds all admissible states (state boundary surface, SBS). As hypoplastic models do not incorporate the state boundary surface explicitly, the primary aim of this paper is to investigate if these models (in particular a hypoplastic model for clays [87]) predict the state boundary surface as a by-product of the constitutive formulation.

In this paper hypoplastic models will be distinguished according to the terminology laid out by Kolymbas [77]. Models without internal structure (*i.e.* with Cauchy stress tensor $\mathbf{T}$ being the only state variable) will be referred to as *amorphous*, whereas models with internal structure (incorporated by means of additional state variables) *endomorphous*. In this work we restrict our attention to *endomorphous* models with a single additional state variable (void ratio e). Solid mechanics sign convention (compression negative) will be adopted throughout, all stresses are considered as effective in the sense of Terzaghi. The

operator arrow is defined as $\vec{\mathbf{X}} = \mathbf{X}/\|\mathbf{X}\|$, trace by $\operatorname{tr}\mathbf{X} = \mathbf{X} : \mathbf{1}$, with $\mathbf{1}$ being the second-order unit tensor. $\hat{\mathbf{T}}$ is the normalised stress defined by $\hat{\mathbf{T}} = \mathbf{T}/\operatorname{tr}\mathbf{T}$, $\|\mathbf{D}\| = \sqrt{\mathbf{D} : \mathbf{D}}$ is the Euclidian norm of $\mathbf{D}$, which stands for the Euler's stretching tensor.

The paper starts by introducing proportional response envelopes and definition of asymptotic (swept-out-memory) states. Thereafter, pointing to the analogy with the limit and bounding surfaces of *amorphous* hypoplastic models, a mathematical formulation of the surface in the stress-void ratio space which covers all asymptotic states (named *swept-out-memory* surface) is developed. Further, using the concept of so-called normalised incremental stress response envelopes, it is demonstrated that swept-out-memory surface is a close approximation of the state boundary surface. Finally, the influence of model parameters on the shape of the swept-out-memory surface is discussed.

3.2 Response envelopes and swept-out-memory states

Response envelopes in axisymmetric stress space [50] were proposed as a graphical representation of resulting stress rates imposed by different unit strain rates $\sqrt{D_a^2 + 2D_r^2} = 1$ at one particular initial state (D_a and D_r being axial and radial strain rates, respectively). This concept proved to be useful in studying properties of rate-type constitutive equations, however due to the infinitesimal nature of stress and strain rates they can not be studied experimentally. Hypoplastic models yield elliptic (smooth) response envelopes, whereas elasto-plastic models are characterised by non-smooth envelopes.

A modification of the stress-rate envelopes towards *incremental stress response envelopes*, as defined in Reference [134], may be applied for finite values of stress and strain increments. Linear strain paths with a fixed direction of stretching $\vec{\mathbf{D}}$ and with a fixed length $R_{\Delta\epsilon}$ (Eq. (3.2)) yield the stress response $\Delta\mathbf{T}$ in the stress space $\mathbf{T}$ (see Fig. 3.1 for axisymmetric conditions). The stress increment $\Delta\mathbf{T}$ may be calculated by the time integration of the rate form of the constitutive equation:

$$\Delta\mathbf{T} = \int_{t_0}^{t_1} \mathring{\mathbf{T}} dt \tag{3.1}$$

where $\mathring{\mathbf{T}}$ stands for a co-rotated (Jaumann) stress rate. The shape and size of the incremental stress response envelopes depends on the value of

$$R_{\Delta\epsilon} = \| \int_{t_0}^{t_1} \mathbf{D}\, dt \| \tag{3.2}$$

An inverse procedure with constant $\vec{\mathring{\mathbf{T}}}$ and fixed length stress increments $R_{\Delta\sigma}$, constituting in the strain space *incremental strain response envelopes*, was applied experimentally by Royis and Doanh [120] for sand and Costanzo et al. [31] for clays. These results were followed by numerical investigations using DEM with rigid spheres [24] and used for evaluation of predictive capabilities of different constitutive models [99, 131].

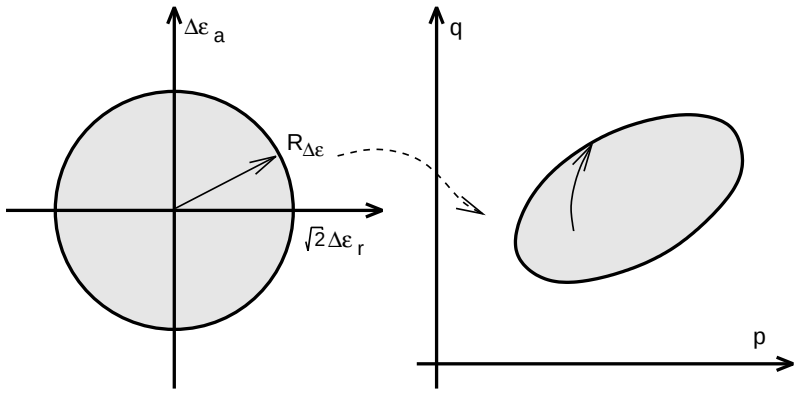

Figure 3.1: On the definition of the *incremental stress response envelope* for the special case of axisymmetric conditions

In addition to incremental responses, constitutive models should predict so-called asymptotic states, as pointed out by Kolymbas [76]. Stress paths of sound constitutive models should tend to proportional stress paths (constant $\vec{\mathbf{T}}$) for sufficiently long proportional strain paths (constant $\vec{\mathbf{D}}$). As corresponding $\vec{\mathbf{T}}$ and $\vec{\mathbf{D}}$ at asymptotic states are independent of the initial state, these states are often denoted as swept-out-memory (SOM) states [55], and may be seen as *attractors* of the soil behaviour [51] (see Fig. 3.2).

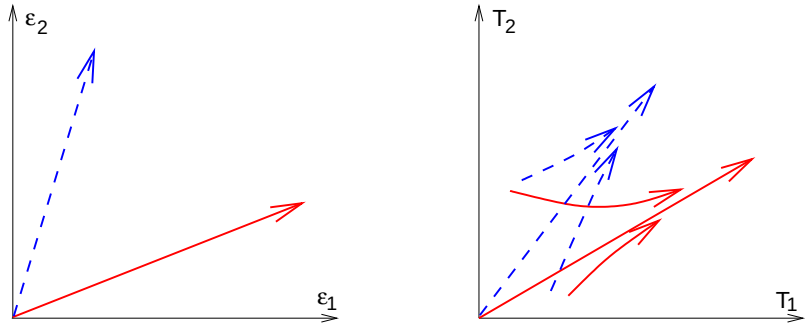

Figure 3.2: SOM-behaviour: proportional stress paths for proportional strain paths

The concept of swept-out-memory states may be extended also to *endomorphous* constitutive models. For pairs of proportional stress and strain paths one can find corresponding void ratios e_p dependent on the mean stress $p = -\operatorname{tr}\mathbf{T}/3$ (Fig. 3.3). Combinations of e_p and p plotted in the $e : p$ space are usually denoted as normal compression lines (NCL). A particular example of SOM-states is the critical state with $\operatorname{tr}\mathbf{D} = 0$ and $\mathring{\mathbf{T}} = \mathbf{0}$, where SOM stress ratio follows from the critical state friction angle φ_c and void ratio from the position of the critical state line in the stress-void ratio space.

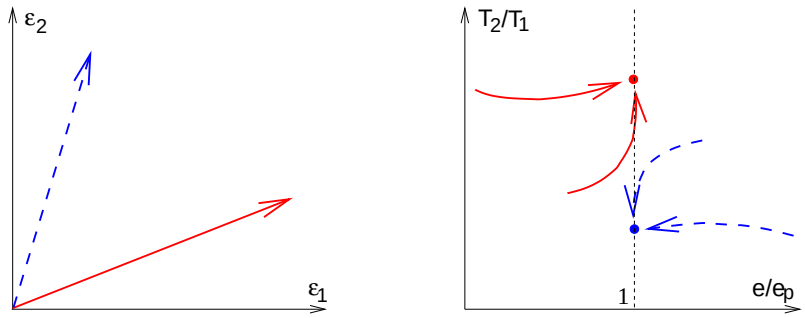

Figure 3.3: Extended SOM-behaviour including void ratio

3.3 Basic properties of the considered constitutive model

This paper focuses on the particular hypoplastic model for clays [87], whose complete mathematical formulation is given in Appendix A. The model may be written in its most general form by

$$\mathring{\mathbf{T}} = \boldsymbol{h}\left(\mathbf{T}, \mathbf{D}, e\right) \tag{3.3}$$

The model belongs to the sub-class of hypoplastic models referred to as *endomorphous* (Sec. 3.1). The particular form of the isotropic tensor-valued function $\boldsymbol{h}$ follows from [53] and reads

$$\mathring{\mathbf{T}}\left(\mathbf{T}, \mathbf{D}, e\right) = f_s\left(\operatorname{tr}\mathbf{T}\right)\left[\boldsymbol{\mathcal{L}}(\hat{\mathbf{T}}) : \mathbf{D} + f_d\left(\operatorname{tr}\mathbf{T}, e\right)\mathbf{N}(\hat{\mathbf{T}})\|\mathbf{D}\|\right] \tag{3.4}$$

where f_s and f_d are so-called *barotropy* and *pyknotropy* factors [53], which incorporate the influence of the mean stress and void ratio. Note that differently from [53], the barotropy factor f_s of the hypoplastic model for clays is independent of void ratio e.

The following properties of the considered constitutive equation are important for the developments presented in this paper:

1. The function $\boldsymbol{h}$ is positively homogeneous of degree 1 in $\mathbf{D}$:

$$\boldsymbol{h}\left(\mathbf{T}, \gamma\mathbf{D}, e\right) = \gamma\boldsymbol{h}\left(\mathbf{T}, \mathbf{D}, e\right) \tag{3.5}$$

   for any $\gamma > 0$. This property implies that the behaviour of the material is not influenced by any change in the time scale, i.e. the behaviour is rate-independent.

2. For a constant value of the *pyknotropy* factor f_d, the function $\boldsymbol{h}$ is positively homogeneous of *degree 1* in $\mathbf{T}$, thus

$$\boldsymbol{h}\left(\gamma\mathbf{T}, \mathbf{D}, e\right) = \gamma\boldsymbol{h}\left(\mathbf{T}, \mathbf{D}, e\right) \tag{3.6}$$

   for any $\gamma > 0$. This property follows from the fact that in the considered model the tensors $\boldsymbol{\mathcal{L}}$ and $\mathbf{N}$ are functions of the normalised stress $\hat{\mathbf{T}}$ only, and the ratio $f_s / \operatorname{tr}\mathbf{T}$ is constant (consequence of the assumption of a linear isotropic normal compression line in the $\ln(1+e)$:$\ln p$ space [18]).

For cases described by Eq. (3.6), the behaviour may be normalised by the current mean stress p, or in a general case, by Hvorslev's equivalent pressure on the isotropic normal compression line p_e^*. This procedure will be applied in Sec. 3.5.

3. The model predicts swept-out-memory states, introduced in Sec. 3.2. For a discussion on the prediction of SOM behaviour by hypoplastic models the reader is referred to [106].

Before proceeding to the derivation of the state boundary surface of the considered constitutive model, we recall some basic properties of more simple *amorphous* hypoplastic models.

3.4 Limit surface and Bounding surface

Amorphous hypoplastic constitutive models (e.g. model from [149]) may still be written using Eq. (3.4) [80], considering $f_d = \text{const}$. Eq. (3.3) therefore reduces to

$$\mathring{\mathbf{T}} = \boldsymbol{h}\left(\mathbf{T}, \mathbf{D}\right) \tag{3.7}$$

For brevity, we will consider the factor f_s in Eq. (3.4) embedded in the constitutive tensors $\boldsymbol{\mathcal{L}}$ and $\mathbf{N}$. Therefore, we may write

$$\mathring{\mathbf{T}}\left(\mathbf{T}, \mathbf{D}\right) = \boldsymbol{\mathcal{L}}(\mathbf{T}) : \mathbf{D} + \mathbf{N}(\mathbf{T})\|\mathbf{D}\| \tag{3.8}$$

Based on the fundamental experimental evidence, all reasonable constitutive models for soils must consider the domain of admissible states in the *stress space*, bounded by a surface, formally defined through an isotropic tensor function. In the sequel, we will distinguish between two different notions: *limit surface* and *bounding surface*:

1. *Limit surface* [29] $f(\mathbf{T})$, sometimes referred to as invertibility surface [133], failure surface [154] or yield surface [77], is defined in the *stress* space as a boundary of all states where Eq. (3.7) is invertible.

2. *Bounding surface* [106] $b(\mathbf{T})$ (or bound surface [154]) is defined in the *stress* space as a boundary of all admissible states.[1]

Limit surface has been embedded even in very early versions of hypoplastic models (see, e.g., [76]) as a by-product of a particular choice of tensorial constitutive functions. It has been however soon recognised that the mathematical structure of Eq. (3.8) allows us to define the limit surface explicitly (e.g., [26, 9, 141]).

[1] Note that this definition is different compared to the one usually adopted for bounding surface plasticity models [38] and kinematic hardening elasto-plastic models (e.g., [127]), where the term bounding surface is used for the intersection of the state boundary surface and an elastic wall.

Following [133], Eq. (3.8) may be written as

$$\gamma\mathbf{S} = \boldsymbol{\mathcal{L}} : \mathbf{D} + \mathbf{N}\|\mathbf{D}\| \tag{3.9}$$

with γ being the norm of the stress increment $\gamma = \|\mathring{\mathbf{T}}\|$ and $\mathbf{S}$ its direction $\mathbf{S} = \vec{\mathring{\mathbf{T}}}$. Due to the Property 1. of Sec. 3.3 we may, without loss of generality, assume $\|\mathbf{D}\| = 1$. Eq. (3.9) then reads

$$\gamma\mathbf{S} = \boldsymbol{\mathcal{L}} : \vec{\mathbf{D}} + \mathbf{N} = \boldsymbol{\mathcal{L}} : (\vec{\mathbf{D}} + \mathbf{B}) \tag{3.10}$$

with

$$\mathbf{B} = \boldsymbol{\mathcal{L}}^{-1} : \mathbf{N} \tag{3.11}$$

Expressing (3.11) obviously requires invertibility of the tensor $\boldsymbol{\mathcal{L}}$ of the particular *amorphous* hypoplastic model.

From Eq. (3.10) we get

$$\vec{\mathbf{D}} = \gamma\boldsymbol{\mathcal{L}}^{-1} : \mathbf{S} - \mathbf{B} \tag{3.12}$$

Because $\|\vec{\mathbf{D}}\| = 1$, we have

$$1 = \|\gamma\boldsymbol{\mathcal{L}}^{-1} : \mathbf{S} - \mathbf{B}\| \tag{3.13}$$

and therefore

$$\gamma^2\|\boldsymbol{\mathcal{L}}^{-1} : \mathbf{S}\|^2 - 2\gamma(\boldsymbol{\mathcal{L}}^{-1} : \mathbf{S}) : \mathbf{B} + \|\mathbf{B}\|^2 - 1 = 0 \tag{3.14}$$

For states inside the limit surface we require that Eq. (3.14) has a single real positive solution for the norm of the stress increment γ. It may be shown from the requirement

$$(\boldsymbol{\mathcal{L}}^{-1} : \mathbf{S}) : \mathbf{B} < \sqrt{[(\boldsymbol{\mathcal{L}}^{-1} : \mathbf{S}) : \mathbf{B}]^2 - \|\boldsymbol{\mathcal{L}}^{-1} : \mathbf{S}\|^2(\|\mathbf{B}\|^2 - 1)} \tag{3.15}$$

that this condition is satisfied for

$$\|\mathbf{B}\|^2 - 1 < 0 \tag{3.16}$$

Equation

$$\|\mathbf{B}\|^2 - 1 = 0 \tag{3.17}$$

therefore describes the limit of invertibility of Eq. (3.8) and, according to its definition, the limit surface[2]. The fact that one solution corresponds to $\gamma = 0$ may be represented graphically using the concept of response envelopes (Sec. 3.2). As may be seen from Fig. 3.4, the reference stress point is then located on the response envelope. For states outside the limit surface the solution of Eq. (3.14) is not unique and the reference stress point is located outside the response envelope.

An investigation of Fig. 3.4 reveals that the limit surface $f(\mathbf{T})$ does not coincide with the bounding surface $b(\mathbf{T})$: for some directions of stretching the corresponding stress rates surpass $f(\mathbf{T})$. This fact, which was already described for example in [154], is a common feature of hypoplastic models developed at the University of Karlsruhe (see [133]) and is

[2]Eqs. (3.10)–(3.17) are useful for the subsequent comparison of the limit and bounding surfaces. Limit surface may be also found directly from $\mathring{\mathbf{T}} = 0$ following, e.g., [154]. In that case $\mathbf{0} = \boldsymbol{\mathcal{L}} : (\mathbf{D} + \mathbf{B}\|\mathbf{D}\|)$, thus $\vec{\mathbf{D}} = -\mathbf{B}$ and $\|\mathbf{B}\| - 1 = 0$ at the limit surface, which corresponds to (3.17).

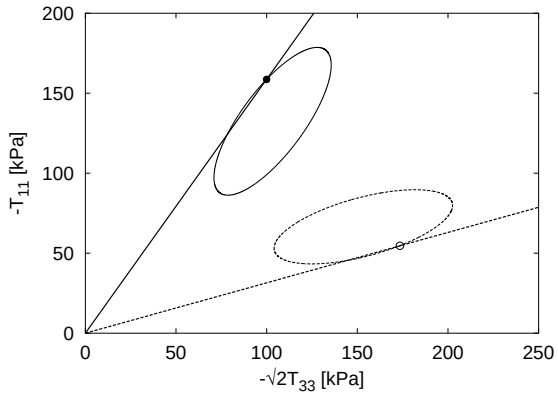

Figure 3.4: Stress rate response envelopes for the initial stress located on the limit surface

related to the derivation of constitutive tensors $\boldsymbol{\mathcal{L}}$ and $\mathbf{N}$. As noticed by [154] and as may be appreciated also from Fig. 3.4, however, the difference between the bounding and limit surfaces is not significant from the point of view of parameter identification.

The bounding surface can be mathematically characterised also by Eq. (3.14) requiring the magnitude of the stress rate $\gamma \geq 0$. Inserting the condition of the *limit surface* ($\|\mathbf{B}\|^2 - 1 = 0$) into Eq. (3.14) yields

$$\gamma^2 \|\boldsymbol{\mathcal{L}}^{-1} : \mathbf{S}\|^2 - 2\gamma(\boldsymbol{\mathcal{L}}^{-1} : \mathbf{S}) : \mathbf{B} = 0 \tag{3.18}$$

which leads to inequality constraining the possible directions of the stress rate $\mathbf{S}$:

$$(\boldsymbol{\mathcal{L}}^{-1} : \mathbf{S}) : \mathbf{B} > 0 \tag{3.19}$$

The bounding surface thus follows [133] from the condition

$$(\boldsymbol{\mathcal{L}}^{-1} : \mathbf{S}) : \mathbf{B} = 0 \tag{3.20}$$

As noted above, Eqs. (3.18)–(3.20), describing the bounding surface, hold for stress states at the limit surface. They may be therefore used to specify conditions for $b(\mathbf{T})$ to coincide with $f(\mathbf{T})$. As shown in [106], it is possible to enforce coincidence of $b(\mathbf{T})$ and $f(\mathbf{T})$ for hypoplastic models by a suitable rotation of the hypoelastic tensor $\boldsymbol{\mathcal{L}}$. Note also that $b(\mathbf{T}) = f(\mathbf{T})$ is a common feature of all CLoE hypoplastic models [29].

3.5 Swept-out-memory surface

Let us now consider the case of *endomorphous* hypoplastic models (particularly the model from [87]) with the rate-formulation given in Eq. (3.4). For these models, the definitions of the limit and bounding surfaces in the *stress* space are not unique, as both depend on the additional scalar state variable, void ratio e. Based on the experimental evidence, which

led in 1960's to the development of the critical state soil mechanics in Cambridge [117, 122], the constitutive model should describe a single surface in the stress-void ratio space, which bounds all admissible states. This surface is traditionally called *state boundary surface* (SBS). It is, in general, a surface in the four-dimensional space of the three principal components of the stress tensor $\mathbf{T}$ and void ratio e.

The property 2. from Sec. 3.3 allows us to simplify the following developments by introducing a normalisation factor taking into account both changes of void ratio and of mean pressure. A suitable quantity is Hvorslev's equivalent pressure p_e^* at the isotropic normal compression line (see Fig. 3.5), following from the formulation of the isotropic NCL:

$$\ln(1+e) = N - \lambda^* \ln\left(\frac{p_e^*}{p_r}\right) \tag{3.21}$$

with p_r being the reference stress of 1 kPa. Using this normalisation the state boundary

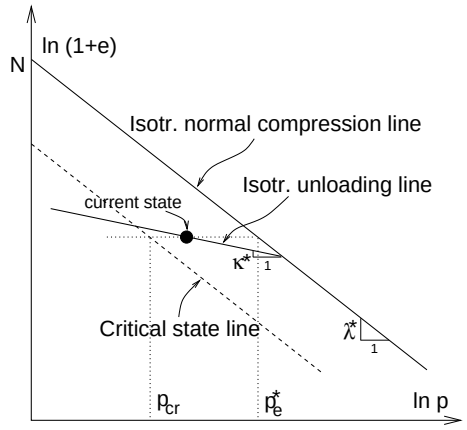

Figure 3.5: On the definition of Hvorslev's equivalent pressure p_e^*.

surface may be, in general, fully characterised in the three-dimensional space defined by the principal components of the normalised stress tensor $\mathbf{T}_n$, where

$$\mathbf{T}_n = \frac{\mathbf{T}}{p_e^*} \tag{3.22}$$

The normalised stress rate $\dot{\mathbf{T}}_n$ follows from (3.22)

$$\dot{\mathbf{T}}_n = \frac{\dot{\mathbf{T}}}{p_e^*} - \frac{\mathbf{T}}{(p_e^*)^2}\dot{p}_e^* \tag{3.23}$$

The stress rate $\dot{\mathbf{T}}$ is, under the assumption of small strains, given by (3.4) and the rate of $\dot{p}_e^*$ is found by the time-differentiation of the isotropic NCL given by Eq. (3.21):

$$\frac{\dot{e}}{1+e} = -\frac{\lambda^*}{p_e^*}\dot{p}_e^* \tag{3.24}$$

From the assumption of grain incompressibility we have

$$\dot{e} = (1+e)\,\mathrm{tr}\,\mathbf{D} \tag{3.25}$$

and thus

$$\dot{p}_e^* = -\frac{p_e^*}{\lambda^*}\,\mathrm{tr}\,\mathbf{D} \tag{3.26}$$

Substituting (3.4) and (3.26) into (3.23) we get

$$\dot{\mathbf{T}}_n = \frac{1}{p_e^*}\left(\boldsymbol{\mathcal{L}}\mathbf{D} + f_d\mathbf{N}\|\mathbf{D}\|\right) + \frac{\mathbf{T}\,\mathrm{tr}\,\mathbf{D}}{p_e^*\lambda^*} \tag{3.27}$$

For brevity, *barotropy* factor f_s has been embedded in the constitutive tensors $\boldsymbol{\mathcal{L}}$ and $\mathbf{N}$.

We first try to find an expression equivalent to the limit surface in the stress-void ratio space. As the limit surface in the *stress* space was defined by $\mathring{\mathbf{T}} = \mathbf{0}$ for one direction of stretching $\vec{\mathbf{D}}$ (Eq. 3.17), we define its equivalent in the stress-void ratio space by $\dot{\mathbf{T}}_n = \mathbf{0}$. By applying this definition on (3.27) we get

$$-\frac{\mathbf{T}}{\lambda^*}\,\mathrm{tr}\,\mathbf{D} = \boldsymbol{\mathcal{L}} : \mathbf{D} + f_d\mathbf{N}\|\mathbf{D}\| \tag{3.28}$$

To solve Eq. (3.28) for a given $\mathbf{T}$ with unknowns $\vec{\mathbf{D}}$ and f_d, we introduce a fourth order tensor $\boldsymbol{\mathcal{A}}$

$$\boldsymbol{\mathcal{A}} = \boldsymbol{\mathcal{L}} + \frac{1}{\lambda^*}\mathbf{T}\otimes\mathbf{1} \tag{3.29}$$

such that

$$\boldsymbol{\mathcal{A}} : \vec{\mathbf{D}} = \boldsymbol{\mathcal{L}} : \vec{\mathbf{D}} + \frac{\mathbf{T}}{\lambda^*}\,\mathrm{tr}\,\vec{\mathbf{D}} \tag{3.30}$$

Eq. (3.28) may be divided by $\|\mathbf{D}\| \neq \mathbf{0}$ and rewritten

$$\boldsymbol{\mathcal{A}} : \vec{\mathbf{D}} + f_d\mathbf{N} = 0 \tag{3.31}$$

Since $\|\vec{\mathbf{D}}\| = 1$, we get

$$f_d = \|\boldsymbol{\mathcal{A}}^{-1} : \mathbf{N}\|^{-1} \tag{3.32}$$

(for invertibility condition of the tensor $\boldsymbol{\mathcal{A}}$ see Appendix B) and

$$\vec{\mathbf{D}} = -\frac{\boldsymbol{\mathcal{A}}^{-1} : \mathbf{N}}{\|\boldsymbol{\mathcal{A}}^{-1} : \mathbf{N}\|} \tag{3.33}$$

As may be seen from the definitions of tensors $\boldsymbol{\mathcal{A}}$ and $\mathbf{N}$, the quantity $\boldsymbol{\mathcal{A}}^{-1} : \mathbf{N}$, and therefore also $\vec{\mathbf{D}}$ and f_d for $\dot{\mathbf{T}}_n = \mathbf{0}$, are constant for a given $\vec{\mathbf{T}}$. As the condition $\dot{\mathbf{T}}_n = \mathbf{0}$ indeed implies $\vec{\mathbf{T}} = \text{const.}$, Eq. (3.28) describes asymptotic (swept-out-memory) states as defined in Sec. 3.2, provided that the evolution equation for f_d is consistent with (3.28). Therefore, we name the equivalent of the limit surface for the stress-void ratio space a *swept-out-memory (SOM) surface*. From (3.28) it is also obvious that condition $\mathrm{tr}\,\mathbf{D} = 0$ directly implies $\mathring{\mathbf{T}} = \mathbf{0}$, so the critical state is predicted as a particular SOM state.

The corresponding response in the $p:e$ space may be found by taking the trace of Eq. (3.28) and considering $\boldsymbol{\mathcal{L}}:\mathbf{D}+f_d\mathbf{N}\|\mathbf{D}\|=\overset{\circ}{\mathbf{T}}$. We get

$$\dot{p}=-\frac{p}{\lambda^*}\operatorname{tr}\mathbf{D} \tag{3.34}$$

which is the rate formulation of the normal compression line with the slope λ^* in the $\ln(1+e):\ln p$ space. Positions of different NCLs in this space (and therefore the shape of the SOM surface) are controlled by the *pyknotropy* factor f_d, which in the considered model reads

$$f_d=\left(\frac{2p}{p_e^*}\right)^{\alpha} \tag{3.35}$$

with α being a constant calculated from the model parameters (see Appendix A) and p_e^* comes from (3.21). Factor f_d is constant along any line characterised by (3.34), which ensures consistency between evolution equation for f_d and (3.28) and thus implies that Eq. (3.28) describes SOM states.

Combining Eqs. (3.32) and (3.35) allows us to calculate the value of p_e^* at the SOM surface at any stress level $\mathbf{T}$ and consequently to find the shape of the SOM surface in the normalised $\mathbf{T}_n$ space:

$$p_e^*=-\frac{2}{3}\operatorname{tr}\mathbf{T}\|\boldsymbol{\mathcal{A}}^{-1}:\mathbf{N}\|^{1/\alpha} \tag{3.36}$$

The shape of the SOM surface in the normalised triaxial stress space, plotted for triaxial stress invariants $q=-(\mathrm{T}_a-\mathrm{T}_r)$ and p, is shown in Fig. 3.6 for material parameters given in Tab. 3.1.

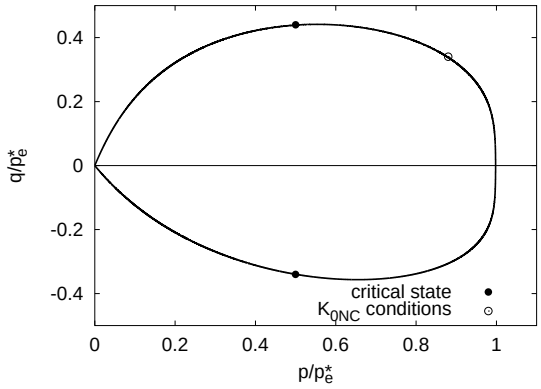

Figure 3.6: Swept-out-memory surface in the normalised triaxial stress space for the hypoplastic model [87] using London clay parameters (Tab. 3.1)

3.6 State boundary surface

In this section we discuss the difference between the swept-out-memory surface, defined in Sec. 3.5, and the state boundary surface. Without loss of generality we again study

response of the considered model in the normalised space $\mathbf{T}_n$. The state boundary surface is defined as an envelope of all admissible states of a soil element. In other words, no outer response in the normalised space $\mathbf{T}_n$ can be generated. Using the concept of response envelopes (Sec. 3.2), stress rate response envelope plotted in the normalised $\mathbf{T}_n$ space (normalised response envelope, NRE) for the states at the state boundary surface must not cross-sect the surface (i.e., must have a common tangent with the state boundary surface).

We first presume that the state boundary surface is equal to the swept-out-memory surface. A tangent to the normalised response envelope may then be found using a similar procedure to that applied in Sec. 3.4 for evaluation of bounding surface of *amorphous* hypoplastic models. Let γ_n be the norm of the normalised stress rate $\dot{\mathbf{T}}_n$ ($\gamma_n = \|\dot{\mathbf{T}}_n\|$) and $\mathbf{S}_n$ its direction ($\mathbf{S}_n = \dot{\mathbf{T}}_n/\|\dot{\mathbf{T}}_n\|$). Using the definition of the tensor $\boldsymbol{\mathcal{A}}$ (Eq. 3.29) and assuming, without loss of generality, $\|\mathbf{D}\| = 1$, Eq. (3.27) reads

$$p_e^* \gamma_n \mathbf{S}_n = \boldsymbol{\mathcal{A}} : \vec{\mathbf{D}} + f_d \mathbf{N} \tag{3.37}$$

or

$$p_e^* \gamma_n \mathbf{S}_n = \boldsymbol{\mathcal{A}} : (\vec{\mathbf{D}} + f_d \mathbf{B}_n) \tag{3.38}$$

with

$$\mathbf{B}_n = \boldsymbol{\mathcal{A}}^{-1} : \mathbf{N} \tag{3.39}$$

Thus (from (3.38))

$$\vec{\mathbf{D}} = p_e^* \gamma_n \boldsymbol{\mathcal{A}}^{-1} : \mathbf{S}_n - f_d \mathbf{B}_n \tag{3.40}$$

taking the norm of (3.40) we get

$$(p_e^*)^2 \gamma_n^2 \|\boldsymbol{\mathcal{A}}^{-1} : \mathbf{S}_n\|^2 - 2 p_e^* \gamma_n f_d \left(\boldsymbol{\mathcal{A}}^{-1} : \mathbf{S}_n\right) : \mathbf{B}_n + f_d^2 \|\mathbf{B}_n\|^2 - 1 = 0 \tag{3.41}$$

For the states at the SOM surface we have $f_d = \|\mathbf{B}_n\|^{-1}$ (3.32). Introducing this condition into (3.41) leads to

$$p_e^* \gamma_n^2 \|\boldsymbol{\mathcal{A}}^{-1} : \mathbf{S}_n\|^2 - 2\gamma_n \left(\boldsymbol{\mathcal{A}}^{-1} : \mathbf{S}_n\right) : \vec{\mathbf{D}}_{SOM} = 0 \tag{3.42}$$

where $\vec{\mathbf{D}}_{SOM}$ is the direction of the proportional stretching corresponding to the swept-out-memory conditions for a given state $\mathbf{T}_n$ (from 3.33):

$$\vec{\mathbf{D}}_{SOM} = -\frac{\mathbf{B}_n}{\|\mathbf{B}_n\|} \tag{3.43}$$

As γ_n represents the norm of $\dot{\mathbf{T}}_n$, it must be positive or null. Therefore, possible directions $\mathbf{S}_n$ must be confined in the half-space defined by

$$\left(\boldsymbol{\mathcal{A}}^{-1} : \mathbf{S}_n\right) : \vec{\mathbf{D}}_{SOM} > 0 \tag{3.44}$$

where the plane

$$\left(\boldsymbol{\mathcal{A}}^{-1} : \mathbf{S}_n\right) : \vec{\mathbf{D}}_{SOM} = 0 \tag{3.45}$$

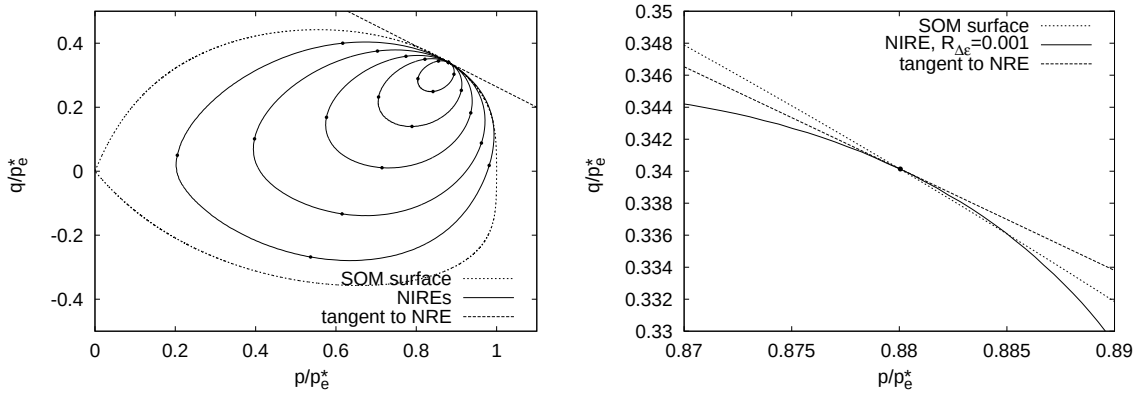

Figure 3.7: NIREs for the initial K_{0NC} conditions. (b) provides detail of (a). NIREs are plotted for $R_{\Delta\epsilon} = 0.001,\ 0.0025,\ 0.005,\ 0.01,\ 0.02$ (a) and $R_{\Delta\epsilon} = 0.001$ (b). Points at NIREs denote compression and extension for $\mathrm{D}_{00} = \mathrm{D}_{11} = \mathrm{D}_{22}$ and $\mathrm{tr}\,\mathbf{D} = \mathbf{0}$)

represents a tangent to the normalised response envelope.

Fig. 3.7a depicts the SOM surface, tangent to the normalised response envelope calculated according to Eq. (3.45) and incremental stress response envelopes (as defined in Sec. 3.2) plotted in the normalised space $\mathbf{T}_n$ (normalised incremental response envelope, NIRE) for different values of $R_{\Delta\epsilon}$. Apparently, the tangent to the normalised response envelope is nearly coincident with the tangent to the SOM surface. A detailed inspection in Fig. 3.7b, however, reveals that the tangent to the NRE is slightly inclined with respect to the tangent to the SOM surface and therefore proves that the state boundary surface, in general, does not coincide with the swept-out-memory surface. The difference between tangents to NRE and SOM surface is even more pronounced for initial states *dry of critical* (defined by $p/p_e^* < 0.5$ in the model considered) as shown in Fig. 3.8[3].

Therefore, similarly to the limit and bounding surfaces of *amorphous* hypoplastic models in the stress space, the state boundary surface is located slightly outside the swept-out-memory surface. Nevertheless, taking into account uncertainties in the experimental determination of the state boundary surface, we may consider the swept-out-memory surface as a sufficient approximation of the state boundary surface. For this reason we restrict our investigations in the next sections to the SOM surface.

Figures 3.7 and 3.8 also demonstrate the asymptotic property of the considered hypoplastic model, as for large $R_{\Delta\epsilon}$ the normalised incremental response envelopes converge towards the SOM surface. The model keeps this property also for the initial states outside the SOM surface (see Fig. 3.9). Therefore, we see that the fact that the model allows to surpass slightly the SOM surface (SBS is located slightly outside the SOM surface) does

[3]In Fig. 3.8 normalised incremental response envelopes are cross-sected by the tangent to normalised response envelopes calculated according to (3.45). This fact is to be expected, as, in general, a tangent to the NRE represents a tangent to the NIRE only for $R_{\Delta\epsilon} \to 0$.

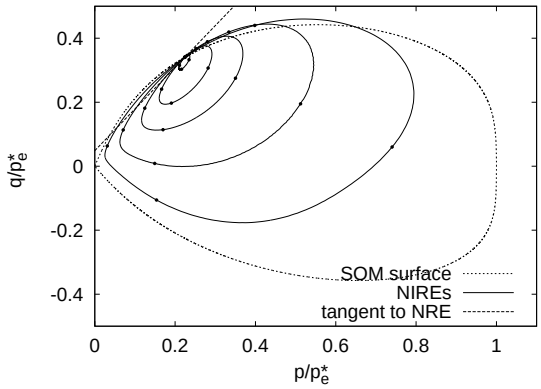

Figure 3.8: NIREs for the initial conditions with $p/p_e^* < 0.5$, plotted for $R_{\Delta\epsilon} = 0.001$, 0.005, 0.01, 0.02, 0.035.

not spoil its abilities to predict asymptotic states.

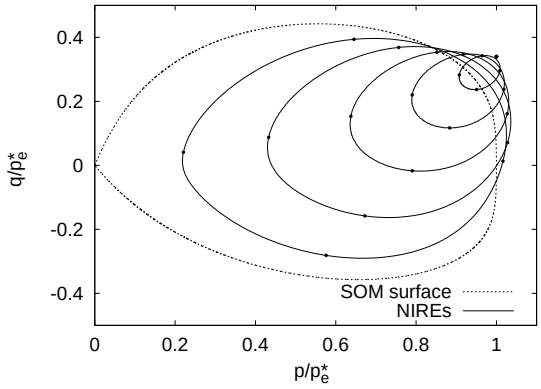

Figure 3.9: NIREs for the initial state outside the SOM surface. The initial state has been *imposed* and does not follow from a model prediction. NIREs are plotted for $R_{\Delta\epsilon} = 0.001, 0.0025, 0.005, 0.01, 0.02$.

3.7 Model performance

3.7.1 The influence of model parameters on the shape of the SOM surface

The SOM surface shown in Fig. 3.6 was found using parameters derived in [87] for London clay (with the exception of $\kappa^* = 0.014$ instead of $\kappa^* = 0.016$). They are summarised in Tab. 3.1.

As follows from the equations representing the SOM surface (Sec. 3.5), its shape is dependent on model parameters. A detailed study of Eq. (3.36) reveals that the parameters

Table 3.1: *Parameters for London clay used in the simulations*

φ_c [°]	λ^*	κ^*	N	r
22.6	0.11	0.014	1.375	0.4

N and λ^* do not independently influence the shape of the SOM surface (see comments further) and the influence of the parameter r is negligible (for its reasonable values). The shape of the SOM surface is controlled by the critical state friction angle φ_c and by the ratio $(\lambda^* - \kappa^*)/(\lambda^* + \kappa^*)$ appearing in the expression for the pyknotropy factor f_d, Eq. (3.58).

The influence of the parameter φ_c is shown in Fig. 3.10a. The value of φ_c was varied in the analyses, while other parameters (Tab. 3.1) were kept constant. In order to normalise the response for the variation in φ_c, the SOM surface is plotted in the space $q/(Mp_e^*)$:p/p_e^* (as suggested in [34]), where the quantity M is defined as:

$$\begin{cases} M = \dfrac{6\sin\varphi_c}{3-\sin\varphi_c} & \text{for triaxial compression} \\ M = \dfrac{6\sin\varphi_c}{3+\sin\varphi_c} & \text{for triaxial extension} \end{cases} \tag{3.46}$$

The influence of the ratio $(\lambda^* - \kappa^*)/(\lambda^* + \kappa^*)$ is demonstrated in Fig. 3.10b. The value of the parameter $\lambda^* = 0.11$ was kept constant, whereas the parameter κ^* was varied. The corresponding values of the ratio $(\lambda^* - \kappa^*)/(\lambda^* + \kappa^*)$ are also given in the figure.

Fig. 3.10 reveals that although the influence of the parameter φ_c and of the ratio $(\lambda^* - \kappa^*)/(\lambda^* + \kappa^*)$ on the shape of the SOM surface is significant, for reasonable values of the involved parameters the shape remains close to the one predicted by the Modified Cam clay model. Only for low values of the ratio $(\lambda^* - \kappa^*)/(\lambda^* + \kappa^*)$ (large ratio κ^*/λ^*, i.e. soft response in isotropic unloading), the SOM surface becomes non-convex in the vicinity of isotropic stress states[4].

3.7.2 K_0 normally compressed conditions

Finally, the equations for swept-out-memory conditions are applied in a study of the influence of model parameters on K_0 conditions in the normally compressed state (K_{0NC}), see Fig. 3.11. The parameter φ_c and the ratio $(\lambda^* - \kappa^*)/(\lambda^* + \kappa^*)$ were varied as in Sec. 3.7.1. Predictions of K_{0NC} by the hypoplastic model are compared with Jáky's [66] equation

$$K_{0NC} = 1 - \sin\varphi_c \tag{3.47}$$

As demonstrated for example in [101], Eq. (3.47) is suitable for fine-grained soils. Predic-

[4]The issue of convexity of a limit surface in the normalised plane is of relevance in the theory of plasticity, where the convexity of the yield surface is crucial in order to properly define loading/unloading conditions. In hypoplasticity, whether a non-convex SOM surface is acceptable or not can be judged only with reference to available experimental data.

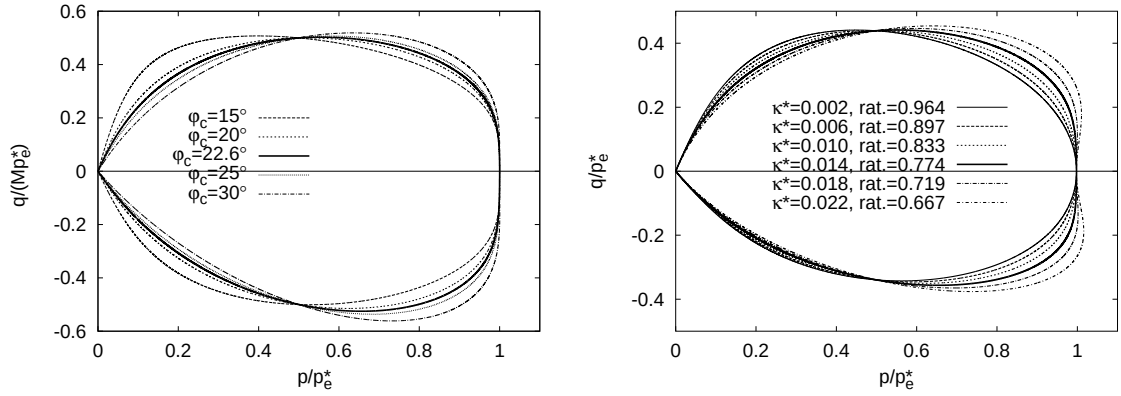

Figure 3.10: The influence of (a) the parameter φ_c and (b) of the ratio $(\lambda^* - \kappa^*)/(\lambda^* + \kappa^*)$ on the shape of the SOM surface

tions by the Modified Cam clay model [117] are also included in Fig. 3.11. In the calculation with the Modified Cam clay model, the influence of elastic strain increments, which are at the yield surface negligible compared to the plastic strain increments, is omitted. Consequently,

$$K_{0NC} = \frac{3 - \eta}{3 + 2\eta} \tag{3.48}$$

for the Modified Cam clay model, with

$$\eta = \frac{\sqrt{9 + 4M^2} - 3}{2} \quad \text{and} \quad M = \frac{6 \sin \varphi_c}{3 - \sin \varphi_c} \tag{3.49}$$

It can be seen in Fig. 3.11 that the considered hypoplastic model predicts correctly the trend of decreasing K_{0NC} with increasing φ_c. Although the hypoplastic model overpredicts K_{0NC} as compared to Eq. (3.47), its predictions are still significantly closer to Eq. (3.47) than the predictions by the Modified Cam clay model.

Further discussion on the direction of stretching $\vec{\mathbf{D}}$ at SOM conditions with respect to the corresponding $\vec{\mathbf{T}}$, as well as on the SOM conditions predicted by different *endomorphous* hypoplastic models, may be found in [96].

3.8 Concluding remarks

The present paper studied if the hypoplastic model for clays [87] predicts, as a by–product of the constitutive formulation, the existence of the state boundary surface, which may be seen as a key characteristics of the behaviour of fine–grained soils.

It has been shown that for the given model it is possible to derive an explicit formulation for the so-called swept-out-memory surface, which may be defined as an envelope of asymptotic

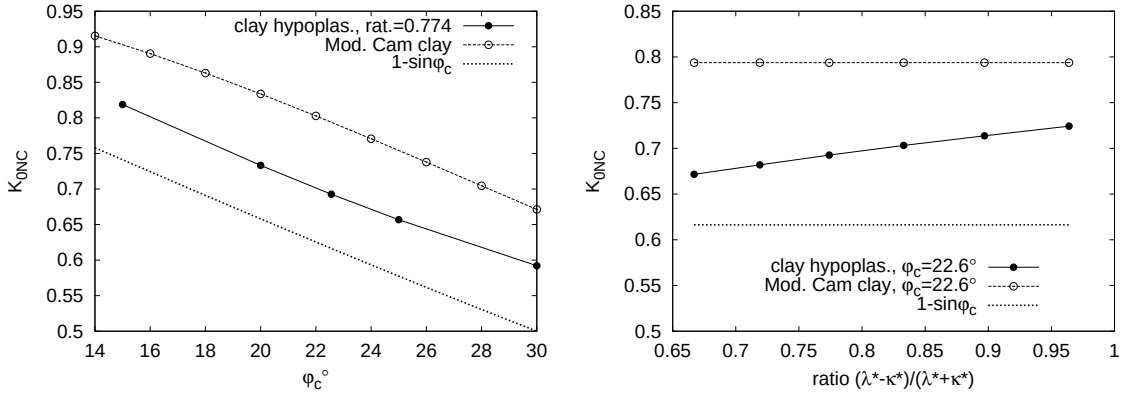

(a) (b)

Figure 3.11: K_{0NC} conditions predicted by the considered model, compared to Jáky's [66] formula and predictions by the Modified Cam clay model [117].

(swept-out-memory) states in the stress-void ratio space. The concept of the normalised incremental stress response envelopes and the derivation of the tangent to the normalised rate response envelopes was subsequently used to demonstrate that the swept-out-memory surface is a close approximation of the state boundary surface, although, in general, they do not coincide. It has been shown that there is a direct parallel between the swept-out-memory and the state boundary surfaces defined in the stress-void ratio space for *endomorphous* hypoplastic models, and limit and bounding surfaces defined in the stress space for *amorphous* hypoplastic models.

Finally the influence of the constitutive parameters on the shape of the swept-out-memory surface has been studied by means of a parametric study. For parameters suitable for fine-grained soils, the considered hypoplastic model predicts a swept-out-memory surface of a similar shape to the state boundary surface of the Modified Cam clay model. However, the K_0 values at normally compressed states are better predicted by the hypoplastic model than by the Modified Cam clay model.

A study of the shape of the SOM surface (Sec. 3.7) and invertibility condition of $\boldsymbol{\mathcal{A}}$ (Appendix B) reveal limitation of the hypoplastic model for clays, which does not perform correctly for soils very soft in isotropic unloading. As a *very rough* guide, condition $\kappa^* < \lambda^*/4$ should be satisfied when using model [87]. More precise investigation requires to plot the SOM surface and to ensure that the condition (3.66) is not satisfied.

Appendix A

The mathematical structure of the hypoplastic model for clays is discussed in detail in [87]. The constitutive equation in rate form reads:

$$\mathring{\mathbf{T}} = f_s \boldsymbol{\mathcal{L}} : \mathbf{D} + f_s f_d \mathbf{N} \|\mathbf{D}\| \tag{3.50}$$

where:

$$\boldsymbol{\mathcal{L}} = 3\left(c_1\boldsymbol{\mathcal{I}} + c_2 a^2 \hat{\mathbf{T}}\otimes\hat{\mathbf{T}}\right) \qquad \mathbf{N} = \boldsymbol{\mathcal{L}} : \left(-Y\frac{\mathbf{m}}{\|\mathbf{m}\|}\right) \qquad \hat{\mathbf{T}} := \frac{\mathbf{T}}{\operatorname{tr}\mathbf{T}} \tag{3.51}$$

$\mathbf{1}$ is the second–order identity tensor and $\boldsymbol{\mathcal{I}}$ is the fourth–order identity tensor, with components:

$$(\mathcal{I})_{ijkl} := \frac{1}{2}\left(1_{ik}1_{jl} + 1_{il}1_{jk}\right) \tag{3.52}$$

In eq. (3.50), the functions $f_s(\operatorname{tr}\mathbf{T})$ (*barotropy* factor) and $f_d(\operatorname{tr}\mathbf{T}, e)$ (*pyknotropy* factor) are given by:

$$f_s = -\frac{\operatorname{tr}\mathbf{T}}{\lambda^*}\left(3 + a^2 - 2^\alpha a\sqrt{3}\right)^{-1} \qquad f_d = \left[-\frac{2\operatorname{tr}\mathbf{T}}{3p_r}\exp\left(\frac{\ln(1+e) - N}{\lambda^*}\right)\right]^\alpha \tag{3.53}$$

where p_r is the reference stress 1 kPa. The scalar function Y and the second–order tensor $\mathbf{m}$ appearing in Eq. (3.51) are given, respectively, by:

$$Y = \left(\frac{\sqrt{3}a}{3+a^2} - 1\right)\frac{(I_1 I_2 + 9I_3)\left(1 - \sin^2\varphi_c\right)}{8I_3\sin^2\varphi_c} + \frac{\sqrt{3}a}{3+a^2} \tag{3.54}$$

in which:

$$I_1 := \operatorname{tr}\mathbf{T} \qquad I_2 := \frac{1}{2}\left[\mathbf{T}:\mathbf{T} - (I_1)^2\right] \qquad I_3 := \det\mathbf{T}$$

and

$$\mathbf{m} = -\frac{a}{F}\left[\hat{\mathbf{T}} + \hat{\mathbf{T}}^* - \frac{\hat{\mathbf{T}}}{3}\left(\frac{6\ \hat{\mathbf{T}}:\hat{\mathbf{T}} - 1}{(F/a)^2 + \hat{\mathbf{T}}:\hat{\mathbf{T}}}\right)\right] \tag{3.55}$$

in which:

$$\hat{\mathbf{T}}^* = \hat{\mathbf{T}} - \frac{\mathbf{1}}{3} \qquad F = \sqrt{\frac{1}{8}\tan^2\psi + \frac{2 - \tan^2\psi}{2 + \sqrt{2}\tan\psi\cos 3\theta}} - \frac{1}{2\sqrt{2}}\tan\psi \tag{3.56}$$

$$\tan\psi = \sqrt{3}\|\hat{\mathbf{T}}^*\| \qquad \cos 3\theta = -\sqrt{6}\frac{\operatorname{tr}\left(\hat{\mathbf{T}}^*\cdot\hat{\mathbf{T}}^*\cdot\hat{\mathbf{T}}^*\right)}{\left(\hat{\mathbf{T}}^*:\hat{\mathbf{T}}^*\right)^{3/2}} \tag{3.57}$$

Finally, the scalars a, α, c_1 and c_2 appearing in eqs. (3.51)–(3.55), are given as functions of the material parameters φ_c, λ^*, κ^* and r by the following relations:

$$a = \frac{\sqrt{3}\left(3 - \sin\varphi_c\right)}{2\sqrt{2}\sin\varphi_c} \qquad \alpha = \frac{1}{\ln 2}\ln\left[\frac{\lambda^* - \kappa^*}{\lambda^* + \kappa^*}\left(\frac{3+a^2}{a\sqrt{3}}\right)\right] \tag{3.58}$$

$$c_1 = \frac{2\left(3 + a^2 - 2^\alpha a\sqrt{3}\right)}{9r} \qquad c_2 = 1 + (1 - c_1)\frac{3}{a^2} \tag{3.59}$$

The model requires five constitutive parameters, namely φ_c, λ^*, κ^*, N and r, state is characterised by the Cauchy stress $\mathbf{T}$ and void ratio e.

Appendix B

In this Appendix invertibility of the tensor $\boldsymbol{\mathcal{A}}$ is discussed. Eq. (3.29) can be written with help of Eqs. (3.51) and (3.53) as

$$\begin{aligned}\boldsymbol{\mathcal{A}} &= -\frac{\mathrm{tr}\mathbf{T}}{\lambda^*}\left[f_s^* 3c_1\boldsymbol{\mathcal{I}} - \hat{\mathbf{T}}\otimes\mathbf{1} + f_s^* 3c_2 a^2\hat{\mathbf{T}}\otimes\hat{\mathbf{T}}\right] \\ &= -\frac{\mathrm{tr}\mathbf{T}}{\lambda^*}\left[f_s^* 3c_1\boldsymbol{\mathcal{I}} - \hat{\mathbf{T}}\otimes\mathbf{1} + f_s^*\left[3a^2+9(1-c_1)\right]\hat{\mathbf{T}}\otimes\hat{\mathbf{T}}\right] \end{aligned} \tag{3.60}$$

with

$$f_s^* = \left(3 + a^2 - 2^\alpha a\sqrt{3}\right)^{-1} > 0 \tag{3.61}$$

for any realistic values of a and α. Eq. (3.60) can be also written as

$$\boldsymbol{\mathcal{A}} = -\frac{\mathrm{tr}\mathbf{T}}{\lambda^*}\left[C_1\boldsymbol{\mathcal{I}} - \hat{\mathbf{T}}\otimes\mathbf{1} + C_2\hat{\mathbf{T}}\otimes\hat{\mathbf{T}}\right] \tag{3.62}$$

with C_1, C_2 being scalar constants calculated from model parameters.

$$C_1 = \frac{2}{3r} \quad \text{and} \quad C_2 = \frac{2a^2 + 6(1-c_1)}{3rc_1} \tag{3.63}$$

To study the invertibility condition of $\boldsymbol{\mathcal{A}}$, it is sufficient to consider tensor $\boldsymbol{\mathcal{A}}^* = -\lambda^*\boldsymbol{\mathcal{A}}/\mathrm{tr}\mathbf{T}$ (only $\mathrm{tr}\mathbf{T} < 0$ is allowed). In the principal stress components the determinant of $\boldsymbol{\mathcal{A}}^*$ reads

$$\det\boldsymbol{\mathcal{A}}^* = C_1^3 - C_1^2\left[(\hat{T}_1 + \hat{T}_2 + \hat{T}_3) - C_2(\hat{T}_1^2 + \hat{T}_2^2 + \hat{T}_3^2)\right] \tag{3.64}$$

Inversion of the tensor $\boldsymbol{\mathcal{A}}$ is possible if $\det\boldsymbol{\mathcal{A}}^* \neq 0$. Because $C_1 \neq 0$ and $\hat{T}_1 + \hat{T}_2 + \hat{T}_3 = 1$, this condition reads

$$C_1 - 1 + C_2(\hat{T}_1^2 + \hat{T}_2^2 + \hat{T}_3^2) \neq 0 \tag{3.65}$$

Taking into account definitions of scalars C_1 and C_2 (3.63) and the fact that for compressive stresses $1/3 < (\hat{T}_1^2 + \hat{T}_2^2 + \hat{T}_3^2) < 1$, we find that the invertibility of $\boldsymbol{\mathcal{A}}$ is *not* guaranteed if

$$\frac{1}{3}\left[\frac{2a^2 + 6(1-c_1)}{c_1}\right] < (3r-2) < \frac{2a^2 + 6(1-c_1)}{c_1} \tag{3.66}$$

A detailed study of the condition (3.66) reveals that for reasonable values of material parameters the tensor $\boldsymbol{\mathcal{A}}$ is invertible. For example for London clay parameters (Tab. 3.1) the condition (3.66) reads $3.31 < -0.8 < 9.94$. The invertibility of $\boldsymbol{\mathcal{A}}$ may not be guaranteed for unrealistically low values of the ratio $(\lambda^* - \kappa^*)/(\lambda^* + \kappa^*)$.

Chapter 4

Directional response of a reconstituted fine-grained soil: Performance of different constitutive models

4.1 Introduction

The directional character of the mechanical response of fine-grained soils, i.e., its dependence on the loading direction, has been the subject of several studies throughout the last decades, including both experimental and theoretical investigations. On the experimental side, some pioneering contributions were provided in the early seventies, see e.g., References [81, 147]. Notable examples of more recent contributions can be found in the works of Graham *et al.* [48], Atkinson *et al.* [6], Smith *et al.* [123] and Callisto and Calabresi [20]. On the theoretical side, a major improvement of classical plasticity as applied to clays has been provided by the introduction of the so-called nested-surface kinematic hardening theories of plasticity, originating from the works of Prevost [113], Mróz *et al.* [102] and Hashiguchi [57]. These latter studies were essentially motivated by the need of improving available design approaches for those practical applications where soil is subject to cyclic loading conditions, e.g., earthquakes, offshore engineering, etc.

Later studies on shear banding in soils as a bifurcation problem [121, 115] showed the need to take into account the *incrementally non-linear* character of the material response – i.e., a dependence of soil tangent stiffness on the strain rate direction, see, e.g., References [39, 132] – and motivated the development of a class of constitutive theories which depart from the framework of plasticity and rather can be seen as a generalization of Truesdell theory of hypoelasticity [137]. A distinctive feature of this approach is the absence of any kinematic decomposition of strain rates into reversible and irreversible parts. An important example in this respect is provided by the theory of hypoplasticity, as defined by Kolymbas

[77], see also Reference [80].

More generally, it turns out that a proper description of soil behavior as a function of loading direction not only is useful for modelling the response of geotechnical structures to cyclic loading or for analyzing localization phenomena, but it is also a key ingredient in the analysis of any geotechnical structure where different zones of soil experience widely different stress-paths, both in size and direction, e.g., deep excavations and tunnels. This has been demonstrated in a number of practical applications, see, e.g. References [124, 146, 45, 140].

The objective of this work is to assess, both qualitatively and quantitatively, the performance of some advanced constitutive models in reproducing the stress-strain behavior of a soft, normally consolidated reconstituted clay as observed in laboratory tests performed along a number of different stress-paths originating from a common initial state. Two particular classes of inelastic models have been selected for the comparison. On the one hand, the three-surface kinematic hardening model proposed by Stallebrass [125]; Stallebrass and Taylor [127] has been chosen as the representative candidate of modern soil plasticity approaches. On the other hand, three different versions of hypoplasticity have been considered, which differ from each other in terms of history-related state variables, namely the CLoE model [29], the clay K-hypoplastic model recently proposed by Mašín [87], and a modified version of this last model, embedding the concept of intergranular strain [108] as additional internal state variable. Finally, the classical critical-state Modified Cam-Clay model with associative flow rule [117] has been also considered as a reference.

The companion paper by Costanzo *et al.* [31] presents the results of a large program of stress-probing tests on normally consolidated, reconstituted Beaucaire Marl. These results are used herein both for the calibration of the different models, and as a benchmark for the evaluation of the models performance. The results obtained from standard isotropic or triaxial compression and extension tests, starting from an isotropic state, were used for the calibration of the different models. The assessment of models' performance was carried out with reference to a different set of data, obtained from axisymmetric stress-probing tests starting from an anisotropic initial stress state.

The outline of the paper is as follows. The details of the experimental program are shortly recalled in Sect. 4.2. A summary of the main features of the constitutive models considered is provided in Sect. 4.3. The procedures adopted for the calibration of the different models are thoroughly discussed in Sect. 4.4, before presenting the comparison between predicted and observed directional response, in Sect. 4.5, where a quantitative assessment of the performance of the models is attempted by introducing suitable scalar measures of the prediction error. Finally, some concluding remarks are drawn and perspectives for further research are provided in Sect. 4.6.

In the following, the usual sign convention of soil mechanics (compression positive) is adopted throughout. In line with Terzaghi's principle of effective stress, all stresses are *effective* stresses, unless otherwise stated. Both direct and index notation will be used to represent tensor quantities, according to convenience. Calligraphic letters are used to represent fourth-order tensors and their components (e.g., $\boldsymbol{\mathcal{L}}$ and $\mathcal{L}_{ijkl}$). In the representation

of stress and strain states, use is sometimes made of the following invariant quantities: $p := (1/3)\ \mathrm{tr}\,\boldsymbol{\sigma}$ (mean stress); $q := \sqrt{(3/2)}\ \|\mathrm{dev}(\boldsymbol{\sigma})\|$ (deviatoric stress); $\epsilon_v := \mathrm{tr}\,\boldsymbol{\epsilon}$ (volumetric strain); and $\epsilon_s := \sqrt{(2/3)}\ \|\mathrm{dev}(\boldsymbol{\epsilon})\|$ (deviatoric stress).

4.2 Experimental data from stress-probing tests

The material tested is a low plasticity silty clay, with a liquid limit of 38%, and a plasticity index of 17%. The stress-probing tests were performed on reconstituted material, consolidated in a large consolidometer up to a nominal vertical effective stress of 75 kPa. Full details of the experimental procedures employed in the testing program are given by Costanzo *et al.* [31]. Overall, the measurement system is capable of resolving strains of approximately 0.0005.

The testing program consisted of a large number of drained stress probes, starting from a common initial stress state and pointing in different directions in the triaxial plane. Two different initial stress states were considered: the first one (state A) is located on the isotropic axis at $p = 150$ kPa; the second one (state B) is characterized by the same mean stress as state A and a deviator stress $q = 60$ kPa. Both states A and B were reached upon stress-controlled consolidation along a constant q/p path ($q/p = 0$ for state A, $q/p = 0.4$ for state B). Each stress probe from an initial state $(\sigma_{a0}, \sigma_{r0})$ is described by the following parametric equations:

$$\Delta\sigma_a := \sigma_a - \sigma_{a0} = R_\sigma \sin\alpha_\sigma \tag{4.1}$$

$$\sqrt{2}\,\Delta\sigma_r := \sqrt{2}\,\sigma_r - \sigma_{r0} = R_\sigma \cos\alpha_\sigma \tag{4.2}$$

where $R_\sigma = \|\Delta\boldsymbol{\sigma}\|$ denotes the norm of the stress increment, and α_σ represents its direction in the Rendulic plane of stress increments ($\Delta\sigma_a : \sqrt{2}\,\Delta\sigma_r$, see Fig. 4.1a). Each stress probe was continued up to a R_σ value corresponding either to a "failure" state, or to a prescribed maximum value of the cell pressure. The loading directions α_σ prescribed for each probe are listed in Tab. 4.1. Note that for each initial state the testing program included as particular cases conventional triaxial, constant p and isotropic, compression and extension paths. The stress probe direction in the $q : p$ plane, α_σ^{pq}, calculated from the stress invariant increments $\Delta\,p$ and $\Delta\,q$ as:

$$\Delta\,p = \frac{1}{3}\,(\Delta\sigma_a + 2\Delta\sigma_r) \qquad \Delta\,q = \Delta\sigma_a - \Delta\sigma_r \tag{4.3}$$

$$\sin\alpha_\sigma^{pq} = \frac{\Delta\,q}{\sqrt{(\Delta\,p)^2 + (\Delta\,q)^2}} \qquad \cos\alpha_\sigma^{pq} = \frac{\Delta\,p}{\sqrt{(\Delta\,p)^2 + (\Delta\,q)^2}} \tag{4.4}$$

is also reported in the same table. A picture of the stress paths originating from initial state B in the $q : p$ plane is shown in Fig. 4.2.

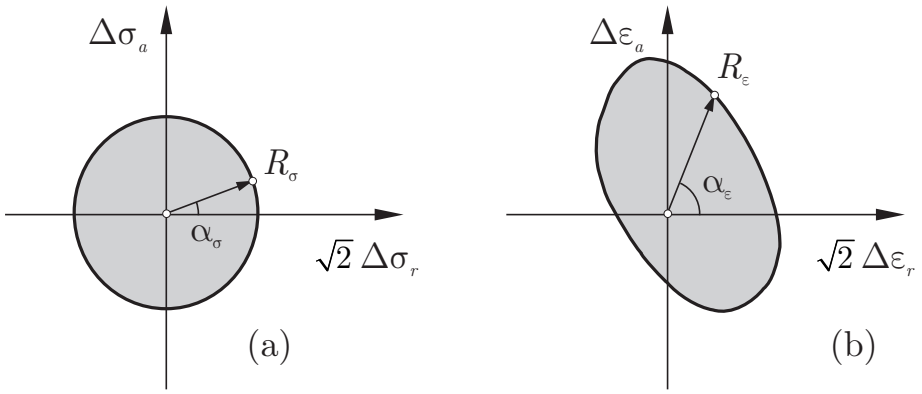

Figure 4.1: Response envelope concept: a) input stress probes; b) output strain envelope.

Test #	Initial state	α_σ (deg.)	α_σ^{pq} (deg.)	Test #	Initial state	α_σ (deg.)	α_σ^{pq} (deg.)
Tx124	A	0	303.69	Tx118	B	0	303.69
Tx128	A	35	0.00	Tx115	B	35	0.00
—	—	—	—	Tx130	B	46	21.91
Tx121	A	90	71.57	Tx132	B	90	71.57
Tx126	A	126	90.00	Tx119	B	126	90.00
—	—	—	—	Tx116	B	154	104.49
Tx123	A	180	123.69	—	—	—	—
Tx127	A	215	180.00	Tx134	B	215	180.00
—	—	—	—	Tx129	B	226	201.91
Tx122	A	270	251.57	Tx117	B	270	251.57
Tx125	A	305	270.00	Tx113	B	305	270.00

Table 4.1: Details of the experimental stress-probing program, after Costanzo *et al.* [31].

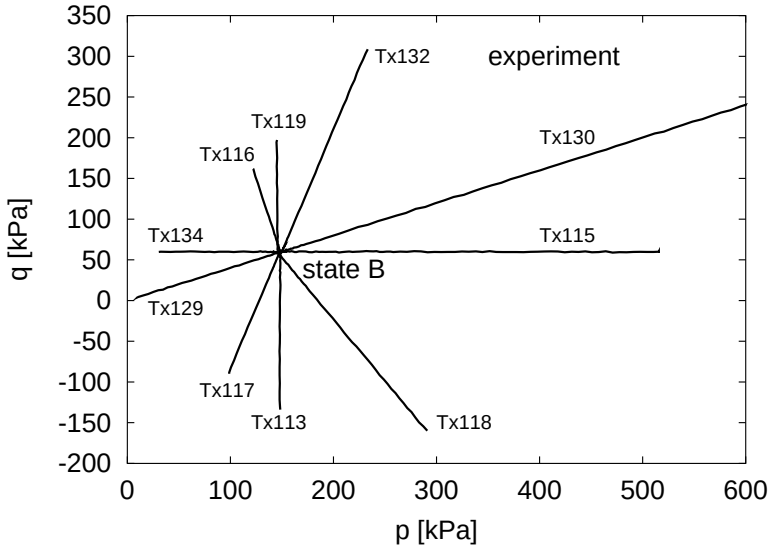

Figure 4.2: Experimental stress-probes performed from state B

4.3 Constitutive models considered

4.3.1 The 3–SKH model

The 3–SKH model is an advanced example of the kinematic hardening plasticity models originating from the pioneering work of Prevost [113] and Mróz *et al.* [102]. The model is based on the principles of critical state soil mechanics and represents an evolution of the classical Modified Cam-Clay model [117], and the two-surface kinematic hardening model proposed by Al Tabaa and Wood [1]. The main feature of the 3–SKH model consists in the introduction of an additional kinematic *history surface* - as defined in Reference [125], see Fig. 4.3 - motivated by experimental findings about the influence of the recent stress history on soil behavior [6]. While kinematic hardening models are capable of dealing with cyclic loading conditions and, more generally, of reproducing the observed non-linear behavior inside the state boundary surface, 3–SKH model provides significantly improved predictions in the small strain range, see [127]. Successful applications of this model at both the single-element level and in the analysis of typical boundary value problems are reported, *e.g.*, by Grant *et al.* [49], Ingram [65], Baudet [7] and Mašín [86]. The general formulation of the 3–SKH model is given in Appendix B.

4.3.2 The CLoE hypoplastic model

The origins of CLoE hypoplasticity — where the acronym CLoE stands for *Consistance et Localisation Explicite* — can be traced back to the pioneering work of Chambon and Desrues on strain localization in incrementally non-linear materials [28, 43]. The

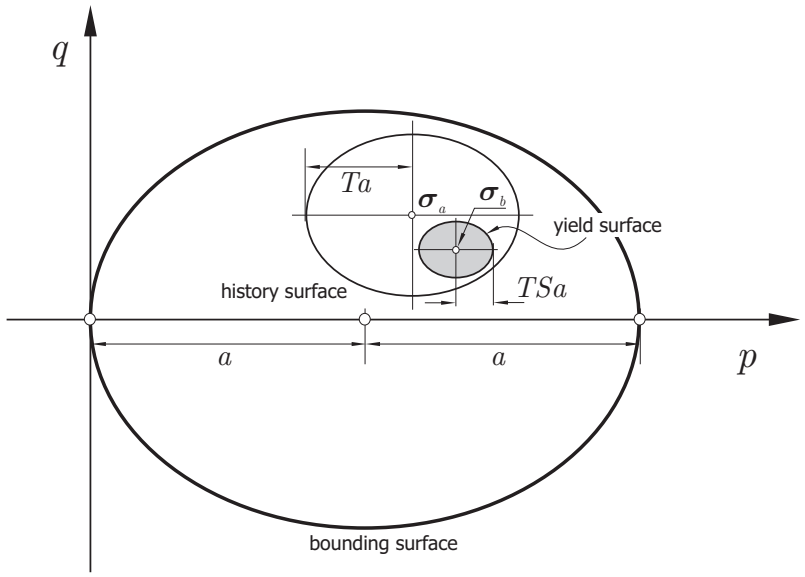

Figure 4.3: Sketch of the characteristic surfaces of the 3–SKH model

constitutive equation is given, in rate-form, by:

$$\dot{\boldsymbol{\sigma}} = \boldsymbol{\mathcal{A}}(\boldsymbol{\sigma})\dot{\boldsymbol{\epsilon}} + \boldsymbol{b}(\boldsymbol{\sigma})\ \|\dot{\boldsymbol{\epsilon}}\| \tag{4.5}$$

see Reference [29]. The first term on the right-hand side yields an incrementally linear response, while the second accounts for incremental non-linearity via a linear dependence on the norm of the strain rate tensor. To keep the formulation as simple as possible, the set of state variables for the material is limited to the Cauchy stress tensor.

An essential feature of CLoE model is that the constitutive response in stress space is bounded by an explicitly assumed limit surface, separating admissible from impossible stress states. The particular form adopted for the limit surface is given by the equation proposed by van Eekelen [138], which allows for different values of friction angle in compression and extension. When the stress state reaches the limit surface, it is explicitly assumed that no outer stress rate response can be generated by any applied strain rate (*consistency condition*).

The two constitutive tensors $\boldsymbol{\mathcal{A}}$ and $\boldsymbol{b}$ appearing in (4.5) are homogeneous functions of degree one of the stress tensor, for which no explicit expression is assumed. Rather, $\boldsymbol{\mathcal{A}}$ and $\boldsymbol{b}$ are obtained via an interpolation procedure based on the assigned material responses at some suitably defined image points, located along special loading paths (*basic paths*). These are selected among those stress-paths that are experimentally accessible by means of conventional laboratory tests. The consistency condition at limit states implies a series of additional requirements for the components of $\boldsymbol{\mathcal{A}}$ and $\boldsymbol{b}$, see Reference [29]. Details on the basic paths and on the constitutive functions employed to represent the stress-strain behavior of the soil along them will be given when detailing the calibration procedure.

4.3.3 The K-hypoplastic model for clays

The K-hypoplastic model considered in the present study has been recently developed by Mašín [87] with the specific aim of describing the behavior of fine-grained soils. The model combines the mathematical structure of K-hypoplastic models – see *e.g.*, Reference [153] and references therein – with key concepts of critical state soil mechanics [122] through the notion of generalised hypoplasticity, as defined by Niemunis [106]. In fact, the model can be considered an evolution of both von Wolffersdorff [141] model for sands, and the more recent Herle and Kolymbas [61] model for soils with low friction angles

The constitutive equation is given, in rate-form, by:

$$\dot{\boldsymbol{\sigma}} = f_s \boldsymbol{\mathcal{L}} : \dot{\boldsymbol{\epsilon}} + f_s f_d \boldsymbol{N} \left\| \dot{\boldsymbol{\epsilon}} \right\| \tag{4.6}$$

Explicit, closed form expressions for the two tensors $\boldsymbol{\mathcal{L}}(\boldsymbol{\sigma})$ and $\boldsymbol{N}(\boldsymbol{\sigma})$ and for the scalar functions $f_s(p)$ and $f_d(p, e)$ are provided in Appendix B. It must be noted that, although Eq. (4.6) and (4.5) appear quite similar, a major difference of K-hypoplasticity as compared to CLoE stems from including void ratio in the set of state variables for the material through the so-called *pyknotropy factor* f_d [53]. It is precisely this ingredient which allows the critical state concept to be incorporated in the constitutive equation. A more general comparison between the two frameworks of CLoE- and K-hypoplasticity can be found in Reference [133].

4.3.4 The K-hypoplastic model for clays with intergranular strain

The K-hypoplastic model discussed in the previous section is capable of predicting the behavior of fine-grained soils upon monotonic loading at medium to large strain levels. In order to prevent excessive ratcheting upon cyclic loading and to improve model performance in the small-strain range, its mathematical formulation has been enhanced by the intergranular strain concept [108].

The mathematical formulation of this enhanced version of the K-hypoplastic model for clays is given by:

$$\dot{\boldsymbol{\sigma}} = \boldsymbol{\mathcal{M}} \left(\boldsymbol{\sigma}, e, \boldsymbol{\delta}, \boldsymbol{\eta} \right) : \dot{\boldsymbol{\epsilon}} \tag{4.7}$$

where $\boldsymbol{\mathcal{M}}$ is the fourth-order tangent stiffness tensor of the material, $\boldsymbol{\eta} := \dot{\boldsymbol{\epsilon}} / \left\| \dot{\boldsymbol{\epsilon}} \right\|$ denotes the strain rate direction, and the additional state variable $\boldsymbol{\delta}$ is a symmetric second order tensor called *intergranular strain*. Full details of the mathematical structure of the model are provided in appendix B.

In this formulation, the total strain can be thought of as the sum of a component related to the deformation of interface layers at integranular contacts, quantified by $\boldsymbol{\delta}$, and a component related to the rearrangement of the soil skeleton. For reverse loading conditions ($\boldsymbol{\eta} : \hat{\boldsymbol{\delta}} < 0$, where $\hat{\boldsymbol{\delta}}$ is defined in Appendix B) and neutral loading conditions ($\boldsymbol{\eta} : \hat{\boldsymbol{\delta}} = 0$), the observed overall strain is related only to the deformation of the intergranular interface layer and the soil behaviour is hypoelastic, whereas in continued loading conditions ($\boldsymbol{\eta} : \hat{\boldsymbol{\delta}} > 0$) the observed overall response is also affected by particle rearrangement in the soil skeleton.

From a mathematical standpoint, the response of the model is determined by interpolating between the following three special cases:

$$\dot{\boldsymbol{\sigma}} = m_R f_s \boldsymbol{\mathcal{L}} : \dot{\boldsymbol{\epsilon}} \qquad (\boldsymbol{\eta} : \hat{\boldsymbol{\delta}} = -1 \ \wedge \ \boldsymbol{\delta} = 0) \tag{4.8}$$

$$\dot{\boldsymbol{\sigma}} = m_T f_s \boldsymbol{\mathcal{L}} : \dot{\boldsymbol{\epsilon}} \qquad (\boldsymbol{\eta} : \hat{\boldsymbol{\delta}} = 0) \tag{4.9}$$

$$\dot{\boldsymbol{\sigma}} = f_s \boldsymbol{\mathcal{L}} : \dot{\boldsymbol{\epsilon}} + f_s f_d \boldsymbol{N} \, \|\dot{\boldsymbol{\epsilon}}\| \qquad (\boldsymbol{\eta} : \hat{\boldsymbol{\delta}} = 1) \tag{4.10}$$

the last case corresponding to the so-called *swept-out-memory* conditions [55]. The quantities m_R and m_T appearing in Eqs. 4.8 and 4.9 are material constants. The particular structure adopted for the constitutive tensor $\boldsymbol{\mathcal{L}}$ [87] should allow, in principle, to get a good performance in both the very small and large strain ranges.

4.4 Model calibration

When comparing the performance of different constitutive models in predicting the observed directional response of the material, particular care must be taken in the proper selection of the procedure adopted for their calibration. In the present case, this task is somewhat made easier by the fact that all the constitutive models discussed in the previous section, with the only exception of the CLoE hypoplastic model, incorporate the basic principles of Critical State Soil Mechanics, and thus some of the material constants share the same physical meaning.

In order to separate the data used for the calibration of the five models considered and the data used for the evaluation of their performance, the material constants of each model have been determined from the results of the stress probes starting from the isotropic initial state A. This is also consistent with the procedure typically used in practical applications, where most of the experimental data provided by the site investigation refer to isotropically consolidated, drained or undrained triaxial tests.

For some of the constitutive models considered, the available data from stress probes at point A do not provide enough information to calibrate all the relevant constants. This is the case, for example, of the material parameters controlling the response of the 3–SKH or K-hypoplastic models upon load reversal in the very small strain range. In such cases, the choice has been made to evaluate such material constants based on the experience gathered in previous experimental investigations on similar soils. Although such a choice necessarily introduces a certain degree of subjectivity in the comparative evaluation of the model responses, it can still be considered acceptable for our purposes, considering that the typical range of variation of such parameters for different soils is relatively limited, and the model response is not very sensitive to their variation, see *e.g.*, References [108, 125, 65, 30, 86].

It is important to note that, although the initial conditions of all the specimen belonging to a single stress probing "rosette" were nominally identical, some small differences in their initial effective stress and void ratio have been observed for both initial states A and B. In all the simulations discussed in this and in the next section, the average values reported in Tab. 4.2 have been assumed.

	p_0 (kPa)	q_0 (kPa)	e_0 (–)
State A	147.3	0.0	0.746
State B	148.4	60.0	0.752

Table 4.2: Initial conditions assumed for the two sets of stress-probing tests

4.4.1 Modified Cam-Clay model

In the Modified Cam-Clay model, the parameters N, and λ provide the position and the slope of the isotropic virgin compression line in the $(1+e)$:$\ln p$ plane, while the constant κ represents the slope of isotropic unloading/reloading lines in the same plane. Those constants have been determined using the results of the isotropic compression and extension probes, Tx128 and Tx127, as shown in Fig. 4.4a.

The value of the friction angle at critical state, φ_c, has been determined from the results of all the stress probes leading the material to failure (Tx121–Tx126). In Fig. 4.4b, these results are plotted in terms of mobilized friction angle

$$\varphi_{\text{mob}} := \sin^{-1}\left\{\frac{\sigma_1 - \sigma_3}{\sigma_1 + \sigma_3}\right\}$$

as a function of the deviatoric strain norm $|\epsilon_s|$. From the figure it is apparent that critical state conditions are attained at approximately the same friction angle in all the probes considered. From the results shown in the figure, a value of $\varphi_c = 33°$ has been selected. The critical state stress ratio in triaxial compression, M, can be easily determined from φ_c by considering that

$$M = \frac{6\sin\varphi_c}{3 - \sin\varphi_c}$$

The elastic shear modulus G was evaluated by trial and error, starting from the results of the $p = $ const. compression probe (Tx126), as shown in Fig. 4.4c. From the results shown in the figure, a value of $G = 5$ MPa was adopted. The complete set of parameters for the Modified Cam-Clay model is summarized in Tab. 4.3.

N (–)	λ (–)	κ (–)	M (–)	G (MPa)
2.245	0.097	0.017	1.33	5.0

Table 4.3: Parameters of the Modified Cam-Clay model.

As for the initial conditions, it is worth noting that, due to the creep strains accumulated before the stress probing, the average e_0 value assumed for the specimens (reported in Tab. 4.2) is slightly lower than the void ratio on the virgin compression line calculated

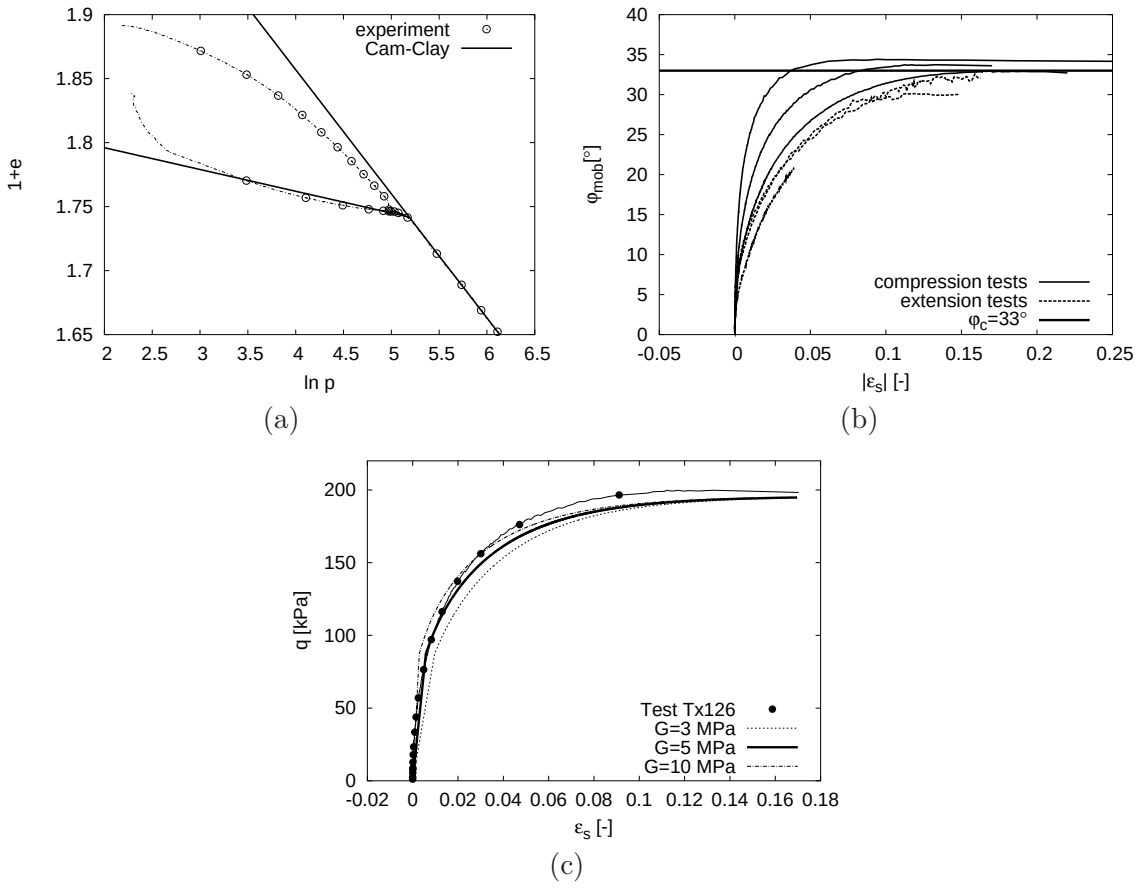

Figure 4.4: Calibration of the Modified Cam-Clay model: a) determination of parameters N, λ and κ from isotropic compression and extension probes; b) determination of critical state friction angle φ_c, from probes leading to failure; c) determination of elastic shear modulus, G, from the p = const. compression probe.

for $p = p_0$ with the N and λ values given in Tab. 4.3. Therefore, the initial value of the preconsolidation pressure p_{c0} (*i.e.*, the size of the elliptical yield locus along the isotropic axis) is slightly larger than p_0 and the soil appears as slightly overconsolidated ("quasi-preconsolidation" effect). The value of p_{c0} consistent with the assumed position of the virgin compression line and initial void ratio can be computed by the following equation:

$$1 + e_0 = N - \lambda \ln p_{c0} + \kappa \ln \frac{p_{c0}}{p_0} \tag{4.11}$$

with p_0 and e_0 provided by Tab. 4.2 and N, λ and κ as in Tab. 4.3.

4.4.2 3–SKH model

In the 3–SKH model, the material constants λ^* and N^* define the slope and position of the virgin compression line in the $\ln(1+e)$:$\ln p$ plane. Their numerical values have been determined by interpolating the experimental data from the isotropic compression probe, Tx128, shown in Fig. 4.4a.

According to eq. $(4.34)_2$ of Appendix B, the constants A, m and n quantify the dependence of the elastic shear modulus G on mean effective stress p and preconsolidation pressure $2a$ (size of the Bounding Surface along the isotropic axis). Due to the lack of reliable information on the influence of such state variables on G, the values for the constants m and n have been set equal to those provided by Mašín [86] for London Clay. The constant A was determined by comparing the shear stiffness value predicted by eq. $(4.34)_2$ with the tangent shear moduli measured in a number of deviatoric probes (Tx121–Tx123, Tx125 and Tx126) at very small strain levels. These tangent shear moduli are plotted in Fig. 4.5a as a function of the deviatoric strain. From the figure, it is apparent how the experimental data in the very small strain range ($\epsilon_s < 1.0 \cdot 10^{-4}$) are quite scattered, due to the lack of accurate strain measurements. For the purpose of model calibration, the average value $A = 653$ was selected, which is well inside the range of values reported for similar soils.

The constant κ^* controls the value of the bulk modulus of the material in the elastic range, see eq. $(4.34)_3$. In principle, it could be determined from the isotropic extension probe, Tx127, as the slope of the tangent to the unloading curve in the $\ln(1+e)$:$\ln p$ plane at very small volumetric strains. However, due to the lack of accurate volume change measurements in the very small strain range, κ^* was determined from the elastic shear stiffness, as:

$$\kappa^* = \frac{p}{K} = \frac{3(1-2\nu)}{2(1+\nu)} \frac{p}{G}$$

by assuming a value of the Poissons ratio $\nu = 0.25$, at $p = 150$ kPa.

The parameter M, controlling the slope of the Critical State Line for axisymmetric compression in the q:p plane can be assumed equal to 1.33, as for the Modified Cam-Clay model. No ad-hoc experimental tests were performed to calibrate the parameters T and S. Therefore, in lack of sufficient information and since the values reported in the literature for these two constants lie in a very narrow range – see References [125, 7, 65, 86] – the values determined by Mašín [86] for London Clay were adopted.

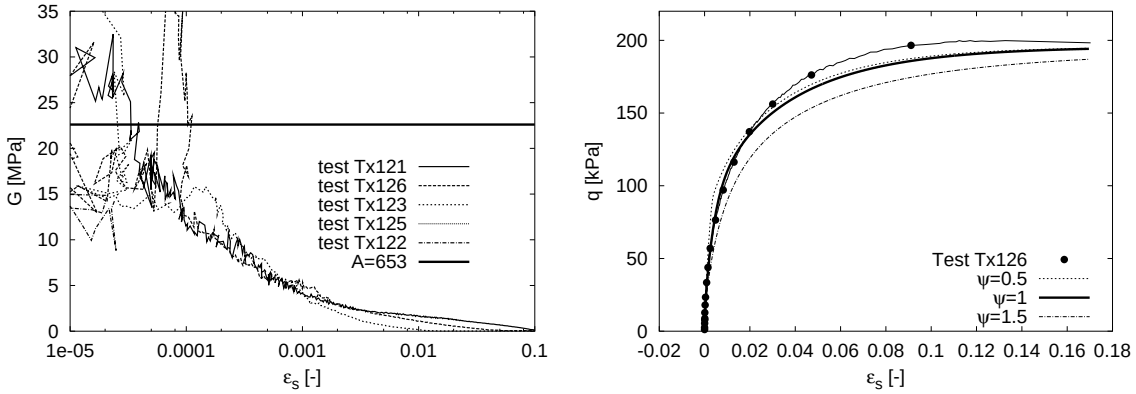

(a) (b)

Figure 4.5: Calibration of the 3–SKH model: a) determination of parameter A from deviatoric probes; b) determination of parameter ψ from the p = const. compression probe.

The last material constant of the model – namely the exponent ψ appearing in the expression of the hardening moduli H_1 and H_2, eq. (4.51) – was determined by trial and error, by comparing the model response with the experimental results obtained in the p = const. compression probe Tx126. From the results shown in Fig. 4.5b, a value of $\psi = 1.0$ has been considered appropriate.

The complete set of parameters for the 3–SKH model is summarized in Tab. 4.4.

N^*	λ^*	A	n	m	κ^*	M	T	S	ψ
0.85	0.057	653	0.71 †	0.27 †	0.004	1.33	0.24 †	0.16 †	1.0

Table 4.4: Parameters of the 3–SKH model. Quantities indicated with the symbol † have been assumed from data reported by Mašín [86] for London Clay.

The definition of the initial conditions requires the determination of the initial values of the internal variable a – controlling the size of the elliptic Bounding Surface, see eq. (4.38) – and of the two back-stresses, $\boldsymbol{\sigma}_a$ and $\boldsymbol{\sigma}_b$, defining the centers of the yield surface and history surface, respectively (see Fig. 4.3).

As previously discussed in sect. 4.4.1, the initial state of the material appears to be slightly overconsolidated due to the quasi-preconsolidation effect induced by creep strains. In defining the initial value of the parameter a, this effect can be easily taken into account by fixing the position of the virgin compression line of the material. From the expressions of the virgin compression and unloading/reloading curves in the $\ln(1+e)$:$\ln p$ plane, the following relation between a and the initial void ratio e_0 and mean stress p_0 can be derived:

$$\ln(1+e_0) = N - \lambda^* \ln 2a + \kappa^* \ln \frac{2a}{p_0} \tag{4.12}$$

Eq. (4.12) can be solved for a, with p_0 and e_0 provided by Tab. 4.2 and N^*, λ^* and κ^* as

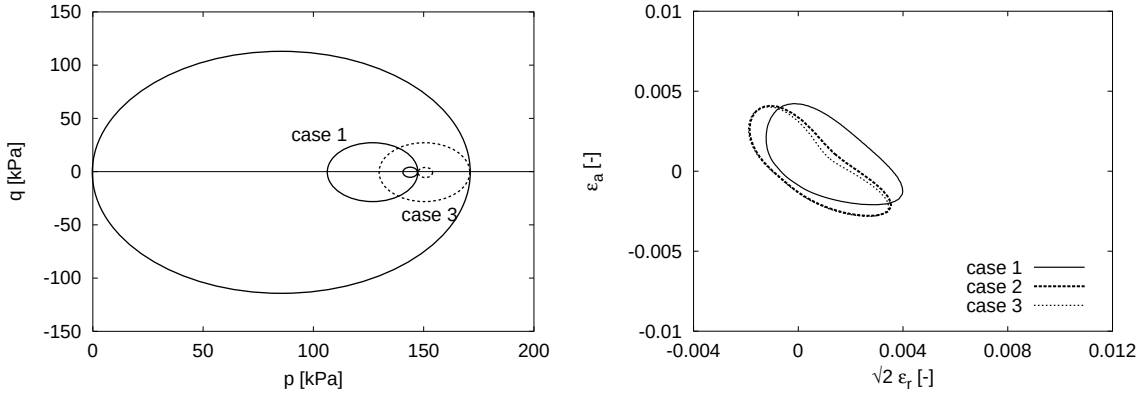

(a) (b)

Figure 4.6: Effect of initial position of kinematic hardening surfaces on the directional response of 3–SKH model. a) Initial positions of kinematic surfaces assumed for Cases (1) and (3); Strain response envelopes for axisymmetric probes from initial state A, and R_σ = 50 kPa.

in Tab. 4.4.

On the contrary, it is not clear how the back stresses $\boldsymbol{\sigma}_a$ and $\boldsymbol{\sigma}_b$ should evolve with creep strain. This introduces some uncertainty in the definition of the initial conditions, which must be considered in the evaluation of the model predictions. In order to assess the potential effect of the assumed initial conditions on the predicted directional behavior of the model, three possible scenarios were considered:

- Case 1: History surface and yield surface touch each other at the current stress state, and are both located at its left, as shown in Fig. 4.6a;
- Case 2: History surface and yield surface both centered about the current stress state: $\boldsymbol{\sigma} = \boldsymbol{\sigma}_a = \boldsymbol{\sigma}_b$;
- Case 3: History surface is in contact with the Bounding Surface at the isotropic stress state $p = 2a$; yield surface touches the current stress state and is located at its right, as shown in Fig. 4.6a;

The strain response envelopes obtained for Cases 1–3 under axisymmetric probes with R_σ = 50 kPa, starting from initial state A, are shown in Fig. 4.6b. While the results obtained for Cases (2) and (3) are almost coincident, some quantitative differences are apparent between the response envelopes for Cases (1) and (2). This is due to the fact that, in Case (1), plastic loading conditions with relatively low values of the plastic modulus occur even at very small strain levels in all the probes characterized by a net increase in mean stress p, whereas in the other two cases the response of the material in the very small strain range is always elastic or almost elastic.

In the following, the assumption made in Case (1) – i.e., that the quasi–preconsolidation due to creep affects only the sizes of the three surfaces, but not the position of history

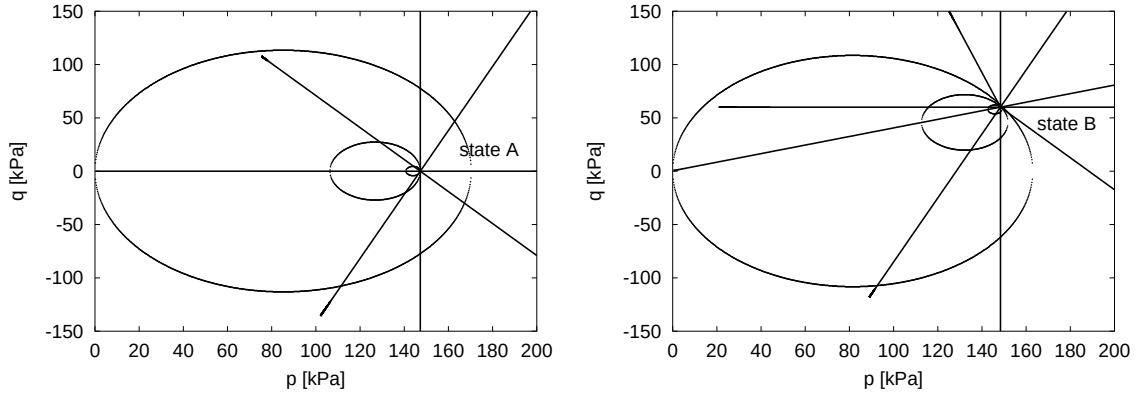

(a) (b)

Figure 4.7: Initial configuration assumed for the kinematic surfaces of 3–SKH model: a) initial state A; b) initial state B. Stress probe directions are also shown in the figures.

and yield surfaces with respect to the current stress state – has been assumed both for the calibration of the 3–SKH model and for the simulation of the stress probing experiments from state B, discussed in Sect. 4.5. The initial configuration assumed for the kinematic surfaces for states A ad B is shown in Fig. 4.7. Note that, while the state A appears as slightly overconsolidated, according to the value of the average initial void ratio reported in Tab. 4.2, the state B lies on the Bounding Surface. The initial configuration of the kinematic hardening surfaces at state B, shown in Fig. 4.7b, is the only possible under the assumption of Case (1), due to the non-intersection condition. However, it is worth recalling that Clayton and Heymann [30] report experimental evidence showing an initially stiff, "elastic" behavior after some period of rest.

4.4.3 CLoE hypoplastic model

As discussed by Chambon *et al.* [29], the calibration of the CLoE model requires experimental data from some prescribed "basic paths", including:

i) conventional drained triaxial compression and extension;

ii) isotropic compression or extension;

iii) "pseudo-isotropic" (*i.e.*, isotropic loading from an anisotropic stress state) compression and extension.

Four of these basic paths are included among the stress probes originating from the isotropic initial state A (Tx121, Tx122 and Tx127 or Tx128). As for the pseudo-isotropic tests, use was made of the results of the stress probe Tx115, originating from the initial state B. This is the only case in which some information from the stress-probing experiments conducted from the anisotropic state B was used in the calibration process.

The various constants of the CLoE model cannot be evaluated directly from the experimental results, since care must be taken in preserving the consistency of the constitutive tensors at isotropic states and on the limit surface, which bounds the region of admissible stress states in stress space. Rather, a complex calibration procedure must be followed in order to obtain a consistent set of parameters, see Reference [29] for details. In this case, the calibration procedure was carried out using a specifically designed software tool, kindly provided by Desrues [42]. The results of the calibration process are summarized in Tab. 4.5, providing the complete set of parameters adopted in the simulations with the CLoE model.

φ_c (deg)	c (kPa)	χ_{ca} (–)	y_{ca} (–)	y_{rc} (–)	p_{fc} (–)	p_{ref} (kPa)	$\epsilon_{v,\text{ref}}$ (–)	λ_c (–)	φ_e (deg)
34.0	0	0.17	0.055	3.1	0	147.26	0.0	183.34	33

χ_d (–)	χ_c (–)	χ_{m2} (–)	y_e (–)	p_{fe} (–)	m_c (–)	m_e † (–)	n † (–)	ω † (–)	
-1.0	-0.1	-0.05	0.011	0.02	-0.2	0.0	-0.2	0.36	

Table 4.5: Parameters of the CLoE model. Quantities indicated with the symbol † have been estimated according to Desrues [42].

The comparison between model predictions and material response observed on the calibration paths is shown in Fig. 4.8. The model provides a fairly good match with experimental results for all calibration paths, with the only exception of the isotropic compression path (Fig. 4.8c), for which the model significantly underestimates the compressibility of the soil. This clear limitation is due to the fact that, in its current version, the model does not allow to prescribe independently the bulk and shear tangent moduli (in both compression and extension) at isotropic states, see Reference [92]. A change in the bulk stiffness in isotropic compression is reflected in the deviatoric response, so that any attempt to improve the model response in isotropic compression would unavoidably deteriorate the performance of the model along the other paths. The set of parameters shown in Tab. 4.5 was taken as the best possible compromise in terms of predictive capability of the model along the entire set of basic paths.

4.4.4 K-hypoplastic models for clays

A detailed discussion of the procedures required for the calibration of the K-hypoplastic model for clays can be found in Reference [87]. The standard version of the model is fully characterized by five constitutive constants, namely N^*, λ^*, κ^*, φ_c and r.

The constants N^* and λ^* control the position and slope of the isotropic normal compression line in the $\ln(1+e)$:$\ln p$ plane. As such, they have the same physical meaning as the corresponding constants of the 3–SKH model (Sect. 4.3.1), and can be determined as discussed in Sect. 4.4.2. For the determination of the constant κ^* – which controls the

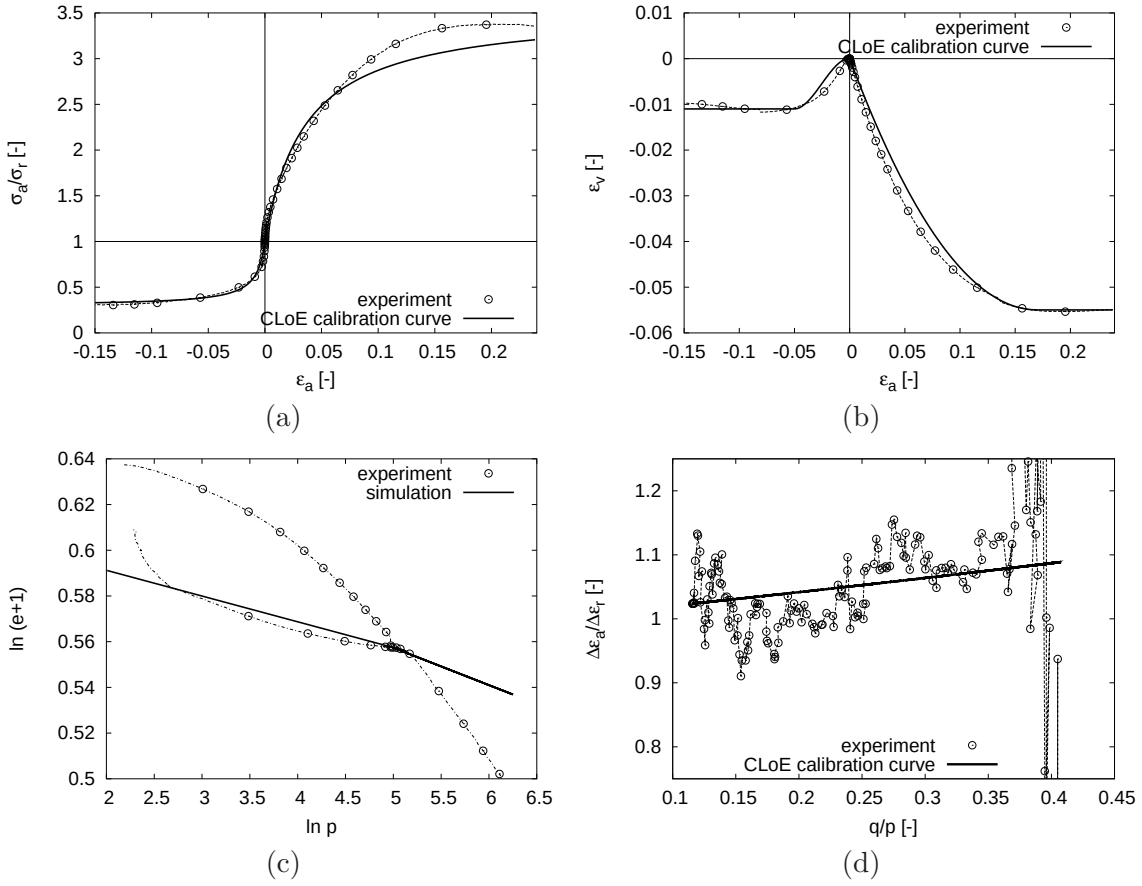

Figure 4.8: Calibration of the CLoE model: comparison of predicted and observed response for: a) conventional triaxial compression and extension tests, in the σ_a/σ_r:ϵ_a plane; b) conventional triaxial compression and extension tests, in the ϵ_v:ϵ_a plane; c) isotropic compression and extension probes, in the $\ln(1+e)$:$\ln p$ plane; d) pseudo-isotropic compression test, in the $\Delta\epsilon_a/\Delta\epsilon_r : q/p$ plane.

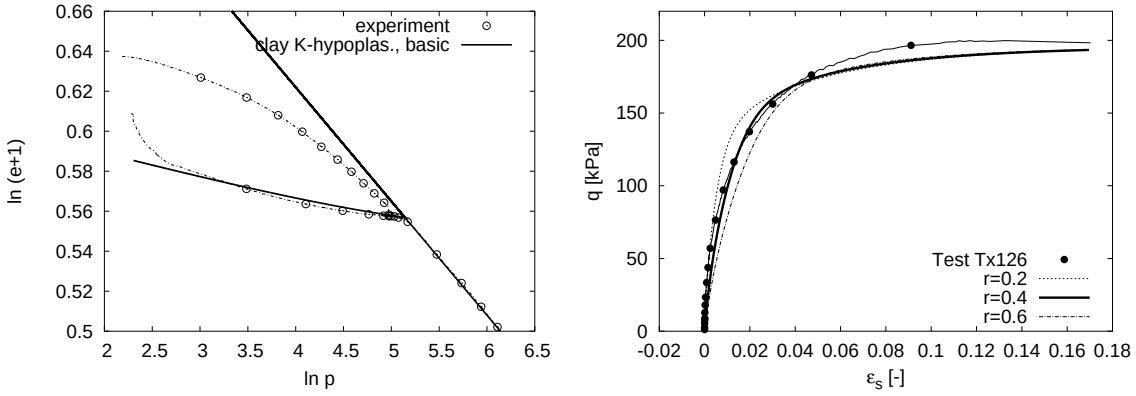

(a) (b)

Figure 4.9: Calibration of the K-hypoplastic model for clays: comparison of predicted and observed response for: a) isotropic compression and extension tests, in the $\ln(1+e)$:$\ln p$ plane; b) constant p triaxial compression, in the q:ϵ_s plane.

compressibility of the soil in isotropic unloading – the choice has been made to use the results of the stress probe Tx127 in the medium strain range. A reasonably good fit to the available experimental data was obtained with $\kappa^* = 0.007$, as shown in Fig. 4.9a.

The constant φ_c defines the friction angle of the material in critical state conditions. Its determination has been already discussed in Sect. 4.4.1. The last constant, r, controls the ratio between shear and bulk stiffness in isotropic virgin states. It was calibrated by trial and error, by comparing the model response with the experimental data from the stress probe Tx126, *i.e.*, a constant p compression test from the isotropic virgin state A. The best fit between predictions and measurements was obtained with $r = 0.4$, see Fig. 4.9b.

The extension of the K-hypoplastic model to include the effects of previous loading history by means of the intergranular strain concept requires five additional constants to be identified, namely m_R, m_T, R, β_r and χ (see Reference [108]). In principle, their calibration requires experimental data from non-conventional laboratory experiments involving complex loading paths – such as those considered by Atkinson *et al.* [6] in the experimental evaluation of the effects of recent stress history – and small-strain stiffness measurements using dynamic testing techniques. Such experiments are not included in the experimental program considered in this study. However, as suggested by Mašín [87], the constants R, β_r and χ, which provide the extent of the quasi-elastic range for the material and the stiffness degradation rate with increasing strain, typically show a relatively limited range of variation for different soils, and therefore have been estimated with reference to the experimental data available for London Clay [86].

The constant m_R, which controls the hypo-elastic stiffness upon stress path reversal in the very small strain range, was estimated by means of the following relation between m_R and

the small-strain shear modulus G_0 in isotropic conditions [87]:

$$G_0 \simeq \frac{m_R p}{r\lambda^*} \qquad \Leftrightarrow \qquad m_R \simeq \frac{G_0 r \lambda^*}{p} \tag{4.13}$$

with $G_0 = 23.0$ MPa at $p = 150$ kPa, see Fig. 4.5a. This guarantees that the enhanced K-hypoplastic model and the 3–SKH model are characterized by identical shear stiffnesses in the very small strain range. Finally, in the absence of any other experimental indication, m_T was assumed equal to m_R. The results of the calibration process are summarized in Tab. 4.6.

N^* (–)	λ^* (–)	κ^* (–)	φ_c (deg)	r (–)	m_R (–)	m_T (–)	R (–)	β_r (–)	χ (–)
0.85	0.057	0.007	33.0	0.4	3.5	3.5	10^{-4} †	0.2 †	6.0 †

Table 4.6: Parameters of the K-hypoplastic models for clays. Quantities indicated with the symbol † were assumed from data reported by Mašín [86] for London Clay.

The definition of the initial conditions requires the determination of the initial values of the void ratio and of the intergranular strain tensor $\boldsymbol{\delta}$. As for the void ratio, the values provided in Tab. 4.2 were adopted. Note that, with the values of N^* and λ^* given in Tab. 4.6, the void ratio assumed for the isotropic state A is slightly lower than the void ratio on the virgin compression line at the same mean stress. This implies that the material appears slightly overconsolidated, as already noted in Sect. 4.4.2. The initial values of the intergranular strain for the two states A and B were determined by numerically simulating the two constant q/p compression paths imposed to the material before the start of the stress-probing. This guarantees that the initial values of $\boldsymbol{\delta}$ are consistent with the initial configuration of the kinematic surfaces in the 3–SKH model.

4.5 Comparison of observed and predicted response

4.5.1 Strain response envelopes

In the following, the response of reconstituted Beaucaire Marl to the stress probing program detailed in Tab. 4.1, as well as the predictions of the different models described above, is depicted by using the so-called *incremental strain response envelope*, as defined in Reference [133]. Such a representation directly follows from the concept of stress response envelope, first proposed by Gudehus [50] as a convenient tool for visualizing the properties of rate-type constitutive equations. According to Gudehus, a stress (strain) response envelope is defined as the image in the stress (strain) rate space of the unit sphere in the strain (stress) rate space, under the map defined by the constitutive equation. By simply replacing rates with finite-size increments, the same definitions apply to the incremental response envelopes. In the general case, an incremental strain response envelope (RE, hereafter) is a surface

in a six-dimensional space. However, for the particular loading conditions considered, the most natural choice is to represent the section of the REs in the plane of work-conjugated strain increment quantities, $(\Delta\epsilon_a, \sqrt{2}\,\Delta\epsilon_r)$, see Fig. 4.1b. The size of each strain increment vector defining the RE can be directly interpreted as a directional secant compliance of the material, for the associated loading direction and stress increment magnitude.

Figures 4.10 and 4.11 show the computed REs for all the models considered at small to medium stress increment levels ($R_\sigma = 20$, 30, 40 and 50 kPa), and at medium to large stress increment levels ($R_\sigma = 50$ and 90 kPa), respectively. The corresponding experimentally obtained REs are also shown in both figures on the top left corner.

For small to medium stress increment levels, the experimental REs indicate that the softest response is associated with those paths which are characterized by a large deviatoric component (*e.g.*, tests Tx119 and Tx113). As R_σ increases, the envelopes progressively shift upward to the left, due to the fact that the initial state is closer to the critical state line for axisymmetric compression than to the corresponding line for axisymmetric extension. For $\eta = 0.4$ loading paths (Tx130 and Tx129), the material response is softer when the probe points in the direction of continued loading, and stiffer upon unloading (*i.e.*, upon full stress path reversal with respect to the consolidation history). In fact, this last path corresponds to the stiffest response of the material. A direct consequence of the above observations is that the experimental REs are markedly non-symmetric about the origin of the strain increment space.

The predictions of the different models considered appear, from a qualitative standpoint, all in fair agreement with the salient features of the experimental response discussed above. The only notable exception is represented by the predictions of CLoE model upon $\eta = 0.4$ loading paths, where – contrary to experimental evidence – no significant difference between secant stiffness in compression and extension is observed. From a quantitative standpoint, however, all models appear to significantly underpredict the secant stiffness of the material. The REs predicted with the two elastoplastic models show a convex shape, except for the expected, yet minor irregularity of the Modified Cam-Clay envelopes, close to neutral loading in extension. The REs of the two K-hypoplastic models, and (to a much lesser extent) those of CLoE show some degree of non-convexity in a region located around the $\eta = 0.4$ loading direction. This feature is also shown by the two largest experimental REs, although such an observation is based on the results of one single stress-probe.

At large stress increment level ($R_\sigma = 90$ kPa, Fig. 4.11), both the elastoplastic and the K-hypoplastic models provide response envelopes which appear in fairly good agreement with the experimental results, from both a qualitative and a quantitative point of view. On the contrary, CLoE significantly overestimates soil stiffness for loading paths close to deviatoric compression (Tx116 and Tx119).

4.5.2 Normalized stress-paths

In addition to response envelopes, the performance of the five models can be also assessed by representing the prescribed stress paths in the normalized plane $q/p_e^* : p/p_e^*$, where p_e^*

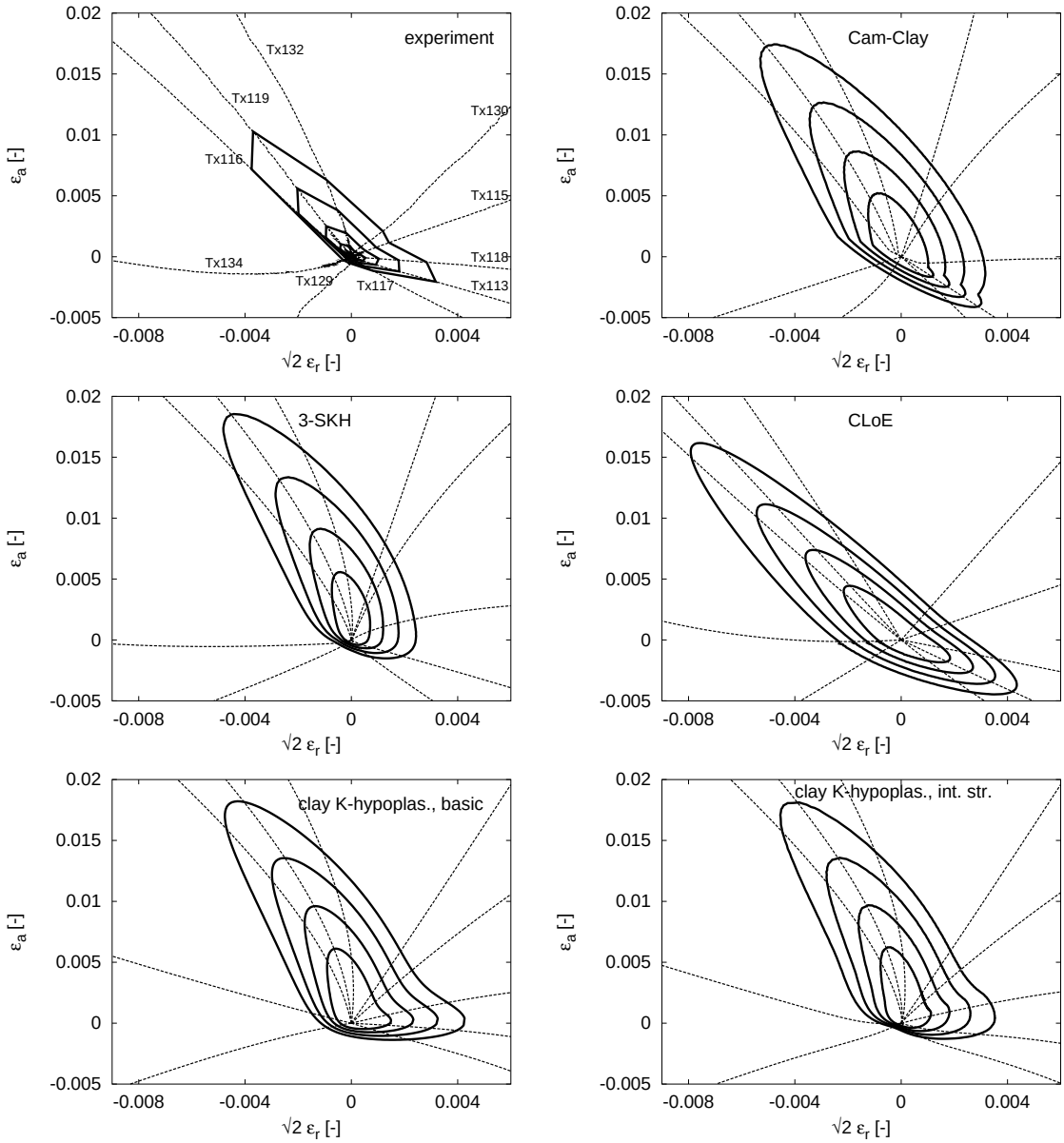

Figure 4.10: Experimental *vs.* simulated strain response envelopes for $R_\sigma = 20$, 30, 40 and 50 kPa

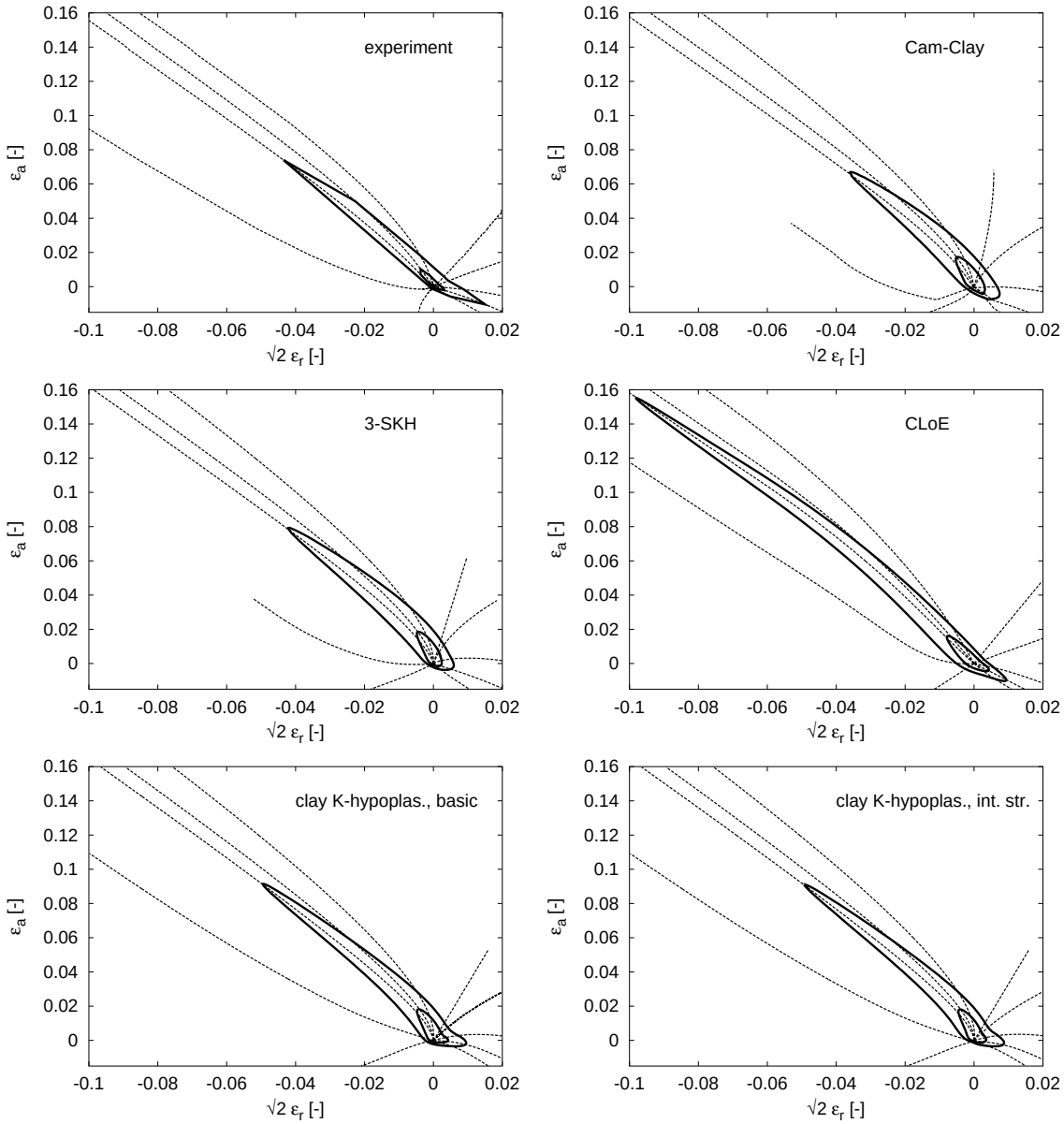

Figure 4.11: Experimental *vs.* simulated strain response envelopes for $R_\sigma = 50$, and 90 kPa

is the equivalent pressure, given by:

$$p_e^* := \exp\left\{\frac{N-1-e}{\lambda}\right\} \qquad \text{for Modified Cam-Clay;} \tag{4.14}$$

$$p_e^* := \exp\left\{\frac{N^*-\ln(1+e)}{\lambda^*}\right\} \qquad \text{otherwise.} \tag{4.15}$$

Figure 4.12 shows such normalized stress-paths for both the constitutive models and the actual experiments. For the latter, the equivalent pressure was evaluated using eq. (4.15).

For the two elastoplastic models, the normalized stress-paths clearly define a single limit surface – of nearly elliptic shape – in the normalized plane, due to the isotropic volumetric hardening law adopted to describe the evolution in size of the Bounding Surface of the material (coinciding with the yield surface for the Modified Cam-Clay model). It is worth noting that the initial portion of the experimental stress-paths Tx115, Tx130 and Tx132 show a sharp bend which can be attributed to a quasi-preconsolidation effect similar to the one observed for the initial state A. This effect is not captured by the two elastoplastic models, due to an inadequate characterization of the initial state.

Interestingly, the response predicted by the two K-hypoplastic models is quite satisfactory when compared to the experimental data, although no such concept as a Bounding Surface is introduced in their formulation. The appearance of a state boundary surface in the model predictions is, in this case, a combined effect of the assumed barotropy and pyknotropy functions, which endow this particular version of K-hypoplasticity with a single critical state line and a unique virgin isotropic compression line [97].

The response of CLoE model is somewhat different from that of all the other models considered in two respects. First, although the response along essentially deviatoric stress paths (probes Tx116, Tx119, Tx132, Tx117 and Tx113) is in reasonable agreement with the data, the normalized stress paths do not converge towards a unique point, which is consistent with the absence of the concept of a critical state line in the model formulation. Second, the performance of CLoE appears quite poor for stress-paths in the region bounded by probes Tx118 and Tx130. This is due to the same factors which originate the problems observed when calibrating the model response along a purely isotropic compression path.

4.5.3 Accuracy of directional predictions

While the strain response envelopes plotted in Figs.4.10 and 4.11 provide a clear qualitative picture of the performance of the five models considered, a more quantitative comparison of model predictions can be obtained by introducing a suitable scalar measure of the "distance" between model response and experimental results.

Herein, the following quantities have been adopted. Let the quantities α_σ^{pq} denote the orientation of the generic stress probe of size R_σ in the q:p plane, and let the stress probe be subdivided into N increments, of length $\Delta R_\sigma = R_\sigma/N$. Then, for each model, the

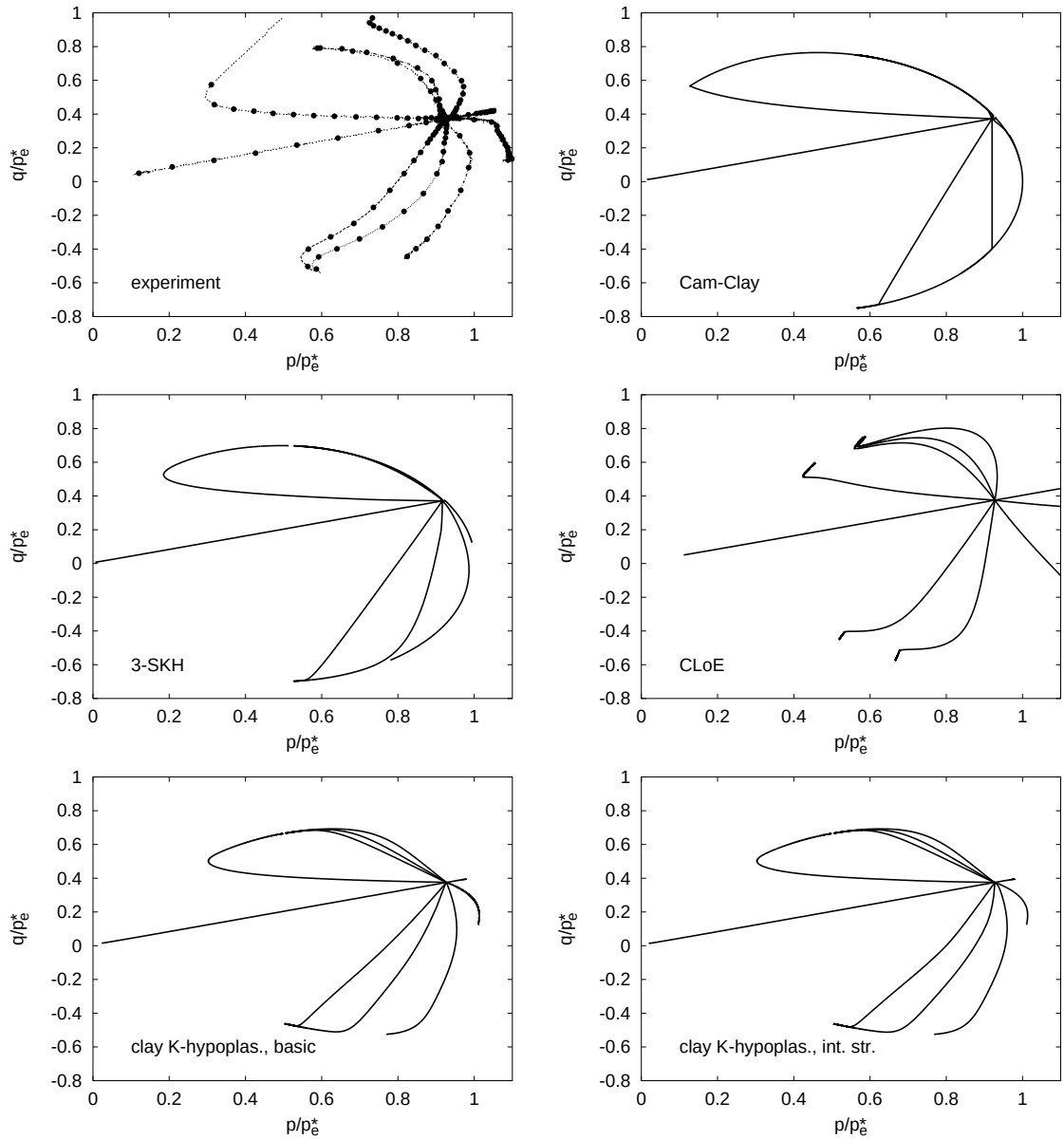

Figure 4.12: Experimental *vs.* simulated stress paths in the normalized plane q/p_e^*:p/p_e^*.

simulation error $\mathrm{err}(\alpha_\sigma^{pq}, R_\sigma)$ can be defined as:

$$\mathrm{err}(\alpha_\sigma^{pq}, R_\sigma) = \sum_{k=1}^{N} \left\| \Delta\boldsymbol{\epsilon}_{\mathrm{sim}}^{(k)} - \Delta\boldsymbol{\epsilon}_{\mathrm{exp}}^{(k)} \right\| \tag{4.16}$$

where $\Delta\boldsymbol{\epsilon}_{\mathrm{exp}}^{(k)}$ and $\Delta\boldsymbol{\epsilon}_{\mathrm{sim}}^{(k)}$ are the measured and predicted strain increment tensors, respectively, corresponding to the k-th stress increment of size ΔR_σ.

To assess the relative size of the prediction error, as compared to the strain-path length, a second, normalized error measure is introduced as follows:

$$\mathrm{err}_{\mathrm{norm}}(\alpha_\sigma^{pq}, R_\sigma) = \frac{\mathrm{err}(\alpha_\sigma^{pq}, R_\sigma)}{\sum_{k=1}^{N} \left\| \Delta\boldsymbol{\epsilon}_{\mathrm{exp}}^{(k)} \right\|} \tag{4.17}$$

Figures 4.13 and 4.14 show computed values of err and $\mathrm{err}_{\mathrm{norm}}$ as a function of the probe direction α_σ^{pq}. Two stress increment ranges have been considered, namely $R_\sigma = 30$ kPa (Fig. 4.13) and $R_\sigma = 90$ kPa (Fig. 4.14). In both cases, the evaluation of the two error measures has been carried out with $\Delta R_\sigma = 5$ kPa, which was considered to be the smallest stress increment for which experimental results are not significantly affected by scatter in the measurements.

For $R_\sigma = 30$ kPa, the performance of the two elastoplastic models is compared in Fig. 4.13a. The largest prediction error, err $\simeq 0.006$, corresponds to probe directions with α_σ^{pq} around 72° (conventional triaxial compression). This is a consequence of the fact that, while the initial state for the two models lies on the Bounding Surface, the experimental data clearly indicate that the soil possesses some degree of overconsolidation (see Fig. 4.12), probably induced by creep strains accumulated during the rest period before probing. The best predictions, in absolute terms, are obtained in the range $200° < \alpha_\sigma^{pq} < 300°$. This is not surprising, since in this region the response of the two models is quite stiff, hence the strain increment magnitudes are quite small. The effect of loading direction is less important when considering the relative error, $\mathrm{err}_{\mathrm{norm}}$, as this quantity accounts for the dependence of soil stiffness on loading direction. The two models provide almost identical predictions for the entire range of probing directions, except for the zone in which Modified Cam-Clay undergoes elastic unloading ($200° < \alpha_\sigma^{pq} < 300°$). Again, this is to be expected, since when the initial state is on the Bounding Surface, the 3–SKH model behaves as a standard Modified Cam-Clay for all probes which are directed outwards. On the contrary, when the stress-probes are directed inwards, then the more evoluted nested surface kinematic hardening structure of the 3–SKH model is capable of reproducing much better the experimental response, in both absolute and relative terms.

For the same stress increment range, the performance of the hypoplastic models is shown in Fig. 4.13b. The computed absolute error distributions with probe direction are quite similar, both in shape and magnitude, to those of the two elastoplastic models. The same is also true, to a certain extent, for the normalized error. The response of the two K-hypoplastic models is almost coincident for those probes corresponding to continued

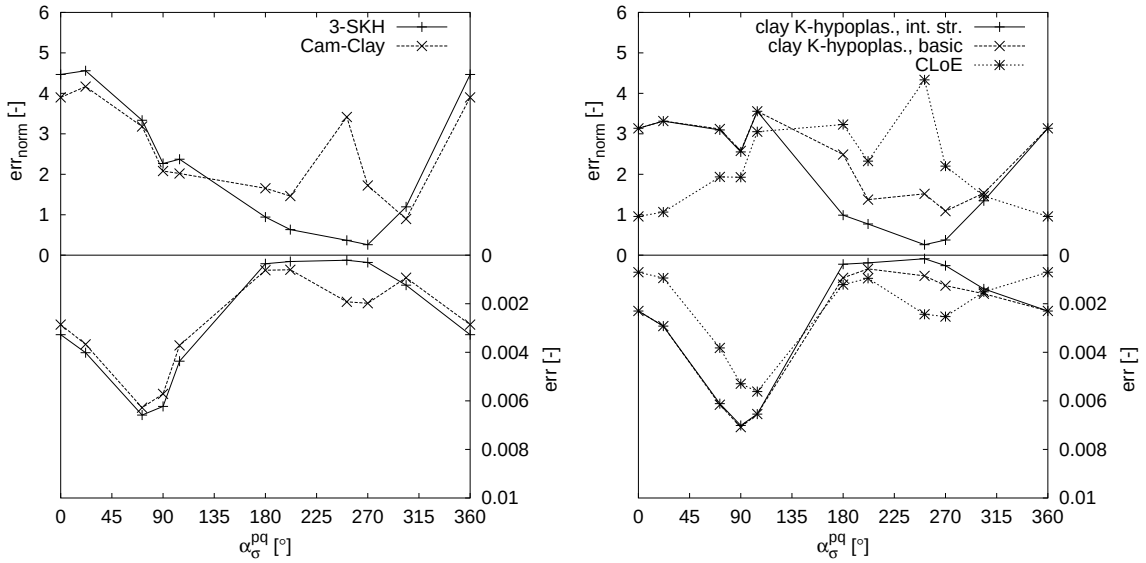

Figure 4.13: Scalar error measures with respect to the stress-path direction α_σ^{pq} in the p:q plane at state B, $R_\sigma = 0 - 30$ kPa

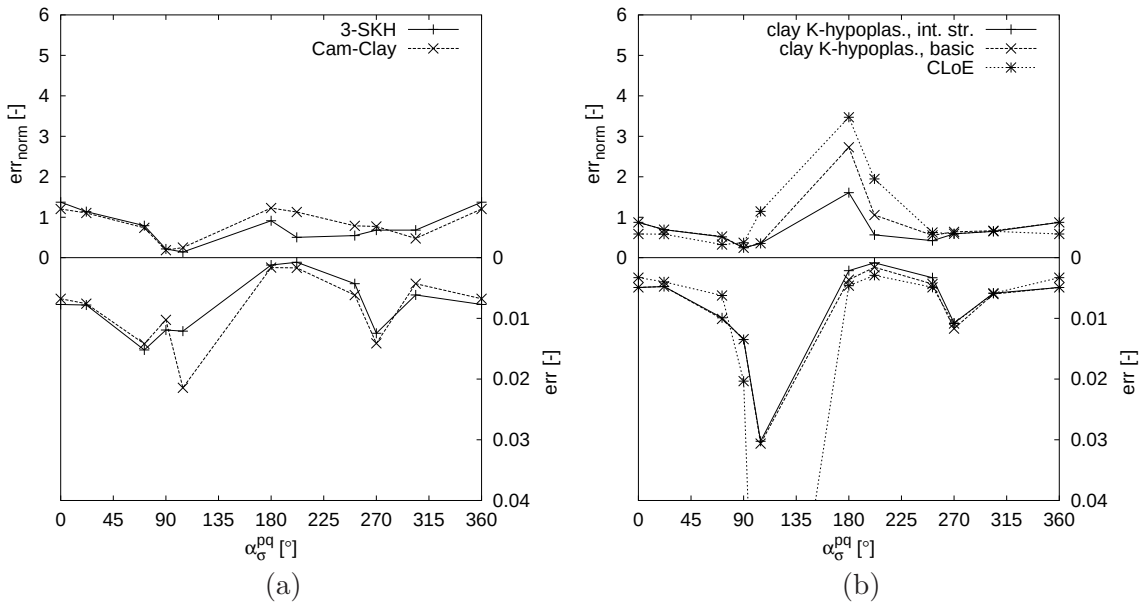

Figure 4.14: Scalar error measures with respect to the stress-path direction α_σ^{pq} in the p:q plane at state B, $R_\sigma = 0 - 90$ kPa

loading conditions, as in this case the material reaches quite rapidly the swept-out-memory conditions. Under reverse loading conditions, the two responses diverge and, as expected, the K-hypoplastic model with intergranular strains performs significantly better. This is even more apparent when considering the normalized error plots. For the same range of probe directions, CLoE performance appears to be substantially poorer, both in absolute and relative terms. On the contrary, for continued loading conditions ($340° < \alpha_\sigma^{pq} < 90°$) CLoE provides the best results among all the models considered. In fact, this is a consequence of a fortuitous combination of two different factors. On the one hand, CLoE calibration has clearly shown that the model is not capable of correctly reproducing the large decrease in stiffness associated with virgin loading upon isotropic or $\eta = \text{const.}$ loading conditions. On the other hand, the actual response of the material for the same range of probing directions appears to be much stiffer than expected for a material in a virgin state, due to the quasi-preconsolidation effect already mentioned.

Overall, data reported in Fig. 4.13 indicate that the best performance is provided by the 3–SKH model and the K-hypoplastic model with intergranular strains, which appear to yield quite similar results in terms of prediction error measures. A somehow different picture emerges by looking at the results for the larger stress increment range (Fig. 4.14). In this case, not only the relative error levels are generally lower, but also the differences between the models are less important. In fact, Modified Cam-Clay performs almost as well as the more refined 3–SKH model, and the same applies to all the hypoplastic models, except for loading directions close to $\alpha_\sigma^{pq} = 180°$. In this case, roughly corresponding to a reduction of mean stress at $q = \text{const.}$, CLoE performance is quite poor, while K-hypoplasticity with intergranular strain provides the best prediction among the models of this class, although not as good as those of the two elastoplastic models.

4.6 Concluding remarks

The comparative evaluation of the performance of different constitutive models in their application to the quantitative solution of practical engineering problems is a very complex task, which – in general – requires a careful consideration of several key factors, among which we recall:

1. Qualitative and quantitative agreement between experimentally observed response and model predictions at the element level (*i.e.*, in the simulation of laboratory tests), in view of the main objectives of the analysis and the type of problem to be solved;

2. Relative complexity of the procedures required to determine the material constants appearing in the model formulation;

3. Type and nature of the internal state variables entering the model to describe the effects of previous loading history, and the relative complexity in the characterization of their initial values;

4. Availability of robust and accurate algorithms for the numerical implementation in FE codes, in view of the solution of the engineering problems at hand.

The comparison between model predictions and experimental results is typically done, in practice, with reference to a limited number of more or less conventional stress paths, whereas the response of the material for different loading conditions is extrapolated in a more or less reasonable way. This can be quite sufficient to assess the model performance in those problems where most of the soil affected by the imposed loading conditions undergoes very similar stress paths, and one of such paths is included in the laboratory testing program. Unfortunately, this is only seldom the case in many important applications where an accurate prediction of soil-structure interaction processes and of the displacement field around the structure is required. Notable examples in this respect are provided by deep excavations and shallow tunnels to be realized in urban environments, as in such cases, different zones of soil experience widely different stress-paths, both in size and direction, and the quality of numerical predictions crucially relies on the ability of the constitutive model adopted for the soil to accurately reproduce the material response along *all* such loading paths.

In this paper, an attempt has been made to evaluate the response of different advanced constitutive models for fine-grained soils in more general terms, considering their predictive capabilities over a quite wide range of loading conditions. In trying to compare the performances of the different models, the experimental data of Costanzo *et al.* [31] have been considered as portraying the actual mechanical response of the soil. However, two main points should be stressed in this respect. First, due to the time required to perform each test, only a few probes were duplicated, and thus most of the data on which the experimental REs are constructed refer to a single specimen only. Therefore, the observed shape of the experimental REs might be affected to some extent by the unavoidable scatter always present in experimental measurements. Second, the occurrence of small amounts of viscous strains may affect both size and shape of the measured response envelopes, even if to a limited extent, see Reference [31]. Interpreting the observed response in light of rate-independent constitutive theories might therefore lead to an underestimation of soil stiffness for some probe directions and to an overestimation of soil stiffness for other probe directions, as thoroughly discussed in the companion paper [31].

Based on the normalized stress paths reported in Sect. 4.5.2 and the scalar error measures introduced in Sect. 4.5.3, the best performance overall appears to be provided by the intergranular strain-enhanced K-hypoplastic model for clays and the 3–SKH model, at both small and large strain levels.

It is interesting to note that, since the soil considered in this study was in a (almost) normally consolidated state, the predictions of the classical Cam-Clay model for continued loading conditions (*i.e.*, those paths pointing outside the yield surface) are equivalent to those obtained with the much more sophisticated 3–SKH model. In unloading, however, the data clearly show the substantial improvement of predictions which can be achieved with the kinematic hardening approach.

As compared to its enhanced version, the performance of the standard K-hypoplastic model is still reasonably good, mainly because the loading programmes considered involve only a very limited number of stress reversals. For the application to monotonic (or quasi-monotonic) loading conditions, the standard K-hypoplastic model may represents a valid alternative to more complex formulations.

On the contrary, the performance of the CLoE model is definitely poor, when compared with the other elastoplastic or hypoplastic models, particularly for those loading paths involving a significant increase in mean stress. This is not surprising, considering that CLoE is a first-generation hypoplastic model, in which the stress tensor is assumed as the only state variable for the material. For this reason, the mathematical structure of CLoE model does not allow to properly distinguish normally consolidated and overconsolidated states, and to correctly describe critical state failure conditions. While CLoE has demonstrated its capability of accurately modelling the response of coarse-grained soils along mainly deviatoric loading paths (see, e.g., Reference [29]), these limitations obviously make it unfit to model the behavior of natural clay deposits. An attempt to modify the current version of CLoE in order to improve its performance for normally consolidated clays has been recently presented by Mašín *et al.* [92].

Although the enhanced K-hypoplastic model and the 3–SKH model provide a great flexibility in describing the effects of recent stress history on the mechanical response of the soil, they are both characterized by a relatively limited number of constants, most of which are linked to standard features of clay behavior. All the constants appearing in these two models can be determined by means of standard laboratory tests, with the only exception of those controlling the stiffness of the material at very low strain levels. As discussed by Mašín [87], these latter quantities can be easily determined from the results of dynamic tests, such as bender element or resonant column tests.

On the contrary, the CLoE model requires a much wider pool of experimental data to calibrate the large number of constants (19) appearing in the functions adopted to describe the material response along the selected basic paths. Moreover, as those parameters typically control more than one specific feature of the material response, they cannot be determined independently. Rather, they have to be found by means of a complex calibration procedure which has to be implemented numerically in a suitable calibration code. This represents a second, major drawback of the CLoE model as compared to the more recent K-hypoplastic models for clays.

The characterization of the initial state of the material is relatively easy for Modified Cam-Clay, CLoE and standard K-hypoplastic models, for which only the initial values of the stress tensor and (possibly) one additional scalar state variable (preconsolidation pressure or void ratio) are required. Defining the initial state is more complex for the enhanced K-hypoplastic model and the 3–SKH model, since it requires the determination of one or two tensorial internal variables (the back-stresses or the intergranular strain). Even in the simple case considered in this study, this has not been a trivial task. The difficulties experienced in the definition of the initial state have had an impact both on the results of the calibration procedures and on the prediction of the material response. It is reasonable

to expect that such difficulties would increase in the application of those models to natural clay deposits, with a more complicated – and possibly unknown – previous loading history. In such a case – based on some experimental observations of Jardine *et al.* [67] and Clayton and Heymann [30], who report an increase in soil stiffness for all loading directions after a relatively short resting period – Niemunis and Herle [108] suggest to assume $\boldsymbol{\delta} = \mathbf{0}$. This is equivalent to setting $\boldsymbol{\sigma}_a = \boldsymbol{\sigma}_b = \boldsymbol{\sigma}$ for the 3–SKH model.

Finally, as far as computational issues are concerned, it can be noted that robust and accurate implicit or explicit integration algorithms are now available for both complex plasticity models (see, e.g., [16, 119, 84]) and advanced hypoplastic models (see, e.g., [44, 40]). However, as the mathematical structure of the K-hypoplastic models appears simpler than that of the 3–SKH model, or of any other kinematic hardening multisurface plasticity model, the former may have some advantage with respect to the latter as far as their numerical implementation into existing FE codes is concerned.

Appendix A

The results of all the stress-probing tests from the anisotropic initial state B, along with the corresponding predictions for the five models considered, are summarized in Figs. 4.15 ($q:\epsilon_s$ plane) and 4.16 ($p:\epsilon_v$ plane). Note that all strain measures are evaluated as natural strains.

Appendix B: Mathematical formulation of the constitutive models

In the description of the relevant constitutive equations, the following invariant quantities for the stress tensor are used:

$$p := \frac{1}{3}\,\boldsymbol{\sigma} : \mathbf{1} \qquad q := \sqrt{\frac{3}{2}\boldsymbol{s} : \boldsymbol{s}} \qquad \cos(3\theta) := -\sqrt{6}\frac{\operatorname{tr}\left(\boldsymbol{s}^3\right)}{\left(\boldsymbol{s} : \boldsymbol{s}\right)^{3/2}} \tag{4.18}$$

where $\boldsymbol{s} = \boldsymbol{\sigma} - p\,\mathbf{1}$ is the deviatoric part of the stress tensor and $\mathbf{1}$ is the second-order identity tensor. Use is made of the fourth-order identity tensor $\boldsymbol{\mathcal{I}}$, with components:

$$(\boldsymbol{\mathcal{I}})_{ijkl} := \frac{1}{2}\,(\delta_{ik}\delta_{jl} + \delta_{il}\delta_{jk}) \tag{4.19}$$

K-hypoplastic model for clays

The mathematical structure of the K-hypoplastic model for clays is discussed in detail in Reference [87]. The constitutive equation in rate form reads:

$$\dot{\boldsymbol{\sigma}} = f_s \boldsymbol{\mathcal{L}} : \dot{\boldsymbol{\epsilon}} + f_s f_d \boldsymbol{N}\,\|\dot{\boldsymbol{\epsilon}}\| \tag{4.20}$$

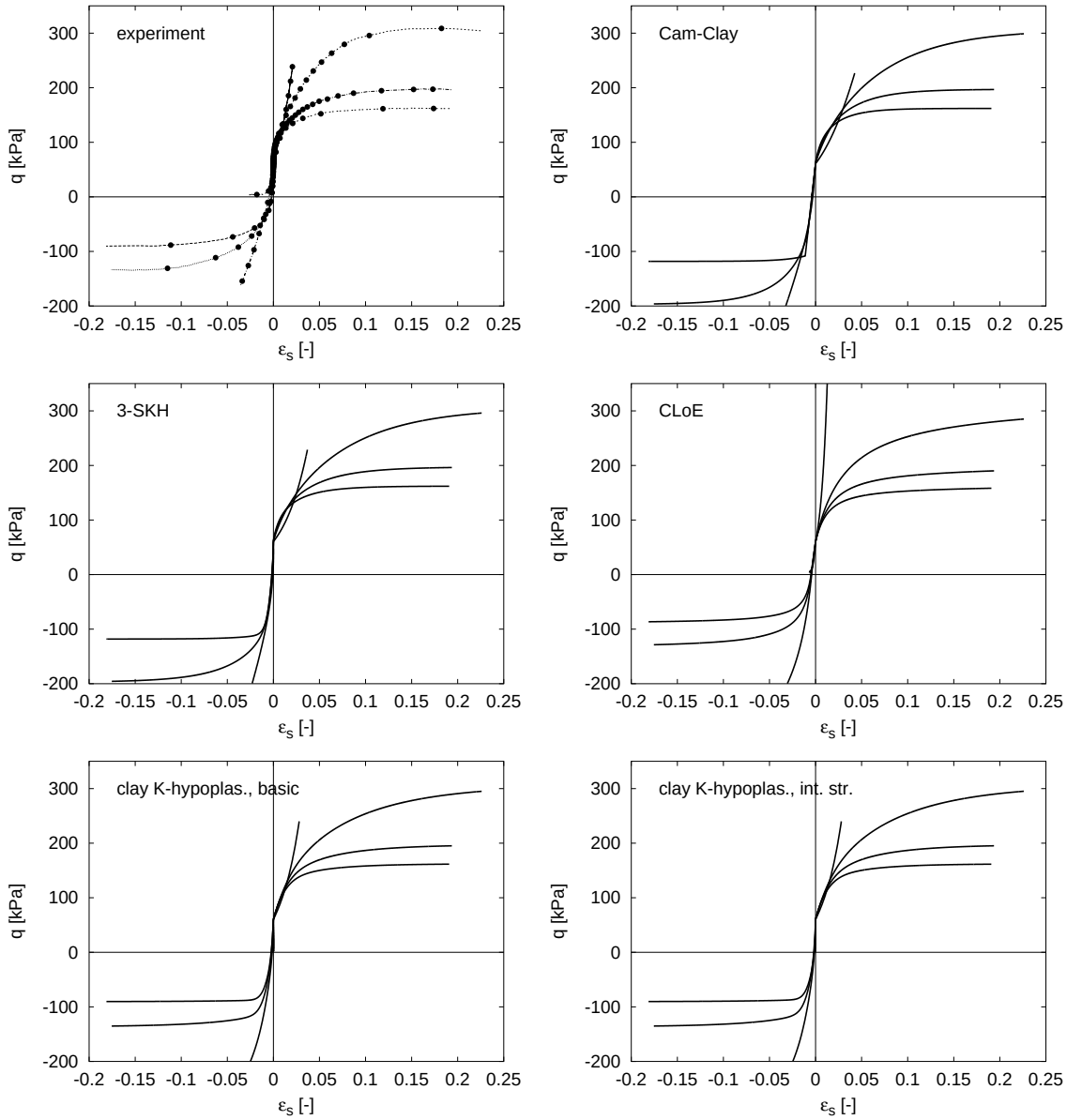

Figure 4.15: Experimental and predicted responses in the q:ϵ_s plane.

where:

$$\boldsymbol{\mathcal{L}} := 3\left(c_1\boldsymbol{\mathcal{I}} + c_2 a^2 \hat{\boldsymbol{\sigma}} \otimes \hat{\boldsymbol{\sigma}}\right) \qquad \boldsymbol{N} = \boldsymbol{\mathcal{L}} : \left(Y \frac{\mathbf{m}}{\|\mathbf{m}\|}\right) \qquad \hat{\boldsymbol{\sigma}} := \frac{1}{3p}\boldsymbol{\sigma} \tag{4.21}$$

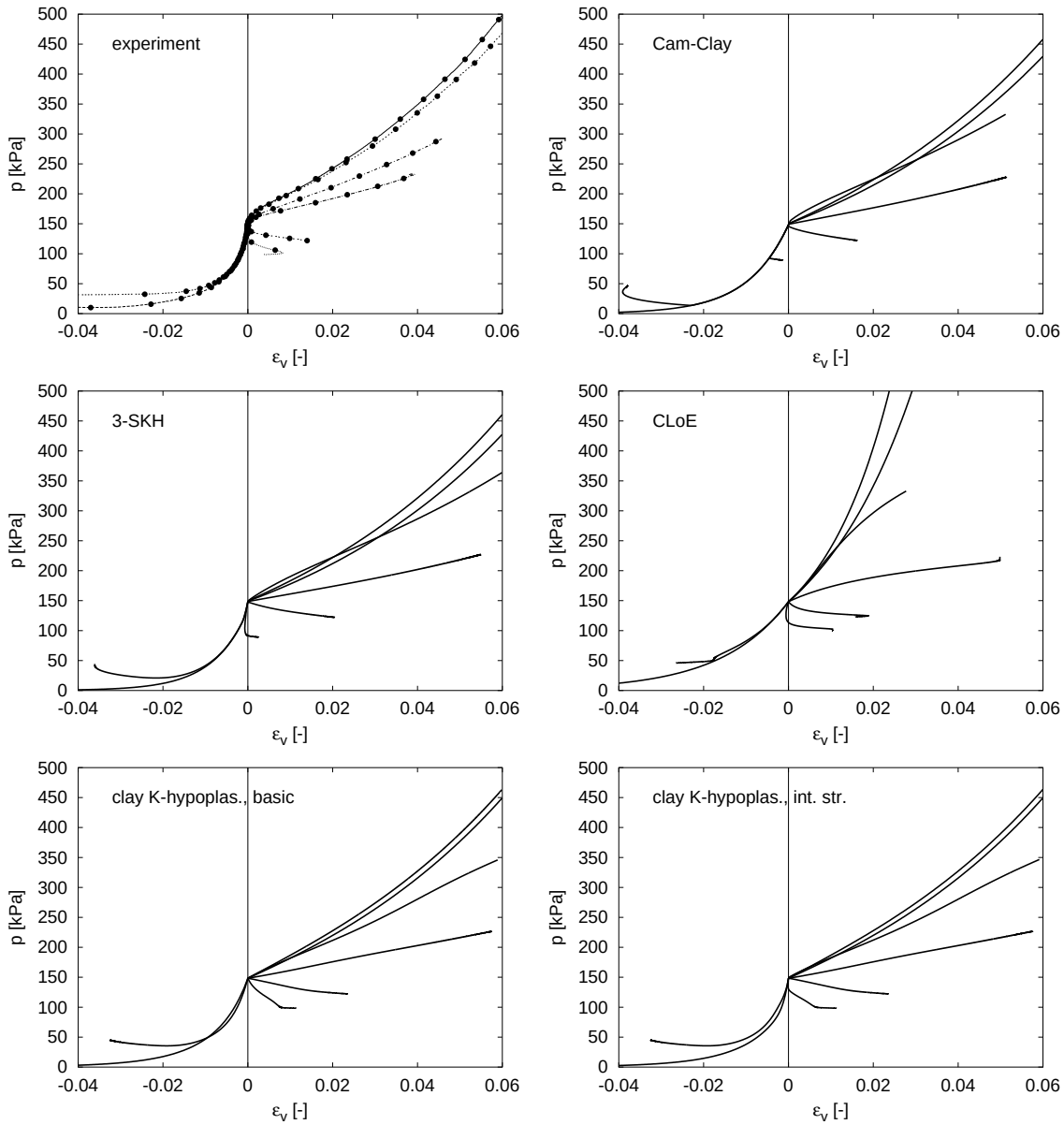

Figure 4.16: Experimental and predicted responses in the p:ϵ_v plane.

In eq. (4.20), the functions $f_s(p,e)$ (barotropy factor) and $f_d(e)$ (pyknotropy factor) are given by:

$$f_s = \frac{3p}{\lambda^*}\left(3 + a^2 - 2^\alpha a\sqrt{3}\right)^{-1} \qquad f_d = \left\{2p\,\exp\left[\frac{\ln(1+e) - N}{\lambda^*}\right]\right\}^\alpha \tag{4.22}$$

The scalar function Y and second-order tensor $\boldsymbol{m}$ appearing in eq. (4.21) are given, respectively, by:

$$Y = \left(\frac{\sqrt{3}a}{3+a^2} - 1\right)\frac{(I_1 I_2 + 9I_3)\left(1 - \sin^2\varphi_c\right)}{8I_3\sin^2\varphi_c} + \frac{\sqrt{3}a}{3+a^2} \tag{4.23}$$

in which:

$$I_1 := \operatorname{tr}(\boldsymbol{\sigma}) \qquad I_2 := \frac{1}{2}\left[\boldsymbol{\sigma}:\boldsymbol{\sigma} - (I_1)^2\right] \qquad I_3 = \det\boldsymbol{\sigma}$$

and:

$$\boldsymbol{m} = -\frac{a}{F}\left[\hat{\boldsymbol{\sigma}} + \operatorname{dev}\hat{\boldsymbol{\sigma}} - \frac{\hat{\boldsymbol{\sigma}}}{3}\left(\frac{6\hat{\boldsymbol{\sigma}}:\hat{\boldsymbol{\sigma}} - 1}{(F/a)^2 + \hat{\boldsymbol{\sigma}}:\hat{\boldsymbol{\sigma}}}\right)\right] \tag{4.24}$$

in which:

$$F = \sqrt{\frac{1}{8}\tan^2\psi + \frac{2 - \tan^2\psi}{2 + \sqrt{2}\tan\psi\cos 3\theta}} - \frac{1}{2\sqrt{2}}\tan\psi \qquad \tan\psi := \sqrt{3}\,\|\operatorname{dev}\hat{\boldsymbol{\sigma}}\| \tag{4.25}$$

Finally, the scalars a, α, c_1 and c_2 appearing in eqs. (4.21)–(4.24), are given as functions of the material parameters φ_c, λ^*, κ^* and r by the following relations:

$$a = \frac{\sqrt{3}\,(3 - \sin\varphi_c)}{2\sqrt{2}\sin\varphi_c} \qquad \alpha = \frac{1}{\ln 2}\,\ln\left[\frac{\lambda^* - \kappa^*}{\lambda^* + \kappa^*}\left(\frac{3+a^2}{a\sqrt{3}}\right)\right] \tag{4.26}$$

$$c_1 = \frac{2\left(3 + a^2 - 2^\alpha a\sqrt{3}\right)}{9r} \qquad c_2 = 1 + (1 - c_1)\frac{3}{a^2} \tag{4.27}$$

The model requires five constitutive parameters, namely φ_c, λ^*, κ^*, N and r.

Integranular strain enhancement of K-hypoplasticity

As proposed by Niemunis and Herle [108], the enhanced K-hypoplastic model is endowed with an additional state variable, $\boldsymbol{\delta}$, a second-order tensor defined as *intergranular strain*, which can be interpreted as a macroscopic manifestation of intergranular slips at grain contacts.

Let $\rho := \|\boldsymbol{\delta}\|/R$ be a suitable normalized magnitude of $\boldsymbol{\delta}$, R being a scalar model parameter. Also, let

$$\hat{\boldsymbol{\delta}} = \begin{cases} \boldsymbol{\delta}/\|\boldsymbol{\delta}\| & \text{for } \boldsymbol{\delta} \neq \mathbf{0} \\ \mathbf{0} & \text{for } \boldsymbol{\delta} = \mathbf{0} \end{cases} \tag{4.28}$$

denote intergranular strain direction. The constitutive equations for enhanced K-hypoplasticity for clays can be written as:

$$\dot{\boldsymbol{\sigma}} = \boldsymbol{\mathcal{M}} : \dot{\boldsymbol{\epsilon}} \tag{4.29}$$

where the fourth-order tangent stiffness tensor $\boldsymbol{\mathcal{M}}$ is calculated from the constitutive tensors tensors $\boldsymbol{\mathcal{L}}$ and $\boldsymbol{N}$ defined in eq. (4.21), the barotropy and pyknotropy factors given in eq. (4.22), and the intergranular strain tensor via the following interpolation:

$$\boldsymbol{\mathcal{M}} = \left[\rho^{\chi} m_T + (1-\rho^{\chi})\, m_R\right] f_s \boldsymbol{\mathcal{L}} + \boldsymbol{\mathcal{B}} \tag{4.30}$$

where:

$$\boldsymbol{\mathcal{B}} := \begin{cases} \rho^{\chi}\,(1-m_T)\, f_s \boldsymbol{\mathcal{L}} : \hat{\boldsymbol{\delta}} \otimes \hat{\boldsymbol{\delta}} + \rho^{\chi} f_s f_d \mathbf{N} \otimes \hat{\boldsymbol{\delta}} & (\hat{\boldsymbol{\delta}} : \dot{\boldsymbol{\epsilon}} > 0) \\ \rho^{\chi}\,(m_R - m_T)\, f_s \boldsymbol{\mathcal{L}} : \hat{\boldsymbol{\delta}} \otimes \hat{\boldsymbol{\delta}} & (\hat{\boldsymbol{\delta}} : \dot{\boldsymbol{\epsilon}} \leq 0) \end{cases} \tag{4.31}$$

and χ, m_T and m_R are material constants.

The evolution equation for the intergranular strain tensor $\boldsymbol{\delta}$ is given by

$$\dot{\boldsymbol{\delta}} = \begin{cases} \left(\boldsymbol{\mathcal{I}} - \hat{\boldsymbol{\delta}} \otimes \hat{\boldsymbol{\delta}} \rho^{\beta_r}\right) : \dot{\boldsymbol{\epsilon}} & (\hat{\boldsymbol{\delta}} : \dot{\boldsymbol{\epsilon}} > 0) \\ \dot{\boldsymbol{\epsilon}} & (\hat{\boldsymbol{\delta}} : \dot{\boldsymbol{\epsilon}} \leq 0) \end{cases} \tag{4.32}$$

As compared to the basic K-hypoplastic model for clay, the enhanced model requires five additional parameters, namely R, m_R, m_T, β_r and χ.

3-SKH model

The 3–SKH model is a nested-surface kinematic hardening plasticity model developed as an extension of classical Modified Cam-Clay. The original formulation is detailed in Reference [125]. Herein, the version proposed by Stallebrass and Taylor [127] is considered. The evolution equation for the effective stress tensor is given by:

$$\dot{\boldsymbol{\sigma}} = \boldsymbol{\mathcal{D}}^e : (\dot{\boldsymbol{\epsilon}} - \dot{\boldsymbol{\epsilon}}^p) \tag{4.33}$$

where $\dot{\boldsymbol{\epsilon}}$ is the plastic strain rate tensor and $\boldsymbol{\mathcal{D}}^e$ is the elastic tangent stiffness tensor, defined by:

$$\boldsymbol{\mathcal{D}}^e := \left(K - \frac{2}{3}G\right) \mathbf{1} \otimes \mathbf{1} + 2G\,\boldsymbol{\mathcal{I}} \qquad \frac{G}{p_r} = A \left(\frac{p}{p_r}\right)^n \left(\frac{p}{2a}\right)^m \qquad K = \frac{p}{\kappa^*}\,, \tag{4.34}$$

In the above equations, the scalar quantity a is an internal variable to be defined later, p_r is a reference stress (set equal to 1.0 kPa), and A, n and m are model parameters.

Nonlinearity and irreversibility are introduced by requiring the stress state to belong to the convex set (known as *elastic domain*):

$$\mathbb{E}_{\sigma} := \left\{ (\boldsymbol{\sigma}, a, \boldsymbol{\sigma}_b) \;\middle|\; f\,(\boldsymbol{\sigma}, a, \boldsymbol{\sigma}_b) \leq 0 \right\} \tag{4.35}$$

where $f(\boldsymbol{\sigma}, a, \boldsymbol{\sigma}_b)$ is the yield function of the material, given by:

$$f(\boldsymbol{\sigma}, a, \boldsymbol{\sigma}_b) = \frac{1}{2}\left[\left(\frac{\bar{q}_b}{M}\right)^2 + \bar{p}_b^2 - T^2 S^2 a^2\right] \tag{4.36}$$

In eq. (4.36), the scalar functions $\bar{p}_b$ and $\bar{q}_b$ are the first and second invariants of the tensor $(\boldsymbol{\sigma}-\boldsymbol{\sigma}_b)$, defined as in eq. (4.18); $\boldsymbol{\sigma}_b$ and a are internal variables, providing the coordinates of the centers of the yield surface and of the Bounding Surface (see eq. (4.38)), respectively, and M, T and S are model parameters.

Inside the yield surface, $\dot{\boldsymbol{\epsilon}}^p = \mathbf{0}$. For stress states on the yield surface, the plastic strain rate is given by the following associative flow rule:

$$\dot{\boldsymbol{\epsilon}}^p = \frac{\langle \boldsymbol{P} : \boldsymbol{\mathcal{D}}^e : \dot{\boldsymbol{\epsilon}} \rangle}{H + \boldsymbol{P} : \boldsymbol{\mathcal{D}}^e : \boldsymbol{P}} \boldsymbol{P} \qquad\qquad \boldsymbol{P} := \frac{\partial f}{\partial \boldsymbol{\sigma}} \tag{4.37}$$

where H is the plastic modulus and the operator $\langle x \rangle := (x + |x|)/2$ denotes the positive part of any scalar function x.

A key characteristic of the 3–SKH model is the definition of two additional surfaces in stress space. The first one, known as Bounding Surface, is given by:

$$F(\boldsymbol{\sigma}, a) = \frac{1}{2}\left[\left(\frac{q}{M}\right)^2 + p^2 - 2pa\right] \tag{4.38}$$

and limits the kinematic hardening of the yield surface. The second surface, called history surface, is given by:

$$f_h(\boldsymbol{\sigma}, a, \boldsymbol{\sigma}_a) = \frac{1}{2}\left[\left(\frac{\bar{q}_a}{M}\right)^2 + \bar{p}_a^2 - T^2 a^2\right] \tag{4.39}$$

where $\boldsymbol{\sigma}_a$ is an additional tensorial internal variable, and the scalar functions $\bar{p}_a$ and $\bar{q}_a$ are the first and second invariants of the tensor $(\boldsymbol{\sigma} - \boldsymbol{\sigma}_a)$.

The evolution equation for the scalar internal variable a is given by:

$$\dot{a} = \frac{a}{\lambda^* - \kappa^*} \dot{\boldsymbol{\epsilon}}^p : \mathbf{1} \tag{4.40}$$

where κ^* and λ^* are material constants. The kinematic hardening rules for the two back-stress tensors are given as follows:

1. *Plastic loading conditions with $f_h < 0$ and $F < 0$*

   In this case, we have:

$$\dot{\boldsymbol{\sigma}}_a = \frac{\dot{a}}{a}\boldsymbol{\sigma}_a \qquad\qquad \dot{\boldsymbol{\sigma}}_b = \frac{\dot{a}}{a}\boldsymbol{\sigma}_b + \dot{Z}_s \boldsymbol{\gamma} \tag{4.41}$$

   where:

$$\boldsymbol{\gamma} = \frac{\boldsymbol{\sigma} - \boldsymbol{\sigma}_b}{S} + \boldsymbol{\sigma}_a - \boldsymbol{\sigma} \tag{4.42}$$

$$\dot{Z}_s = \frac{1}{\boldsymbol{P} : \boldsymbol{\gamma}} \left\{ \boldsymbol{P} : \left(\dot{\boldsymbol{\sigma}} - \frac{\dot{a}}{a} \boldsymbol{\sigma}_b \right) - T^2 S^2 a \dot{a} \right\} \tag{4.43}$$

2. *Plastic loading conditions with* $f_h = 0$ *and* $F < 0$

   In this case, we have:

$$\dot{\boldsymbol{\sigma}}_a = \frac{\dot{a}}{a}\boldsymbol{\sigma}_a + \dot{W}_s\boldsymbol{\beta} \tag{4.44}$$

   where:

$$\boldsymbol{\beta} = \frac{\boldsymbol{\sigma} - \boldsymbol{\sigma}_b}{TS} + a\,\mathbf{1} - \frac{\boldsymbol{\sigma} - \boldsymbol{\sigma}_b}{S} - \boldsymbol{\sigma}_a \tag{4.45}$$

$$\dot{W}_s = \frac{1}{\boldsymbol{P} : \boldsymbol{\beta}} \left\{ \boldsymbol{P} : \left(\dot{\boldsymbol{\sigma}} - \frac{\dot{a}}{a}\boldsymbol{\sigma}_a \right) - T^2 S^3 a \dot{a} \right\} \tag{4.46}$$

   The center of the yield surface, $\boldsymbol{\sigma}_b$ is now calculated explicitly from the non-intersection condition, as:

$$\boldsymbol{\sigma}_b = \boldsymbol{\sigma} - S(\boldsymbol{\sigma} - \boldsymbol{\sigma}_a) \tag{4.47}$$

3. *Plastic loading conditions with* $f_h = 0$ *and* $F = 0$

   In this case, both back-stresses $\boldsymbol{\sigma}_a$ and $\boldsymbol{\sigma}_b$ can be obtained in closed form from the non-intersection condition, as:

$$\boldsymbol{\sigma}_a = \boldsymbol{\sigma} - T(\boldsymbol{\sigma} - a\,\mathbf{1}) \qquad\qquad \boldsymbol{\sigma}_b = \boldsymbol{\sigma} - TS(\boldsymbol{\sigma} - a\,\mathbf{1}) \tag{4.48}$$

The plastic modulus H is given by

$$H = h_0 + H_1 + H_2 \tag{4.49}$$

where:

$$h_0 = -\boldsymbol{P} : \left[\frac{\mathbf{1}}{\lambda^* - \kappa^*} \left(-T^2 S^2 a^2 - \boldsymbol{P} : \boldsymbol{\sigma}_b \right) \right] \tag{4.50}$$

$$H_1 = S^2 \left(\frac{b_1}{b_{1\,\max}} \right)^{\psi} \frac{a^3}{\lambda^* - \kappa^*}\,; \qquad H_2 = \left(\frac{T b_2}{b_{2\,\max}} \right)^{\psi} \frac{a^3}{\lambda^* - \kappa^*} \tag{4.51}$$

$$b_1 = \frac{\boldsymbol{\beta} : \boldsymbol{P}}{TSa}\,; \qquad b_2 = \frac{\boldsymbol{\gamma} : \boldsymbol{P}}{TSa} \tag{4.52}$$

$$b_{1\,\max} = 2a\,(1 - T)\;; \qquad b_{2\,\max} = 2Ta\,(1 - S) \tag{4.53}$$

The 3-SKH model requires 10 model parameters – namely λ^*, N^*, A, n, m, κ^*, M, T, S and ψ – and the definition of the initial conditions for 13 state variables, *i.e.*, the components of the tensors $\boldsymbol{\sigma}_a$ and $\boldsymbol{\sigma}_b$ and the scalar quantity a.

Chapter 5

An evaluation of constitutive models to predict the behaviour of fine-grained soils with different degrees of overconsolidation

5.1 Introduction

It has been recognised since the development of critical state soil mechanics in 1960's that realistic constitutive models should consider void ratio e as a state variable. This approach, in theory, allows to use a single set of material parameters to predict the behaviour of soils with a broad range of overconsolidation ratios and thus simplifies practical application of constitutive models. As a matter of fact, however, qualitatively correct predictions of behaviour of soils with different $OCRs$ based on a single set of material parameters do not necessarily imply satisfactory performance from the quantitative point of view. An engineer aiming to apply the constitutive model for solution of practical geotechnical problems should be aware of the range of $OCRs$ for which a single set of material parameters may be used and design an experimental program accordingly.

In the present paper, performance of three constitutive models of different complexity is evaluated on the basis of triaxial tests by Hattab and Hicher [58]. Reconstituted kaolin clay was isotropically consolidated up to $p_{max} = 1000$ kPa and swelled to a mean effective stress $p = p_{max}/OCR$, with overconsolidation ratios ranging from 1 to 50. From this state a shear phase with constant mean stress p followed up to failure.

5.2 Constitutive models

Modified Cam clay model (CC) has been chosen as a reference for comparison with two advanced constitutive models based on different mathematical backgrounds, namely the three surface kinematic hardening model (3SKH), and a hypoplastic model for clays (HC).

Modified Cam clay model [117] is a basic critical state soil mechanics model. In this work a version which complies with Butterfield's [18] compression law is used, thus the isotropic virgin compression line reads

$$\ln(1+e) = N - \lambda^* \ln(p/p_r) \tag{5.1}$$

with parameters N and λ^* and a reference stress $p_r = 1$ kPa. Slope of the isotropic unloading line is controlled by the parameter κ^*, constant shear modulus G is assumed inside the yield surface and the critical state stress ratio is characterised by parameter M.

The 3SKH model [127] is an advanced example of the kinematic hardening plasticity models for soils. The model, which may be seen as an evolution of the CC model, is characterised by two kinematic surfaces in the stress space (see Fig. 5.1), which determine the extent of the elastic behaviour (yield surface) and the influence of the recent stress history (history surface).

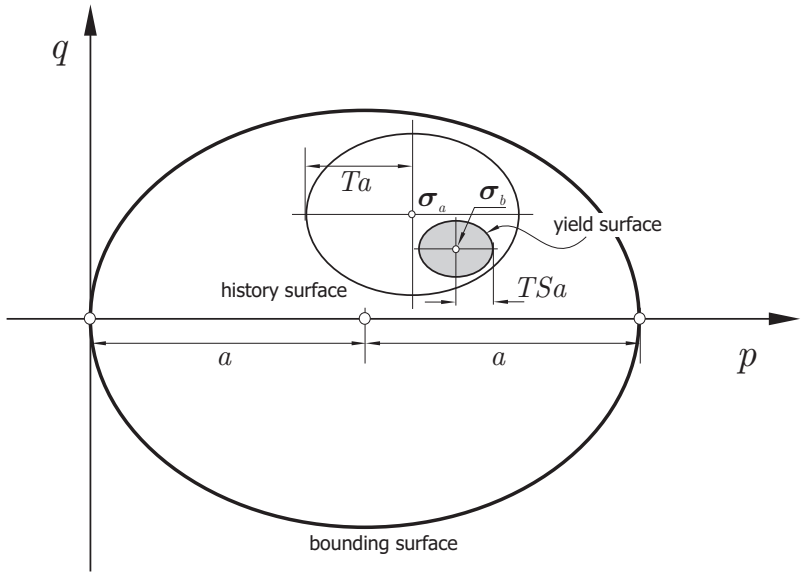

Figure 5.1: Characteristic surfaces of the 3-SKH model, from Mašín et al., 2006.

Parameters N, λ^*, κ^* and M have the same meaning as in the CC model, the shear modulus inside the elastic range G is calculated from

$$\frac{G}{p_r} = A \left(\frac{p}{p_r} \right)^n OCR^m \tag{5.2}$$

with parameters A, n and m. Parameters T and S characterise relative sizes of kinematic surfaces (Fig. 5.1). The last parameter ψ controls the rate of decay of both bulk and shear moduli for states at the yield surface, inside bounding surface (Fig. 5.1).

A hypoplastic constitutive model for clays was proposed by Mašín [87] and investigated further by Mašín and Herle [97]. It combines the mathematical formulation of hypoplastic models (e.g., Reference [77]) with the basic principles of the CC model. The rate formulation is governed by a single non-linear equation

$$\dot{\boldsymbol{\sigma}} = f_s \boldsymbol{\mathcal{L}} : \dot{\boldsymbol{\epsilon}} + f_s f_d \mathbf{N} \|\dot{\boldsymbol{\epsilon}}\| \tag{5.3}$$

with constitutive tensors $\boldsymbol{\mathcal{L}}$ and $\mathbf{N}$ and scalar factors f_s and f_d, no switch function is introduced to distinguish between loading and unloading and strains are not sub-divided into elastic and plastic parts as in elasto-plasticity.

The model requires five parameters with a similar physical interpretation as parameters of the CC model. N and λ^* are coefficients in the Butterfield's [18] compression law (5.1), κ^* controls the slope of the isotropic unloading line in the $\ln(1+e)$ vs. $\ln(p/p_r)$ space, φ_c is the critical state friction angle. The last parameter r determines the shear modulus. Due to non-linear character of Eq. (5.3), the parameter r is usually calibrated by means of a parametric study, similarly to the parameter ψ of the 3SKH model.

5.3 Scalar error measure

A scalar error measure has been introduced in order to asses model performance in the pre-failure regime and in order to eliminate a high amount of subjectivity of model calibration.

The suitable error measure should reflect differences in both predicted and observed stiffnesses and strain path directions. As experiments and simulations are characterised by identical stress paths, simulation error is measured in the strain space. Let the pre-failure part of the stress path be subdivided into L increments, of length $\Delta q = q_{max}/L$. Then, following Mašín et al. [99], the simulation error can be defined as

$$err(OCR, q_{max}) = \frac{\sum_{k=1}^{L} \left\| \Delta\boldsymbol{\epsilon}_{sim}^{(k)} - \Delta\boldsymbol{\epsilon}_{exp}^{(k)} \right\|}{\sum_{k=1}^{L} \left\| \Delta\boldsymbol{\epsilon}_{exp}^{(k)} \right\|} \tag{5.4}$$

where $\Delta\boldsymbol{\epsilon}_{exp}^{(k)}$ and $\Delta\boldsymbol{\epsilon}_{sim}^{(k)}$ are the measured and predicted strain increment tensors, respectively, corresponding to the k–th stress increment of size Δq.

In order to demonstrate the meaning of the numerical value of err, it is plotted for two special cases in Fig. 5.2. First, experiment and simulation with identical strain path directions and different incremental stiffnesses (measured by their ratio $\alpha = \|\Delta\boldsymbol{\epsilon}_{exp}^{(k)}\|/\|\Delta\boldsymbol{\epsilon}_{sim}^{(k)}\|$ from (5.4), i.e. $\alpha = G_{sim}/G_{exp} = K_{sim}/K_{exp}$, where G and K are shear and bulk moduli respectively) are considered. In the second case experiment and simulation are characterised by identical incremental stiffnesses ($\alpha = 1$), but different directions of the strain

paths measured by the angle ψ_ϵ in the Rendulic plane of $\boldsymbol{\epsilon}$ (ϵ_a vs. $\sqrt{2}\epsilon_r$, where ϵ_a and ϵ_r are axial and radial strains respectively). Investigation of (5.4) reveals that $err = |1 - 1/\alpha|$ for the first case and $err = |2\sin(\Delta\psi_\epsilon/2)|$ for the second one (with $\Delta\psi_\epsilon = \psi_{\epsilon\ sim} - \psi_{\epsilon\ exp}$).

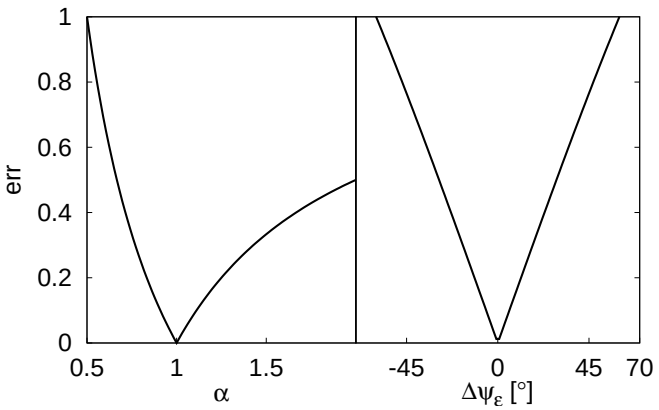

Figure 5.2: Numerical values of *err* for experiments and simulations that differ only in incremental stiffnesses (left) and strain path directions (right).

Calculation of *err* is complicated by the scatter in experimental data, in particular for low p (high OCR). For calculating of *err* the data were approximated by polynomial functions of the form

$$\epsilon_s = a_s q^{b_s} + c_s q^{d_s} + e_s q^{f_s} \ldots \tag{5.5}$$

and

$$\epsilon_v = a_v q^{b_v} + c_v q^{d_v} + e_v q^{f_v} \ldots \tag{5.6}$$

with coefficients a_s, b_s, c_s, d_s, e_s, f_s ... and a_v, b_v, c_v, d_v, e_v, f_v .... In this way a good fit of experimental data was achieved, as demonstrated in Fig. 5.3 for an experiment with $OCR = 10$.

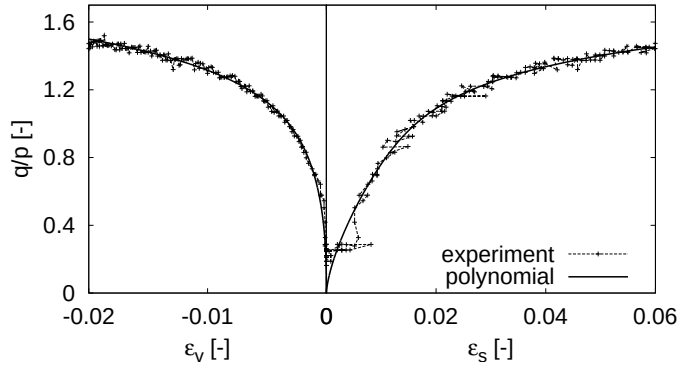

Figure 5.3: Approximation of experimental data for $OCR = 10$ by a polynomial function.

In the present work, for all simulations q_{max} from (5.4) is chosen such that $q_{max} = 0.7q_{peak}$, where q_{peak} is the peak deviator stress achieved in the particular experiment. L in (5.4) is high enough so it does not influence calculated err (typically $L = 100$ was used).

5.4 Calibration

The parameters of the studied constitutive models can be roughly split into two groups. In one group are parameters with a clear physical meaning, which are calibrated by standardized calibration procedures. On the other hand, parameters from the second group are less clearly defined and their calibration is more subjective. These parameters are usually found by means of parametric studies.

5.4.1 The first group of parameters

In the present work, parameters from the first group were calibrated only once and their values were kept constant for all simulations.

To this group belong parameters N, λ^* and κ^*, which were found by evaluation of an isotropic loading and unloading test, as demonstrated for the CC model in Fig. 5.4. Note that the numerical values of the parameter κ^* (Tab. 5.1) differ for the three constitutive models. In the 3SKH model κ^* specifies a bulk stiffness in the *small strain* range and it was calculated from an assumed Poisson ratio (accurate volumetric measurements in the small strain range were not available). In the HC model the slope of the isotropic unloading line is for higher $OCRs$ influenced also by the non-linear character of the hypoplastic equation. For this reason κ^* of the HC model could be considered to belong to the second group of parameters. However, as it has only minor effect on predictions of constant p experiments (which are in scope of this study), its value was kept constant for all simulations. An

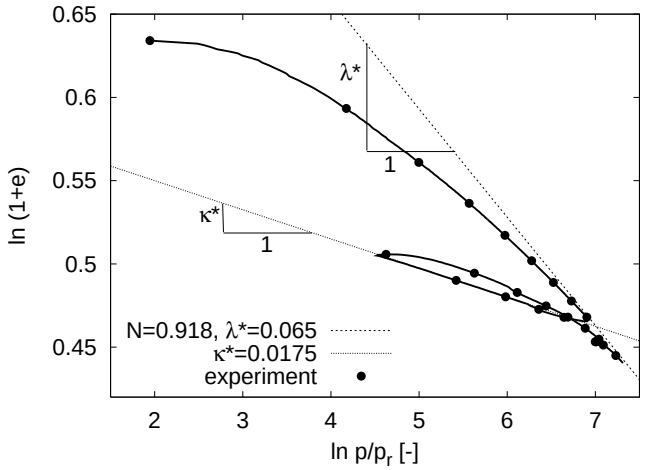

Figure 5.4: Calibration of parameters N, λ^* and κ^* of the CC model.

approximate average value of the critical state friction angle from all shear experiments available was used to calculate the parameter M (φ_c).

The 3SKH model requires five further parameters that control the behaviour in the small strain range and the influence of the recent history (A, n, m, T and S). Data by Hattab and Hicher [58] do not contain experiments required for their calibration. However, as similar soil (Speswhite kaolin) was used by Stallebrass and Taylor [127], the additional parameters of the 3SKH model were taken over from their work.

5.4.2 The second group of parameters

These parameters, namely G (CC), r (HC) and ψ (3SKH), influence significantly results of constant p experiments in the pre-failure regime and their calibration is to some extent subjective. In order to eliminate this subjectivity, these parameters were found by minimizing the scalar error measure err defined in Sec. 5.3. This procedure was applied on constant p experiments at $OCR = 1$ and $OCR = 10$, so two sets of material parameters (optimised for $OCR = 1$ and $OCR = 10$) were obtained (Tab. 5.1).

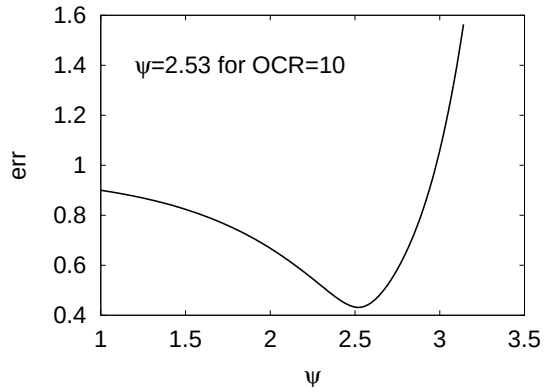

Figure 5.5: Calibration of ψ by means of minimalisation of err for experiment at $OCR = 10$.

Calibration of parameters from the second group is in the following demonstrated by means of calibration of ψ using an experiment at $OCR = 10$.

Relation of err with respect to the value of ψ is shown in Fig. 5.5. The curve has a clear minimum that corresponds to $\psi = 2.53$. This optimised value of ψ, together with two different values, were used for simulation of the experiment at $OCR = 10$ (Fig. 5.6). In the pre-failure regime the value of ψ found by optimisation with respect to err corresponds quite well to the value that could have been chosen by means of a subjective trial-and-error calibration procedure.

Parameters r and G were found using the same procedure as outlined above, a clear minimum of err was obtained in all cases. The only difference was in the calibration of ψ for $OCR = 1$, as the stress state of the 3SKH model is on the bounding surface and therefore ψ does not influence model predictions. In this case ψ was found by trial-and-error by

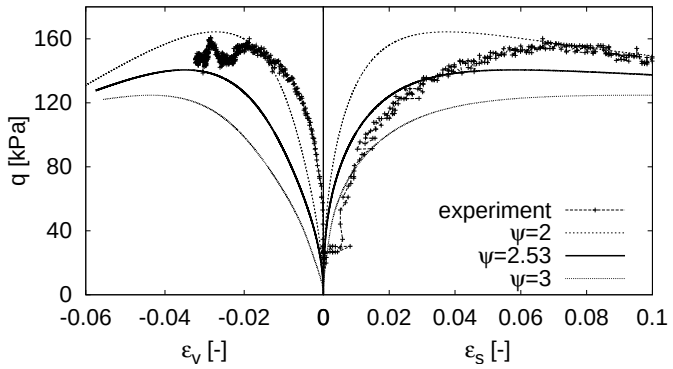

Figure 5.6: Predictions of the test OCR=10 by the 3SKH model with *err*-optimised ($\psi = 2.53$) and two different values of ψ.

simulation of the isotropic unloading test from Fig. 5.4.

Table 5.1: Material parameters

	M, φ_c	λ^*	κ^*	N	
CC	1.1	0.065	0.0175	0.918	
HC	27.5°	0.065	0.01	0.918	
3SKH	1.1	0.065	0.0034	0.918	
	A	n	m	T	S
3SKH	1964	0.65	0.2	0.25	0.08
	G, r, ψ (OCR1)		G, r, ψ (OCR10)		
CC	7330 kPa		2210 kPa		
HC	1.43		0.67		
3SKH	2.3		2.53		

5.5 Performance of the models

The two sets of parameters found in Sec. 5.4 were used in simulating experiments at the whole range of $OCRs$. The initial states of p', q and e measured in the experiments were used in the simulations. In addition, the 3SKH model requires to specify the initial positions of kinematic surfaces. These were aligned to reflect the stress history followed in the experiments (Sec. 5.1).

The obtained scalar error measure *err* is plotted with respect to OCR in Fig. 5.7. From

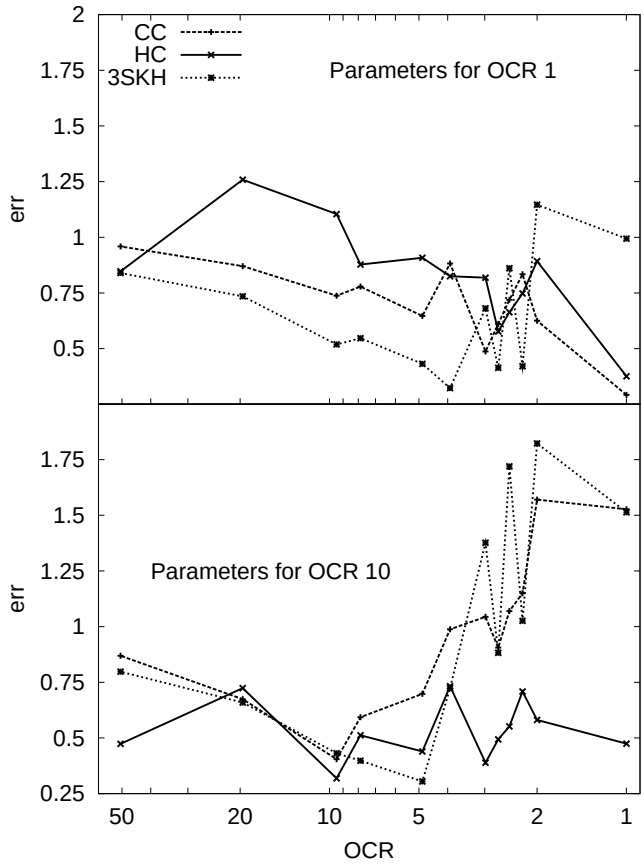

Figure 5.7: *err* for parameters optimised for $OCR = 1$ (top) and $OCR = 10$ (bottom).

this figure it appears that studied elasto-plastic and hypoplastic models have different ranges of validity of different sets of material parameters:

1. Hypoplastic (HC) model performs for higher $OCRs$ less correctly than other two models when calibrated using data for $OCR = 1$. However, when calibrated at higher OCR, it produces the best predictions out of all tested models for the entire range of $OCRs$, with more-or-less constant value of err.

2. Elasto-plastic (CC and 3SKH) models calibrated at $OCR = 10$ perform relatively correctly up to $OCR \approx 4$. For lower $OCRs$ parameters for normally consolidated state lead to better predictions, but in the case of 3SKH still worst than predictions by hypoplasticity.

By definition, the value of err characterises model predictions in the pre-failure regime only. In order to evaluate predictions at failure, observed and predicted peak friction angles φ_p were plotted with respect to OCR. The results were similar for both sets of parameters, Fig. 5.8 shows them for parameters optimised for $OCR = 10$. HC and 3SKH models predict

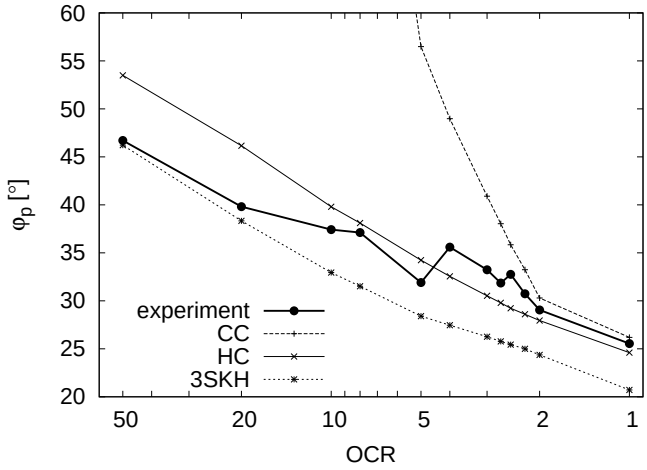

Figure 5.8: Peak friction angles φ_p predicted by the models with parameters optimised for $OCR = 10$.

peak friction angles relatively accurately (HC is more accurate for $OCR \leq 10$, 3SKH for $OCR \geq 20$). CC model overestimates significantly φ_p for all states with $OCR > 2$. This is a well-known shortcoming of the CC model, caused by the elliptical shape of the yield surface.

While *err* gives a convenient quantitative measure of the model performance, it does not specify the source of the prediction error. For qualitative comparison, the stress paths normalised by the Hvorslev equivalent pressure p_e^* are plotted for $OCR = 10$ optimised parameters in Fig. 5.9a. Overprediction of φ_p by the CC model is clear, the shape of the normalised stress paths is predicted relatively correctly by both HC and 3SKH models. All models, however, overestimate dilation. Normalised stress paths of all models head towards a unique critical state point, which has not been reached in the experiments at higher $OCRs$ (Fig. 5.9a top). A possible reason may be in localisation of deformation in shear bands at higher $OCRs$.

q vs. ϵ_s graphs for $OCR = 10$ optimised parameters are shown in Fig. 5.9b. It is clear that higher errors for low $OCRs$ of elasto-plastic models, reflected in Fig. 5.7, are caused by the underestimation of the shear stiffness in the case of CC and overestimation of the shear stiffness in the case of 3SKH (with the exception of $OCR = 1$). Low prediction errors by the HC model (Fig. 5.7) are reflected also in qualitatively correct performance shown in Fig. 5.9b. Volumetric changes shown in Fig. 5.10 reveal a general trend of overestimation of dilation for higher $OCRs$, as already discussed in the previous paragraph. The shape of ϵ_v vs. ϵ_s curves is best predicted by the HC model. For high $OCRs$ the 3SKH model predicts dilatant behaviour immediately after the start of the shear phase, which has not been observed in the experiments. On the other hand, hypoplasticity overestimates the initial contraction for medium $OCRs$.

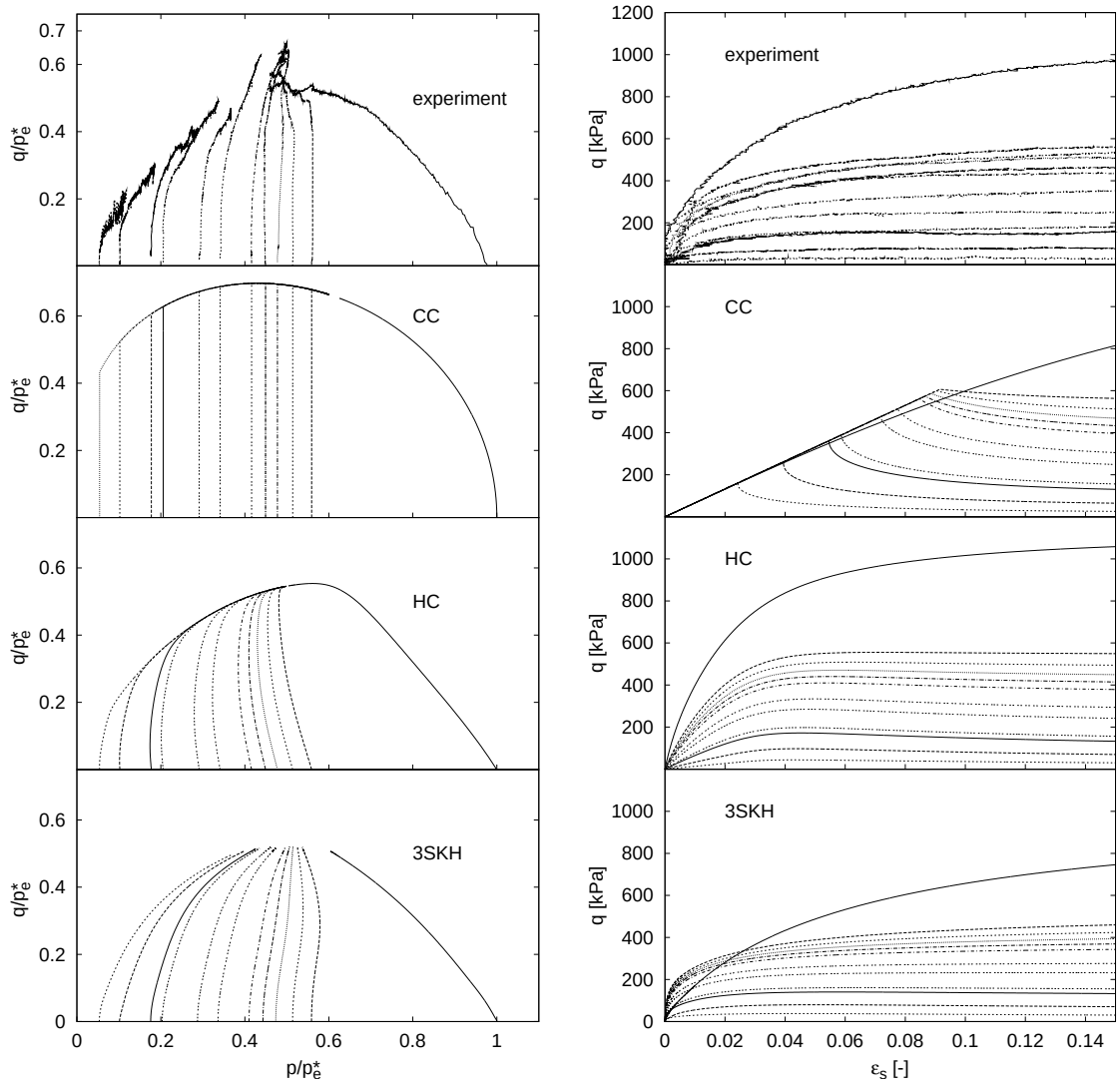

Figure 5.9: Stress paths normalised by p_e^* (a) and q vs. ϵ_s graphs (b) for $OCR = 10$ optimised parameters.

5.6 Concluding remarks

Results of this study must be seen as preliminary, as only one set of experimental data on one particular soil was investigated. Presented results however show that at least two sets of material parameters should be considered for both hypoplastic and elasto-plastic models. It appears that the HC model requires a different set of material parameters only for normally consolidated soil, a single set of parameters, which leads to accurate predictions for a broad range of $OCRs$, is sufficient for $OCR > 1$. Two sets of parameters should also

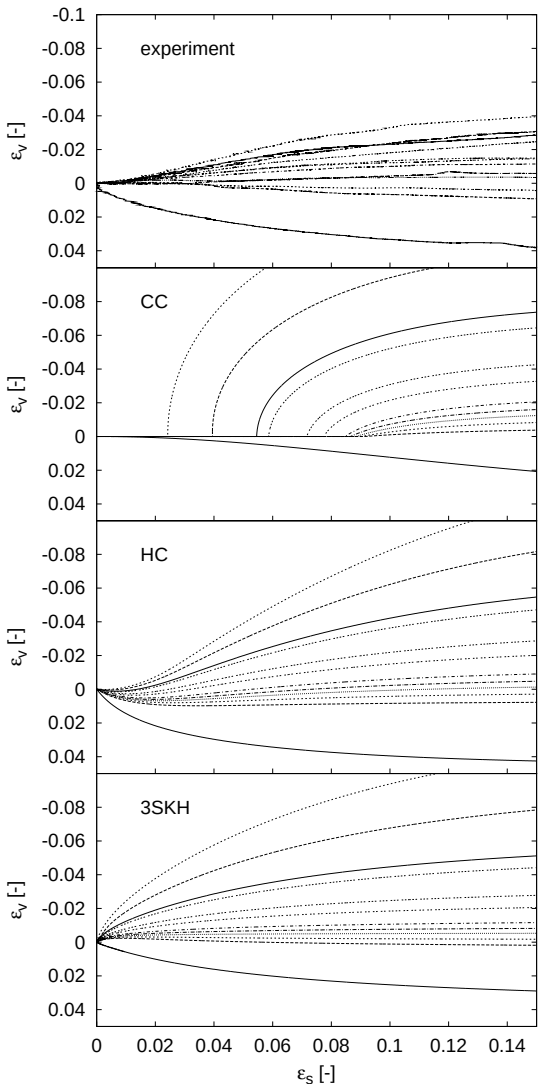

Figure 5.10: ϵ_v vs. ϵ_s graphs for $OCR = 10$ optimised parameters.

be used for studied elasto-plastic models, with the approximate limiting $OCR \approx 4$.

It is perhaps not surprising that the two advanced models performed significantly better than the CC model in predicting the non-linear behaviour in the pre-failure regime and correctly estimating the peak friction angles for high $OCRs$. For higher $OCRs$ the HC model leads to better predictions than the 3SKH, both from the point of view of the scalar error measure *err* and a qualitative performance expressed by the stress - strain diagrams. Also, the 3SKH model can not be effectively calibrated to predict correctly the behaviour of soils in normally consolidated state.

Chapter 6

A hypoplastic constitutive model for clays with meta-stable structure

6.1 Introduction

Constitutive modelling of natural structured clays has observed a notable development in past years. The research is driven by need for suitable design procedures, which would allow a practising engineer to perform analyses which are reliable and safe, but still sufficiently cheap. Apart from the accuracy in reproducing the soil behaviour, the model used for this purpose should be easy to calibrate on the basis of laboratory experiments performed in a standard experimental equipment available in practice. The main objective of the research presented in this paper is to provide an advanced constitutive model for structured clays that fulfills these requirements.

Most of the currently available constitutive models, which describe the destructuration processes in natural clays are developed within the framework of elasto-plasticity and visco-plasticity and may be seen as different extensions of the classical critical state model, developed at Cambridge University in 1960's [117]. This model is usually modified by incorporating the second hardening law, which describes the progressive changes of structure of natural clay. The most simple models (such as the model by Liu and Carter [82]) do not assume any other alteration of the original model, Wheeler et al. [145] include anisotropic effects by modifying the shape of the state boundary surface. These models, however, are not capable of predicting non-linearity of behaviour of overconsolidated soils. This shortcoming is overcome by more advanced models that make use of the kinematic hardening plasticity [103], such as models from References [8, 118, 71, 46]. Different approaches to treat the behaviour of structured soils include the multilaminate framework [37], visco-plasticity [116], and super/subloading yield surface approach [5]. A common feature of these models is that the improvement in accuracy of predictions is often paid

by an increase of complexity of calibration procedures and mathematical formulation, thus reducing their suitability for application in a routine design.

In the text, the usual sign convention of soil mechanics (compression positive) is adopted throughout. In line with the Terzaghi principle of effective stress, all stresses are *effective* stresses. Common tensor notation (see, e.g., Reference [97]) is used.

6.2 Reference constitutive model

The theory of hypoplasticity [75, 77], developed independently at Universities of Karlsruhe and Grenoble (see [133]), was in the past applied successfully in the development of constitutive relations for granular materials [53, 141, 29]. More recently, the research focused on the development of hypoplastic constitutive models for fine-grained soils [105, 54, 61]). Mašín [87] proposed a new hypoplastic constitutive model for clays, which combines mathematical structure of hypoplastic models with the basic principles of the critical state soil mechanics and the Modified Cam clay model. Predictive capabilities of this model, compared with other advanced constitutive models, have been demonstrated, e.g., in References [99, 56]. The hypoplastic model for clays will be used as a reference model for the proposed modification.

The rate formulation of hypoplastic models is, in general [80], characterised by a single equation [53][1]

$$\dot{\boldsymbol{\sigma}} = f_s \boldsymbol{\mathcal{L}} : \dot{\boldsymbol{\epsilon}} + f_s f_d \mathbf{N} \|\dot{\boldsymbol{\epsilon}}\| \tag{6.1}$$

where $\boldsymbol{\mathcal{L}}$ and $\mathbf{N}$ are fourth- and second-order constitutive tensors respectively, f_s is *barotropy* factor that incorporates the influence of the mean stress and f_d is a *pyknotropy* factor, which controls the influence of the relative density (overconsolidation ratio). Cauchy stress $\boldsymbol{\sigma}$ and void ratio e are considered as state variables. Complete mathematical formulation of the reference model is given in Appendix.

The model requires five material parameters, namely φ_c, N, λ^*, κ^* and r. φ_c is the critical state friction angle. Parameters N and λ^* define the position and shape of the isotropic virgin compression line with the formulation according to Butterfield [18]:

$$\ln(1+e) = N - \lambda^* \ln\left(\frac{p}{p_r}\right) \tag{6.2}$$

where p_r is the reference stress 1kPa. The parameter κ^* determines bulk modulus at overconsolidated states and the parameter r controls shear modulus. Although direct calibration of parameters κ^* and r is possible [87], it is suggested to determine their values by means of parametric studies.

[1] To be more precise, the rate formulation of hypoplastic models reads $\mathring{\boldsymbol{\sigma}} = f_s \boldsymbol{\mathcal{L}} : \mathbf{D} + f_s f_d \mathbf{N} \|\mathbf{D}\|$, where $\mathring{\boldsymbol{\sigma}}$ is the objective stress rate and $\mathbf{D}$ the Euler's stretching tensor. See, e.g., References [78, 14] for details.

6.3 Conceptual approach for incorporation of structure effects into constitutive models

A conceptual framework for the behaviour of structured fine-grained soils was presented by Cotecchia and Chandler [34]. They demonstrated that the influence of structure in fine-grained soils can be quantified by the different sizes of the state boundary surfaces[2] of the structured and reference materials (Fig. 6.1), where as the reference material is usually considered soil reconstituted under standard conditions [17]. Cotecchia and Chandler [34] show that assuming a geometric similarity between the state boundary surfaces of natural and reference materials appears to be a reasonable approximation, although strongly anisotropic natural soils may exhibit SBS which is not symmetric about the isotropic axis.

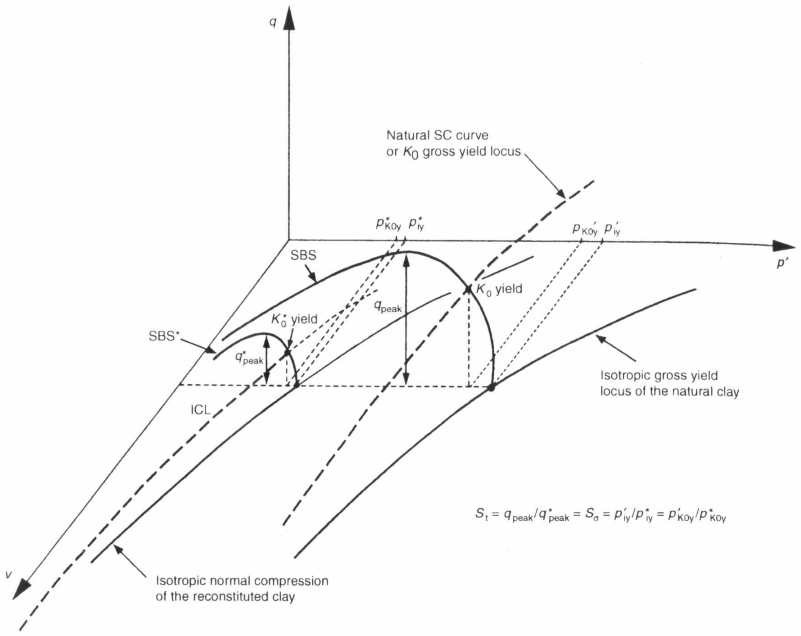

Figure 6.1: Framework for structured fine-grained materials (Cotecchia and Chandler 2000)

These observations are, in principle, applied in most of the currently available constitutive models for structured soils. In general, at least one additional state variable describing the effects of structure is needed, namely the ratio of sizes of SBSs of natural and reference materials, referred to as 'sensitivity' (s). s represents natural fabric and degree of bonding between soil particles. The limit value usually characterise the reference soil ($s = 1$), although higher values may be reasonable for soils with 'stable' elements of structure caused by natural fabric [8]. s is usually considered as a function of accumulated plastic strain.

[2]State boundary surface (SBS) is defined as a boundary of all possible states of a soil element in the stress-void ratio space.

6.4 Incorporation of structure effects into hypoplasticity

As opposed to the most elasto-plastic models, the mathematical formulation of hypoplastic models does not include explicitly the state boundary surface. However, Mašín and Herle [97] demonstrated that the model formulation allows us to derive an expression for the so-called swept-out-memory (SOM) surface, which is a close approximation of the state boundary surface.

They have shown that for any permitted stress state it is possible to calculate explicitly the value of the *pyknotropy* factor f_d on the swept-out-memory surface:

$$f_d = \|f_s \boldsymbol{\mathcal{A}}^{-1} : \mathbf{N}\|^{-1} \tag{6.3}$$

where the fourth-order tensor $\boldsymbol{\mathcal{A}}$ is expressed as

$$\boldsymbol{\mathcal{A}} = f_s \boldsymbol{\mathcal{L}} - \frac{1}{\lambda^*} \boldsymbol{\sigma} \otimes \mathbf{1} \tag{6.4}$$

Equations (6.3) and (6.31) can be combined to find the expression for the Hvorslev equivalent pressure p_e^* for a given stress state $\boldsymbol{\sigma}$ on the swept-out-memory surface and thus to determine the shape of the SOM surface in the normalised space $\boldsymbol{\sigma}/p_e^*$:

$$p_e^* = 2p\|f_s \boldsymbol{\mathcal{A}}^{-1} : \mathbf{N}\|^{1/\alpha} \tag{6.5}$$

where the Hvorslev equivalent pressure p_e^* on the isotropic normal compression line is defined as (from (6.2), Fig. 6.2)

$$p_e^* = p_r \exp\left[\frac{N - \ln(1+e)}{\lambda^*}\right] \tag{6.6}$$

Since the swept-out-memory surface is not given *a priori*, its shape is dependent on the model parameters, namely φ_c and the ratio κ^*/λ^*. For parameters typical to fine-grained soils its shape is similar to the state boundary surface of the Modified Cam clay model (see Fig. 6.3 for different parameter sets).

As summarised in the Introduction, constitutive modelling of structured soils using the framework of elasto-plasticity has recently undergone a notable development. Only few attempts, however, have been made to incorporate structure effects into hypoplastic models. Bauer and Wu [12, 13] enhanced the early version of the hypoplastic model for granular materials [149], which considers Cauchy stress $\boldsymbol{\sigma}$ the only state variable, by the so-called structure tensor $\mathbf{S}$. The Cauchy stress $\boldsymbol{\sigma}$ is in the model replaced by the "transformed stress tensor" $\boldsymbol{\sigma}^t$, defined as

$$\boldsymbol{\sigma}^t = \boldsymbol{\sigma} + \mathbf{S} \tag{6.7}$$

This transformation shifts the limit state locus in the stress space, thus enabling modelling the cohesive behaviour of cemented materials. A suitable evolution equation for the structure tensor $\mathbf{S}$ then allows us to simulate degradation of cementation bonds.

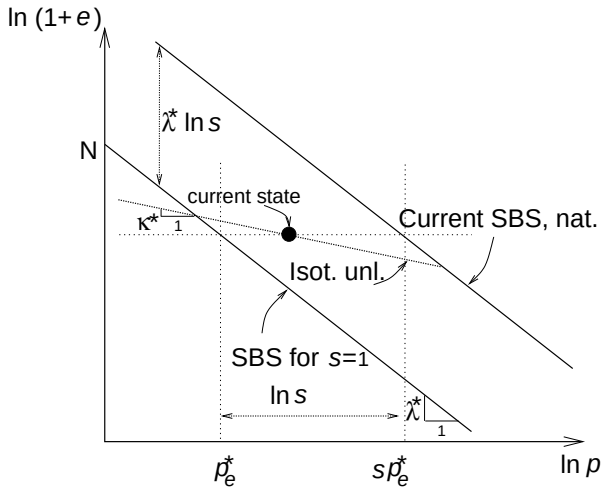

Figure 6.2: On definitions of the sensitivity s, Hvorslev equivalent pressure p_e^* and material parameters N, λ^* and κ^*.

A different approach for incorporating the structure effects into hypoplastic model is proposed in the present work. Soil with stable structure (constant sensitivity) is considered first, following Ingram [65]. As in the present work sensitivity s is measured along *constant volume* sections through the state boundary surfaces (Fig. 6.2), the Hvorslev equivalent pressure of the structured material is calculated by sp_e^* (Fig. 6.2). It follows from the expression of the SOM surface (Eqs. (6.3)-(6.6)) that the reference hypoplastic model may be modified for clays with stable structure by a simple replacement of p_e^* in the expression for f_d (see Eq. (6.31) in Appendix) by sp_e^*:

$$f_d = \left(\frac{2p}{sp_e^*} \right)^{\alpha} \tag{6.8}$$

Eq. (6.8) causes that the SBS of a natural soil is s times larger than the SBS of a corresponding reference material. It also follows from Fig. 6.2 that the normal compression line of a natural soil is shifted along $\ln(1+e)$ axis in the $\ln(1+e)$ vs. $\ln p$ space by $\lambda^* \ln s$. Additional enhancement by the transformed stress tensor $\boldsymbol{\sigma}^t$ (6.7) would shift the SBS along the isotropic axis and thus would allow us to model true cohesive behaviour due to cementation bonds [89]. For simplicity, the latter modification is omitted in this Note.

Second, the model is modified to predict the structure degradation. The proposed evolution equation for sensitivity s reads (similarly to Baudet and Stallebrass [8])

$$\dot{s} = -\frac{k}{\lambda^*}(s - s_f)\dot{\epsilon}^d \tag{6.9}$$

where k is a constitutive parameter that controls the rate of the structure degradation and s_f is the final sensitivity. The damage strain $\dot{\epsilon}^d$ is defined by

$$\dot{\epsilon}^d = \sqrt{(\dot{\epsilon}_v)^2 + \frac{A}{1-A}(\dot{\epsilon}_s)^2} \tag{6.10}$$

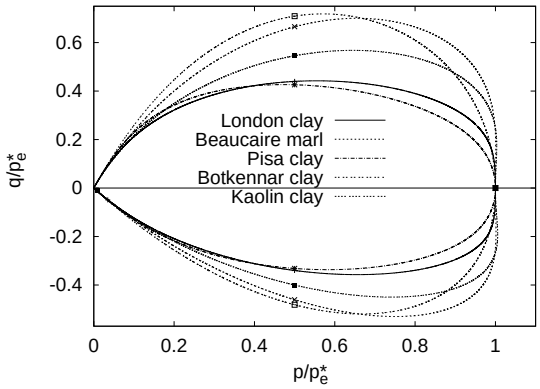

Figure 6.3: SOM surface of the hypoplastic model for clays for five different sets of material parameters (London clay – Mašín 2005; Beaucaire marl – Mašín et al. 2006; Kaolin – Hájek and Mašín 2006; Bothkennar and Pisa clay – this study.).

with the parameter A, which controls the relative importance of the volumetric and shear components (similarly to Rouiania and Wood [118]). Obviously, Eq. (6.10) does not allow modelling purely deviatoric structure degradation process ($A \to 1$). Nevertheless, the research in References [118, 46, 23] indicate that the value of the parameter A may be for most clays expected in the range ($0 < A < 0.5$).

In order to incorporate the variable sensitivity into the hypoplastic model, the *barotropy* factor f_s needs to be modified to ensure consistency between the model predictions and the structure degradation law (6.9). Formulation of the model for the isotropic compression from the isotropic normally compressed state is given by

$$\dot{p} = -\left[\frac{1}{3\,(1+e)} f_s \left(3 + a^2 - 2^{\alpha} a\sqrt{3}\right)\right] \dot{e} \tag{6.11}$$

The isotropic normal compression line of the model incorporating structure reads (see Fig. 6.2)

$$\ln(1+e) = N + \lambda^* \ln s - \lambda^* \ln\left(\frac{p}{p_r}\right) \tag{6.12}$$

Time differentiation of (6.12) results in

$$\frac{\dot{e}}{1+e} = \lambda^* \left(\frac{\dot{s}}{s} - \frac{\dot{p}}{p}\right) \tag{6.13}$$

The isotropic formulation of the structure degradation law (6.9-6.10) is

$$\dot{s} = \frac{k}{\lambda^*}(s - s_f)\frac{\dot{e}}{1+e} \tag{6.14}$$

Combination of (6.13) and (6.14) yields

$$\frac{\dot{p}}{p} = -\left[\frac{s - k(s - s_f)}{\lambda^* s}\right] \frac{\dot{e}}{1+e} \tag{6.15}$$

which may be compared with (6.11) to find an expression for the *barotropy* factor f_s of the new hypoplastic model:

$$f_s = S_i \frac{3p}{\lambda^*} \left(3 + a^2 - 2^\alpha a\sqrt{3}\right)^{-1} \tag{6.16}$$

with the factor

$$S_i = \frac{s - k(s - s_f)}{s} \tag{6.17}$$

Thus the factor f_s of the modified model reads $f_s = S_i f_{sr}$, where f_{sr} is the barotropy factor of the reference model (see Eq. (6.30) in Appendix).

It follows from (6.1) that the factor f_s controls the directional tangential stiffness of material (in terms of response envelopes [50] it controls their size). Therefore, the decrease of the stiffness in isotropic compression to ensure consistency with the structure degradation law (Eqs. (6.11)-(6.17)) has an undesired effect that also shear stiffness (controlled by parameter r) and stiffness in isotropic unloading (controlled by parameter κ^*) is decreased, see Fig. 6.4 (case A). Manipulation with the model reveals that the physical meaning of the parameters r and κ^* is retained if they are both scaled by the factor S_i (Fig. 6.4, case B). Therefore, modification of scalar factors c_1 (6.23) and α (6.24) is required. They now read

$$c_1 = \frac{2\left(3 + a^2 - 2^\alpha a\sqrt{3}\right)}{9 r S_i} \qquad \alpha = \frac{1}{\ln 2} \ln\left[\frac{\lambda^* - \kappa^* S_i}{\lambda^* + \kappa^* S_i}\left(\frac{3 + a^2}{a\sqrt{3}}\right)\right] \tag{6.18}$$

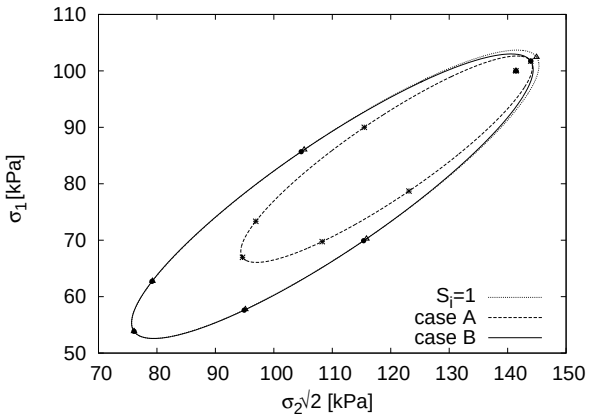

Figure 6.4: Response envelopes of the model with constant sensitivity ($S_i = 1$), model modified only by multiplication of the factor f_s by S_i (case A) and model where the physical meaning of parameters r and κ^* is retained (case B).

Equations (6.8–6.10), (6.16–6.17) and (6.18) are the only modifications of the reference hypoplastic model. The new model assumes one additional state variable s and three additional parameters: k, A, and s_f. Their calibration procedure is detailed in the following text.

6.5 Model performance and calibration

The performance of the proposed hypoplastic model will be evaluated using the concept of the *normalised incremental stress response envelopes* (NIREs, see Fig. 6.5). They have been introduced by Mašín and Herle [97] and follow directly from the concept of incremental response envelopes [134] and rate response envelopes [50].

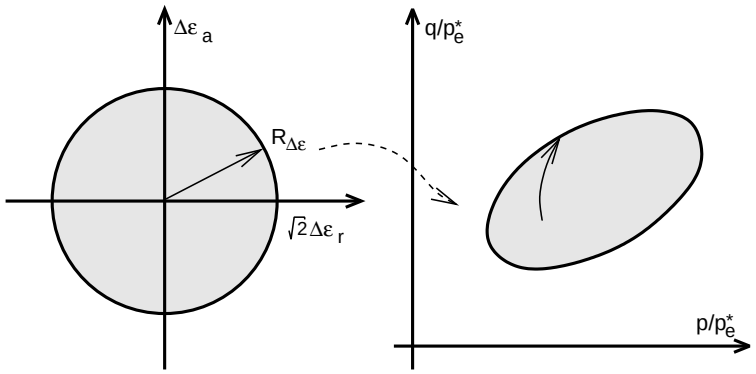

Figure 6.5: Demonstration of the *normalised incremental stress response envelopes* for axisymmetric conditions.

Figures 6.6a and 6.6b show the NIREs for different $R_{\Delta\boldsymbol{\epsilon}} = \|\Delta\boldsymbol{\epsilon}\|$ for natural and reconstituted specimens of Pisa clay (see the next section), with symbols for isotropic and constant volume loading and unloading. For small $R_{\Delta\boldsymbol{\epsilon}}$ (states well inside the swept-out-memory surface, Fig. 6.6a) the NIREs of the natural and reconstituted clays are similar in shape, the sizes of the NIREs of the natural clay are s_0 times larger than corresponding NIREs of the reconstituted clay (where s_0 is the initial sensitivity of the natural clay). We see that although the damage strain (6.10) is defined in terms of total strain rates (instead of plastic strain rates as usual in elasto-plastic models), the model predicts only minor structure degradation for states inside the SBS. Minor structure degradation also inside the SBS is supported by Takahashi et al. [128].

For larger $R_{\Delta\boldsymbol{\epsilon}}$ (Fig. 6.6b) the NIREs of the reconstituted clay coincide with its swept-out-memory surface. The progressive structure degradation of the natural clay, however, causes the NIREs of the natural clay to shrink towards the swept-out-memory surface of the reconstituted material. The heart-like shape of the NIREs of the natural clay for $R_{\Delta\boldsymbol{\epsilon}} > 8\%$ is caused by the low value of the parameter A (Tab. 6.1), which causes more significant influence of the volumetric strain component on the structure degradation.

The influence of the parameter k on model predictions is demonstrated in Fig. 6.7a. The value of the parameter k was varied, while other model parameters (Tab. 6.1) were kept unchanged. The figure demonstrates the faster structure degradation for larger values of the parameter k. The influence of the parameter A is shown in Fig. 6.7b. Larger value of the parameter A increases the influence of shear strains on the structure degradation and thus flattens the NIREs. The common point of all NIREs is at the isotropic stress state.

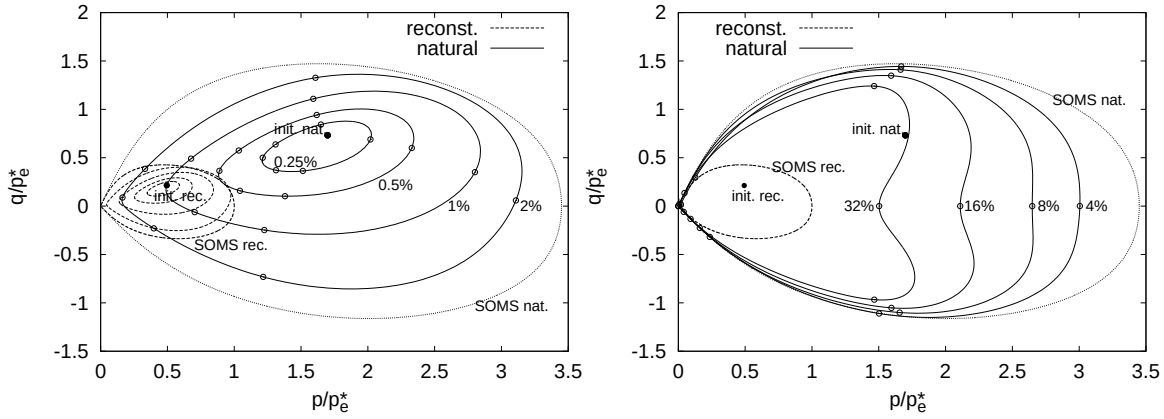

Figure 6.6: Normalised incremental stress response envelopes of the proposed hypoplastic model plotted for medium (a) and large (b) strain range ($R_{\Delta\boldsymbol{\epsilon}}$ is indicated). The envelopes for the reconstituted material obtained with the reference hypoplastic model (Mašín 2005) are also included.

Therefore, the parameter k may be calibrated independently of the parameter A on the basis of an isotropic compression test on natural soil. The parameter A is calibrated with the already known value of k using an experiment where significant shear strains develop.

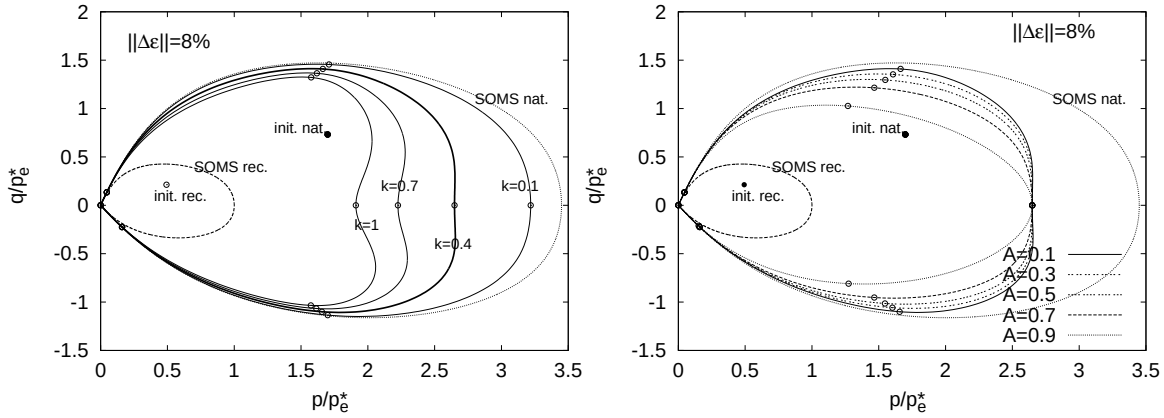

Figure 6.7: The influence of the parameter k (a) and A (b).

The initial value of sensitivity may be determined from an assumption of a geometric similarity between SBSs of natural and reconstituted soil [34] as a ratio of undrained shear strengths of natural and reconstituted soil, or as a ratio of stresses at gross yield in compression tests (e.g., K_0 or isotropic) on natural specimens and equivalent stresses at corresponding normal compression lines of a reconstituted soil. The final value of sensitivity s_f may be derived from compression tests on natural and reference materials performed to

very large strains [7].

6.6 Evaluation of model predictions

The proposed model will be evaluated on the basis of laboratory experiments on two natural clays with meta-stable structure.

Callisto and Calabresi [20] reported laboratory experiments on natural Pisa clay. Drained probing tests were performed, with rectilinear stress paths having different orientations in the stress space. In addition to the tests on natural Pisa clay, experiments with the same stress paths were performed on reconstituted clay. Tests are labelled by prefix 'A' and 'R' for natural and reconstituted clay respectively, followed by the angle of stress paths in the $q : p$ space (measured in degrees anti-clockwise from the isotropic loading direction).

All the parameters of the proposed hypoplastic model, with the exception of parameters related to the effects of structure (k, A and s_f), were be calibrated solely using laboratory experiments on the reconstituted Pisa clay. The parameters N, λ^* and κ^* were calibrated on the basis of an isotropic compression test on reconstituted Pisa clay ([19], Fig. 6.8a). Critical state friction angle φ_c has been found by evaluating the data from shear tests, parameter r has been calibrated on the basis of a parametric study using a single shear test (R60, Fig. 6.8b).

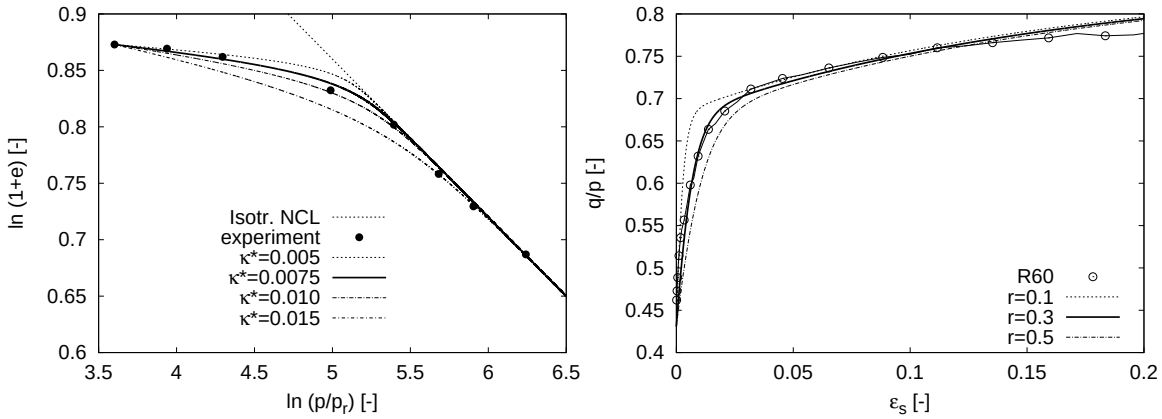

(a) (b)

Figure 6.8: Calibration of the parameters N, λ^* and κ^* on the basis of an isotropic compression test on reconstituted Pisa clay (a), parametric study for the calibration of the parameter r (b).

For the calibration of the structure-related parameters k, A and s_f, it has been *assumed*, following Callisto and Rampello [23], that the experimental procedures adopted for preparation of reconstituted specimens reproduced correctly the stress history of the Pisa clay deposit. Therefore, the stress paths of the equivalent experiments on natural and reconstituted clays should coincide, when plotted in the space normalised with respect to volume

and structure $\boldsymbol{\sigma}/(p_e^* s)$ [34]. The current value of sensitivity s may be found by the time-integration of the structure degradation law (6.9-6.10):

$$s = s_f + (s_0 - s_f) \exp\left[-\frac{k}{\lambda^*}\epsilon^d\right] \tag{6.19}$$

where ϵ^d is the accumulated damage strain

$$\epsilon^d = \int_{t_0}^{t_1} \dot{\epsilon}^d dt \tag{6.20}$$

In this way, parameters k and A (and the initial value of sensitivity s) could be calibrated directly by evaluation of the experimental data, without reference to single element modelling of tests on natural clay. Calibration of the parameter k is demonstrated in Fig. 6.9a. The shear strains in the test A0 are negligible, thus the parameter A does not influence predictions of the structure degradation process (Fig. 6.7b, Eq. (6.10)). The value of the parameter A was calibrated with the already known value of the parameter k using results from shear tests R90 and A90 (Fig. 6.9b). The final value of sensitivity s_f is assumed to be equal to one. This appears to be a reasonable approximation [7], although no compression or shear experiment on natural clay which would lead to a full destructuration is available. Parameters of the hypoplastic model for natural Pisa clay are summarised in Table 6.1 and the initial values of state variables in Table 6.2.

Table 6.1: *Parameters of the proposed hypoplastic model for Pisa clay and Bothkennar clay.*

	φ_c	λ^*	κ^*	N	r	k	A	s_f
Pisa	21.9°	0.14	0.0075	1.56	0.3	0.4	0.1	1
Bothkennar	35°	0.119	0.003	1.344	0.07	0.35	0.5	1

Table 6.2: *The initial values of the state variables for natural and reconstituted Pisa clay and natural Bothkennar clay.*

p [kPa]	q [kPa]	e reconst.	e nat.	s
88.2	38	1.302	1.738	3.45
34	18	–	1.88	6

The evaluated parameters were used for simulation of laboratory experiments on Pisa clay. Experimental data compared with predictions by the proposed hypoplastic model are shown in Figs. 6.10, 6.11 and 6.12. The figures show that the hypoplastic model, due to its non-linear nature, predicts correctly the gradual change of stiffness as the state moves towards the state boundary surface. Consequently, the model predicts in agreement

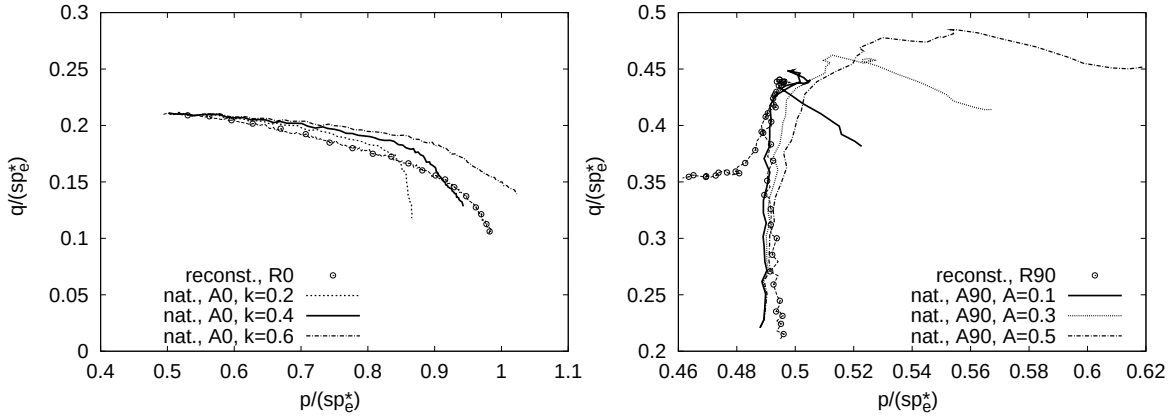

(a) (b)

Figure 6.9: Calibration of parameters k (a) and A (b) using the structure degradation law of the hypoplastic model.

with experiment smooth structure degradation process, which amplifies as the state moves towards the state boundary surface (Fig. 6.10b).

Performance of the model in the strain space is evaluated in Fig. 6.13 using the concept of incremental strain response envelopes (ISREs) [134, 99], defined inversely to the incremental stress response envelopes. The hypoplastic model (Fig. 6.13b) predicts correctly the shape of ISREs, with softer response in compression.

Experimental database by Callisto [19] includes undrained compression (AUC) and extension (AUE) tests on natural Pisa clay samples with the same pre-shear stress history as drained probes A0–A315. These tests were simulated with parameters evaluated using data from drained probes (Fig. 6.14). In compression, the proposed model predicts qualitatively correctly the shape of the stress path, but the shear stiffness and the peak friction angle are underestimated. In extension the stress-strain response is predicted correctly. However, although the final state is reproduced accurately, the model predicts significant decrease in mean stress in initial stages of the experiment that was not be observed experimentally.

Smith et al. [123] performed a series of triaxial stress probing tests on natural Bothkennar clay. The soil, classified as a very silty clay [62], is characterised by relatively high (3-5%) organic content. The soil composition induces somewhat unusual mechanical properties with high plasticity typical to fine-grained soils combined with high critical state friction angles [2]. The stress-probing experiments with constant direction of stress paths in the stress space are labelled by prefix 'LCD' followed by the orientation of the stress paths in $q : p$ space.

The parameters N and λ^* for the Bothkennar clay were calibrated using results of K_0 test on a reconstituted sample ([123], Fig. 6.18). The shape of the swept-out-memory surface of the hypoplastic model was taken into account in calculation of the parameter N from the position of the K_0 normal compression line in the $\ln(1 + e) : \ln(p/p_r)$ space. The

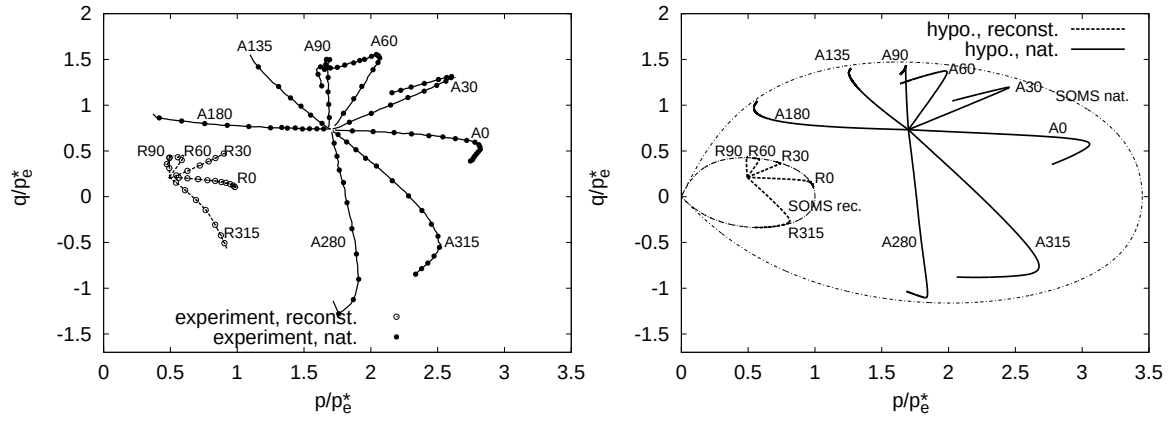

(a) (b)

Figure 6.10: Normalised stress paths of the natural and reconstituted Pisa clay (a) and predictions by the hypoplastic model (b).

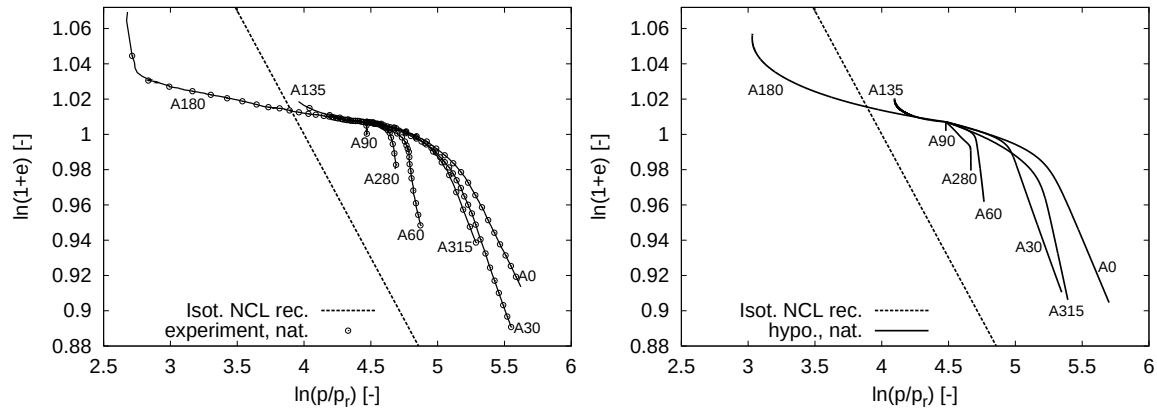

(a) (b)

Figure 6.11: Experiments on natural Pisa clay plotted in the $\ln(p/p_r)$ vs. $\ln(1+e)$ space (a) and predictions by the proposed hypoplastic model (b).

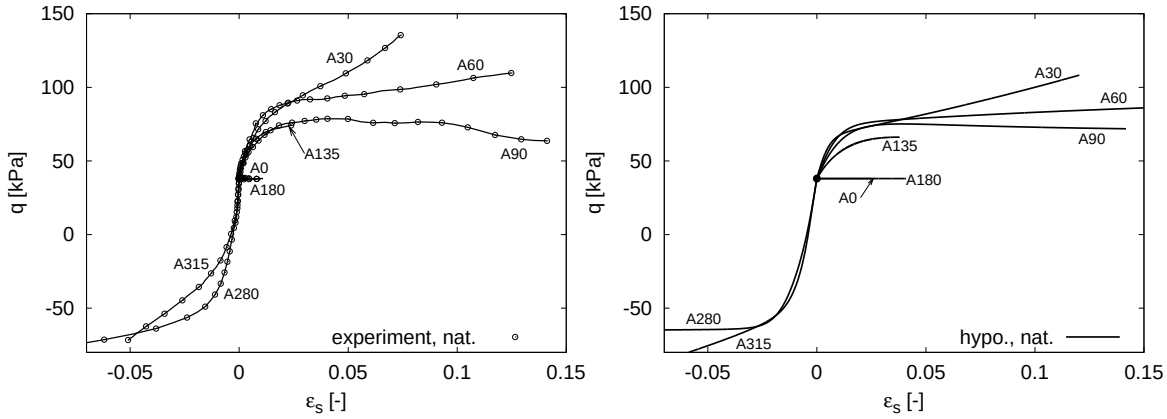

Figure 6.12: ϵ_s vs. q diagrams of experiments on natural Pisa clay (a) and predictions by the proposed hypoplastic model (b).

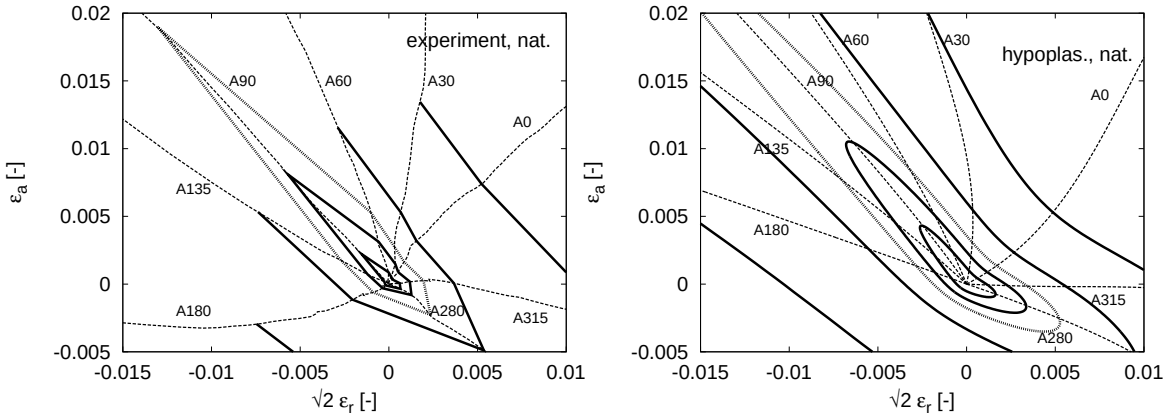

Figure 6.13: Incremental strain response envelopes for $R_{\Delta\boldsymbol{\sigma}} = \|\Delta\boldsymbol{\sigma}\|$=10, 20, 30 (broken line), 50 and 100 kPa, plotted together with strain paths in the $\sqrt{2}\epsilon_r$ vs. ϵ_a space. Experimental data on natural Pisa clay (a) and predictions by the hypoplastic model (b).

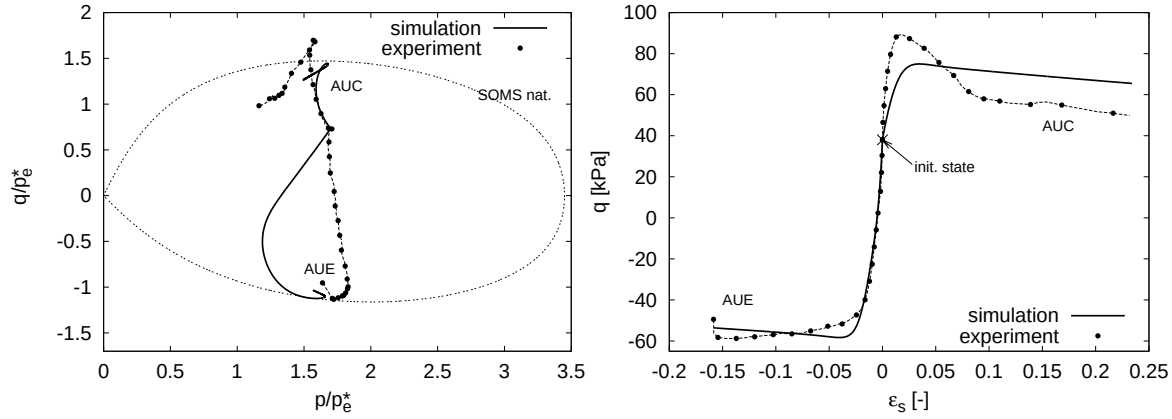

Figure 6.14: Normalised stress paths (a) and ϵ_s vs. q diagrams (b) of undrained compression (AUC) and extension (AUE) experiments on Pisa clay.

final sensitivity s_f is equal to one, as full destructuration is observed in K_0 compression experiments on natural Bothkennar clay ([123], Fig. 6.18). Because the set of stress probing tests published by Smith et al. [123] does not include equivalent experiments on reconstituted soil, other parameters including the initial value of sensitivity were evaluated directly using stress probing data on natural Bothkennar clay by means of parametric studies. The parameters and the initial values of state variables are summarised in Tabs. 6.1 and 6.2.

Comparison of experimental data from drained stress probing experiments on natural Bothkennar clay [123] with predictions by the proposed hypoplastic model are shown in Figs. 6.15–6.17. Similarly to predictions of tests on natural Pisa clay, the proposed model yields results which are in an agreement with experiments. The only notable difference is the normalised stress paths of the test LCD315 which, due to the shape of the swept-out-memory surface of the hypoplastic model, bends later than the experimental normalised stress path. In this case the rotated shape of the swept-out-memory surface would possibly lead to improvement of predictions. The incorporation of anisotropic effects, demonstrated within the hypoplastic framework, for example, by Wu [150] and Niemunis [107], is however outside the scope of this paper.

The set of parameters optimized for predictions of drained stress probing tests LCD was further used to simulate K_0 compression tests on natural Bothkennar clay. Experimental data on Laval and Sherbrooke samples from Smith et al. [123], together with predictions by the proposed hypoplastic model, are shown in Fig. 6.18. It is clear that the parameters optimized for predictions of LCD tests lead to underprediction of the structure degradation process in K_0 compression, which may be possibly attributed to larger disturbance of oedometric specimens in comparison with specimens tested in triaxial apparatuses. Similar observation is reported by Callisto et al. [21] using the kinematic hardening model for structured clays by Rouiania and Wood [118]. A better fit of the experimental data is

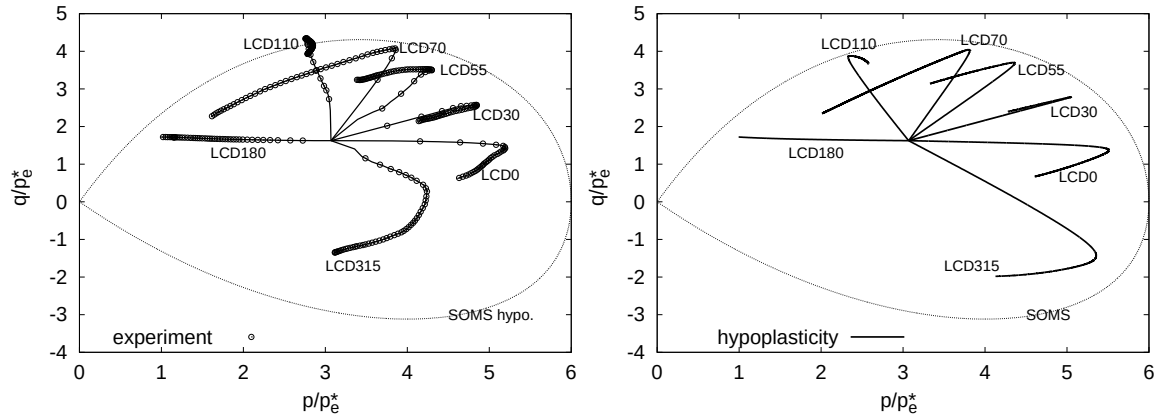

(a) (b)

Figure 6.15: Normalised stress paths of the natural and reconstituted Bothkennar clay (a) and predictions by the proposed hypoplastic model (b).

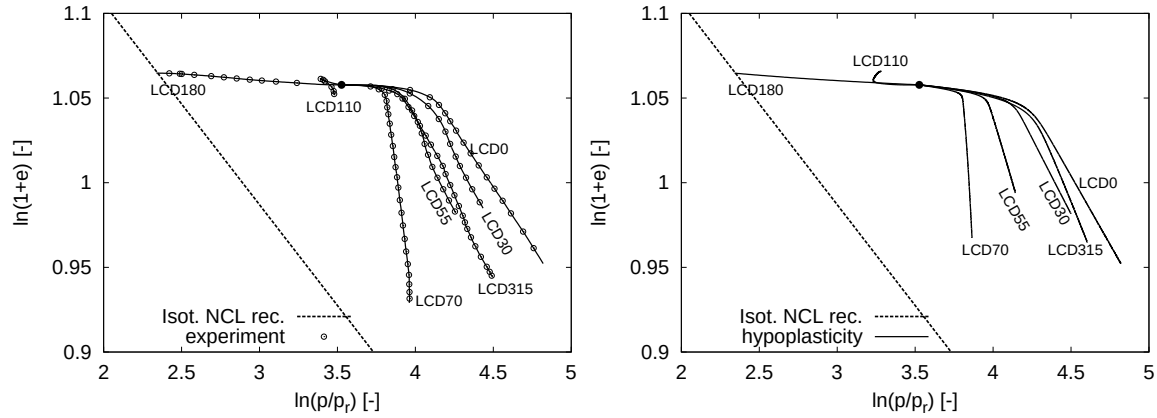

(a) (b)

Figure 6.16: Experiments on natural Bothkennar clay plotted in the $\ln(p/p_r)$ vs. $\ln(1+e)$ space (a) and predictions by the proposed hypoplastic model (b).

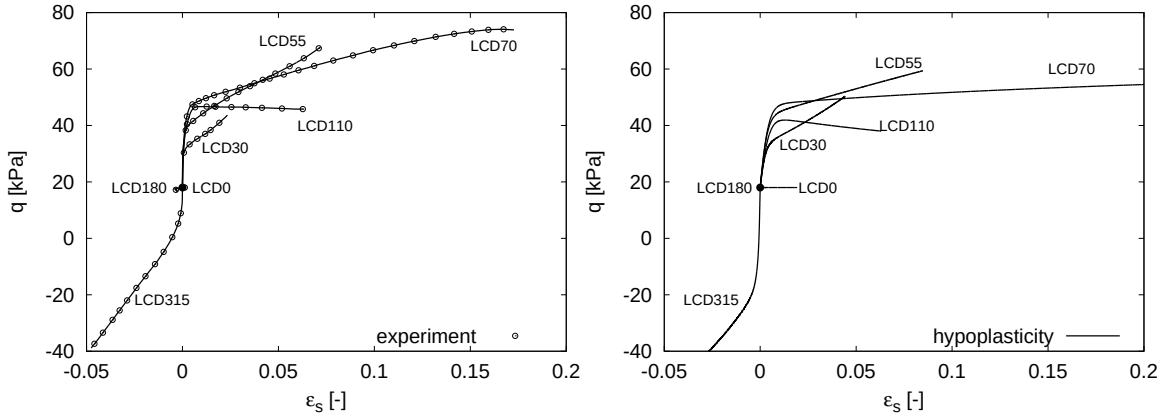

Figure 6.17: ϵ_s vs. q diagrams of experiments on natural Bothkennar clay (a) and predictions by the proposed hypoplastic model (b).

achieved by increasing the value of the parameter k ($k = 0.6$) and decreasing the initial sensitivity ($s_0 = 4$) – see also Fig. 6.18.

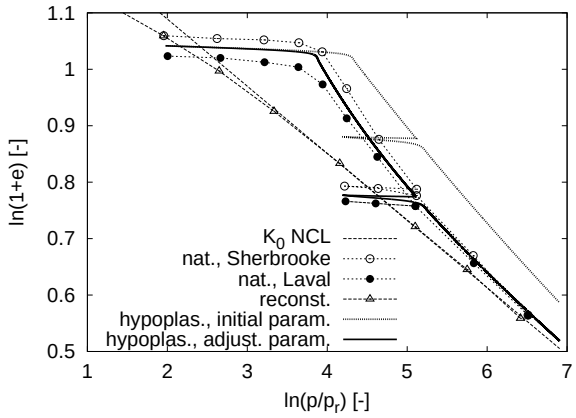

Figure 6.18: K_0 tests on natural Bothkennar clay simulated with the hypoplastic model using two sets of material parameters. "initial param.": parameters optimized for predictions of LCD tests, "adjust. param.": modified value of the parameter k ($k = 0.6$) and lower initial sensitivity ($s_0 = 4$).

6.7 Summary and conclusions

A simple approach to incorporating structure effects into an existing hypoplastic constitutive model for reconstituted clays is presented in the paper. Unlike the previous attempts to incorporate structure effects into hypoplasticity, the proposed approach is based on the

modification of the *barotropy* and *pyknotropy* factors that leads to an increase of the size of the state boundary surface predicted by the model and ensures consistency between the model predictions and the pre-defined structure degradation law. Model predictions compare well with experimental data on two natural clays. In fact, predictions of laboratory experiments on natural Pisa and Bothkennar clays presented in the paper are comparable with predictions by kinematic hardening elasto-plastic models, see [7, 21] for drained probing tests on natural Pisa clay and [8, 7, 46] for LCD tests on natural Bothkennar clay.

The proposed method for incorporating the structure effects into hypoplasticity also opens a way to model other structural effects using hypoplasticity theory, such as mechanical [79] and chemical [111] debonding in cemented granular materials, simulating grain crushing [25], or modelling unsaturated [3] and double-porosity materials [93].

Appendix

The mathematical formulation of a reference hypoplastic model for clays model is summarised briefly in the following. The rate formulation of the hypoplastic model reads

$$\dot{\boldsymbol{\sigma}} = f_s \boldsymbol{\mathcal{L}} : \dot{\boldsymbol{\epsilon}} + f_s f_d \mathbf{N} \, \|\dot{\boldsymbol{\epsilon}}\| \tag{6.21}$$

The fourth-order tensor $\boldsymbol{\mathcal{L}}$ is a hypoelastic tensor given by

$$\boldsymbol{\mathcal{L}} = 3 \left(c_1 \boldsymbol{\mathcal{I}} + c_2 a^2 \hat{\boldsymbol{\sigma}} \otimes \hat{\boldsymbol{\sigma}} \right) \tag{6.22}$$

with the two scalar factors c_1 and c_2 introduced by [61] and modified by [87]:

$$c_1 = \frac{2\left(3 + a^2 - 2^{\alpha} a \sqrt{3}\right)}{9r} \qquad\qquad c_2 = 1 + (1 - c_1)\frac{3}{a^2} \tag{6.23}$$

where the scalars a and α are functions of the material parameters φ_c, λ^* and κ^*

$$a = \frac{\sqrt{3}\,(3 - \sin\varphi_c)}{2\sqrt{2}\sin\varphi_c} \qquad\qquad \alpha = \frac{1}{\ln 2} \ln\left[\frac{\lambda^* - \kappa^*}{\lambda^* + \kappa^*}\left(\frac{3 + a^2}{a\sqrt{3}}\right)\right] \tag{6.24}$$

The second-order tensor $\mathbf{N}$ is given by Niemunis [106]

$$\mathbf{N} = \boldsymbol{\mathcal{L}} : \left(Y \frac{\mathbf{m}}{\|\mathbf{m}\|} \right) \tag{6.25}$$

where the quantity Y determines the shape of the critical state locus in the stress space such that for $Y = 1$ it coincides with the Matsuoka and Nakai [85] limit stress condition.

$$Y = \left(\frac{\sqrt{3}a}{3 + a^2} - 1 \right) \frac{(I_1 I_2 + 9 I_3)\left(1 - \sin^2\varphi_c\right)}{8 I_3 \sin^2\varphi_c} + \frac{\sqrt{3}a}{3 + a^2} \tag{6.26}$$

with the stress invariants

$$I_1 = \mathrm{tr}(\boldsymbol{\sigma}) \qquad I_2 = \frac{1}{2}\left[\boldsymbol{\sigma} : \boldsymbol{\sigma} - (I_1)^2\right] \qquad I_3 = \det(\boldsymbol{\sigma})$$

$\det(\boldsymbol{\sigma})$ is the determinant of $\boldsymbol{\sigma}$. The second-order tensor $\mathbf{m}$ has parallel in the flow rule in elasto-plasticity. It is calculated by

$$\mathbf{m} = -\frac{a}{F}\left[\hat{\boldsymbol{\sigma}} + \mathrm{dev}\,\hat{\boldsymbol{\sigma}} - \frac{\hat{\boldsymbol{\sigma}}}{3}\left(\frac{6\hat{\boldsymbol{\sigma}} : \hat{\boldsymbol{\sigma}} - 1}{(F/a)^2 + \hat{\boldsymbol{\sigma}} : \hat{\boldsymbol{\sigma}}}\right)\right] \tag{6.27}$$

with the factor F

$$F = \sqrt{\frac{1}{8}\tan^2\psi + \frac{2 - \tan^2\psi}{2 + \sqrt{2}\tan\psi\cos 3\theta}} - \frac{1}{2\sqrt{2}}\tan\psi \tag{6.28}$$

where

$$\tan\psi = \sqrt{3}\,\|\mathrm{dev}\,\hat{\boldsymbol{\sigma}}\| \qquad \cos 3\theta = -\sqrt{6}\frac{\mathrm{tr}\,(\mathrm{dev}\,\hat{\boldsymbol{\sigma}} \cdot \mathrm{dev}\,\hat{\boldsymbol{\sigma}} \cdot \mathrm{dev}\,\hat{\boldsymbol{\sigma}})}{[\mathrm{dev}\,\hat{\boldsymbol{\sigma}} : \mathrm{dev}\,\hat{\boldsymbol{\sigma}}]^{3/2}} \tag{6.29}$$

The *barotropy* factor f_s introduces the influence of the mean stress level. The way of its derivation ensures that the hypoplastic model predicts correctly the isotropic normally compressed states.

$$f_s = \frac{3p}{\lambda^*}\left(3 + a^2 - 2^\alpha a\sqrt{3}\right)^{-1} \tag{6.30}$$

The *pyknotropy* factor f_d incorporates the influence of the overconsolidation ratio. The critical state is characterised by $f_d = 1$ and the isotropic normally compressed state by $f_d = 2^\alpha$.

$$f_d = \left(\frac{2p}{p_e^*}\right)^\alpha \qquad p_e^* = p_r \exp\left[\frac{N - \ln(1+e)}{\lambda^*}\right] \tag{6.31}$$

with the reference stress $p_r = 1$ kPa. Finally, evolution of the state variable e (void ratio) is governed by

$$\dot{e} = -(1+e)\,\dot{\epsilon}_v \tag{6.32}$$

Chapter 7

Comparison of elasto-plastic and hypoplastic modelling of structured clays

7.1 Introduction

The recently developed constitutive models for structured clays are based on fundamentally different mathematical backgrounds. The conceptual approach utilised for their development is, however, often very similar. These models are usually based on existing models for reconstituted soils with modified size (and in some cases also shape) of the *state boundary surface* (SBS).

The aim of the paper is a further evaluation of a hypoplastic model for structured clays by Mašín [88]. Predictions by this model are compared with its elasto-plastic alternative developed in the paper. The Structured modified Cam clay (SMCC) model has a similar structure degradation law and the same number of parameters with an equivalent physical meaning as the hypoplastic model. Thus both models are characterised by the same calibration procedure and the same complexity from the standpoint of a practising engineer.

All simulations with the hypoplastic model are taken over from Reference [88]. The aim of the present work is to supplement these simulations by predictions of a simple elasto-plastic model and thus to reveal merits of the non-linear character of the hypoplastic formulation.

7.2 Constitutive models

7.2.1 Hypoplastic model for clays with meta-stable structure

A hypoplastic model for clays with meta-stable structure [88] has been developed by introducing a structure degradation law into the hypoplastic model for clays by Mašín [87]. Incorporation of meta-stable structure into hypoplasticity has been discussed elsewhere [88, 89]. The model assumes additional state variable *sensitivity* s^h, defined as the ratio of the sizes of SBS of structured and reference materials. Sensitivity is in the case of a hypoplastic model measured along a constant volume section through SBS, see Fig. 7.1a. The rate formulation of sensitivity reads

$$\dot{s}^h = -\frac{k}{\lambda^*}(s^h - s^h_f)\dot{\epsilon}^d \tag{7.1}$$

where k, s^h_f (final sensitivity) and λ^* are parameters and $\dot{\epsilon}^d$ is a damage strain rate, defined as

$$\dot{\epsilon}^d = \sqrt{(\dot{\epsilon}_v)^2 + \frac{A}{1-A}(\dot{\epsilon}_s)^2} \tag{7.2}$$

$\dot{\epsilon}_v$ and $\dot{\epsilon}_s$ denote volumetric and shear strain rates respectively and A is a model parameter. For further details of the mathematical structure of the model the reader is referred to Reference [88].

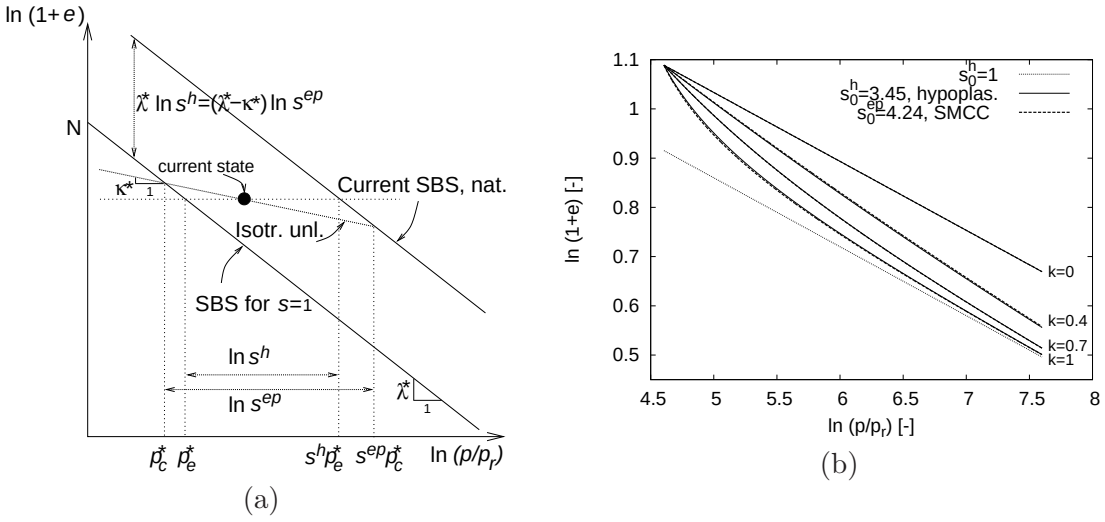

Figure 7.1: (a) Definitions of sensitivities s^{ep} and s^h, quantities p^*_c and p^*_e and material parameters N, λ^* and κ^*. (b) Demonstration of similarity of the two structure degradation laws on the basis of an isotropic compression test. p_r is a reference stress 1 kPa.

7.2.2 Structured modified Cam clay model

The SMCC model, based on the Modified Cam clay model by Roscoe and Burland [117] enhanced by Butterfield's [18] compression law, has been developed as an elasto-plastic equivalent of the hypoplastic model by Mašín [88]. The mathematical formulation of the model is similar to other elasto-plastic models for structured soils, such as the models by Liu and Carter [82] or Bauudet and Stallebrass [8].

As commonly in elasto-plastic models, sensitivity s^{ep} is measured along the *elastic wall*, not along the constant volume section through SBS as in hypoplasticity (see Fig. 7.1a). s^{ep} thus represents the ratio of the sizes of yield surfaces of natural and reference materials. From Fig. 7.1a it is clear that

$$s^{ep} = \left(s^h\right)^{\left(\frac{\lambda^*}{\lambda^* - \kappa^*}\right)} \tag{7.3}$$

The rate formulation for sensitivity s^{ep} reads

$$\dot{s}^{ep} = -\frac{k}{\lambda^* - \kappa^*}(s^{ep} - s_f^{ep})\dot{\epsilon}^d \tag{7.4}$$

and the damage strain rate is defined as

$$\dot{\epsilon}^d = \sqrt{(\dot{\epsilon}_v^p)^2 + \frac{A}{1-A}\,(\dot{\epsilon}_s^p)^2} \tag{7.5}$$

where $\dot{\epsilon}_v^p$ and $\dot{\epsilon}_s^p$ denote *plastic* volumetric and shear strain rates respectively. A complete mathematical formulation of the SMCC model is given in Appendix.

From Eqs. (7.1,7.2) and (7.4,7.5) it is clear that the structure degradation laws of hypoplastic and SMCC models are not completely equivalent. In order to compare both formulations, simulations of isotropic compression of isotropically normally consolidated specimens with varying parameter k are plotted in Fig. 7.1b. The figure demonstrates that for a given parameter k both laws yield similar rates of structure degradation and thus direct comparison of hypoplastic and SMCC models is possible.

7.3 Evaluation of the models

The two constitutive models have been evaluated on the basis of laboratory experiments on natural and reconstituted Pisa clay [19, 20] and natural Bothkennar clay [123]. Details of analyses and predictions by the hypoplastic model are presented in Reference [88].

In the case of Pisa clay, all parameters with the exception of parameters that control the influence of structure (k, A, and s_f^h/s_f^{ep}) were found by simulating experiments on *reconstituted* Pisa clay. Fig. 7.2 demonstrates calibration of parameters N, λ^* and κ^* and parameters that control the shear stiffness, i.e. G (SMCC) and r (hypoplasticity). Structure-related parameters k, A, and s_f^h/s_f^{ep} were found by direct evaluation of experimental data on natural Pisa clay. In the case of Bothkennar clay, experiments on reconstituted soil, which would be equivalent to simulated experiments on natural clay are

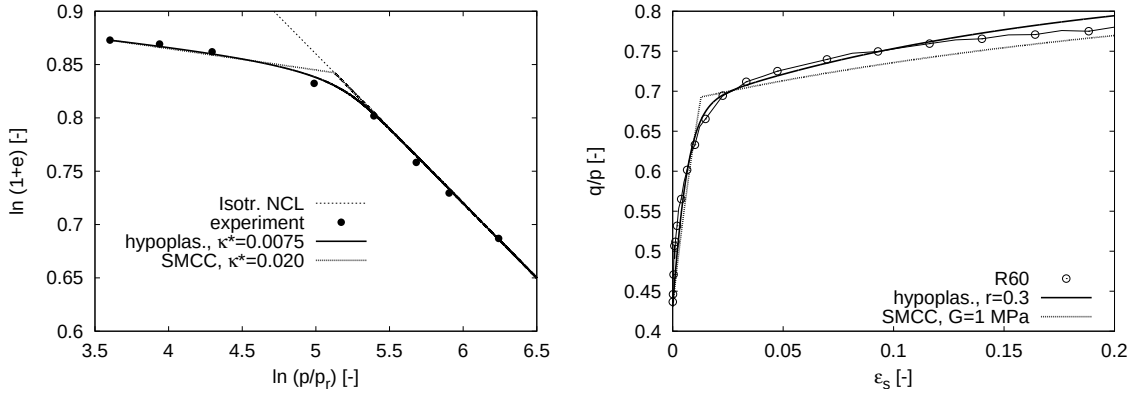

(a) (b)

Figure 7.2: (a) Calibration of the parameters N, λ^* and κ^* of hypoplastic and SMCC models (isotropic compression test on reconstituted Pisa clay from Callisto 1996); (b) Calibration of the parameter r of the hypoplastic model and G of the SMCC model (data from Callisto and Calabresi 1998).

not available, thus all parameters were found by simulation of experiments on natural Bothkennar clay. Parameters of both models are summarised in Tab. 7.1.

Table 7.1: Parameters of the hypoplastic and SMCC models for Pisa and Bothkennar clays.

hypoplasticity	φ_c	λ^*	κ^*	N	r	k	A	s_f^h
Pisa	21.9°	0.14	0.0075	1.56	0.3	0.4	0.1	1
Bothkennar	35°	0.119	0.003	1.344	0.07	0.35	0.5	1
SMCC	M	λ^*	κ^*	N	G	k	A	s_f^{ep}
Pisa	0.85	0.14	0.02	1.56	1 MPa	0.4	0.1	1
Bothkennar	1.42	0.119	0.01	1.344	2 MPa	0.35	0.5	1

Fig. 7.3 shows results of simulations of experiments on Pisa clay, namely stress paths normalised by the Hvorslev equivalent pressure p_e^* (a) and response in $\ln(p/p_r)$ vs. $\ln(1+e)$ space (b). Normalised stress paths of natural Bothkennar clay are in Fig. 7.4a, ϵ_s vs. q curves in Fig. 7.4b. Figures 7.3 and 7.4 demonstrate some common features and some differences in predictions by the hypoplastic and SMCC models. Both models predict apparently similar shape of the SBS and, in general, a similar stress-strain behaviour at larger strains. The main difference stems from the non-linear character of the hypoplastic equation that facilitates the non-linear response also inside the SBS, with a gradual decrease of shear and bulk moduli and a smooth structure-degradation process.

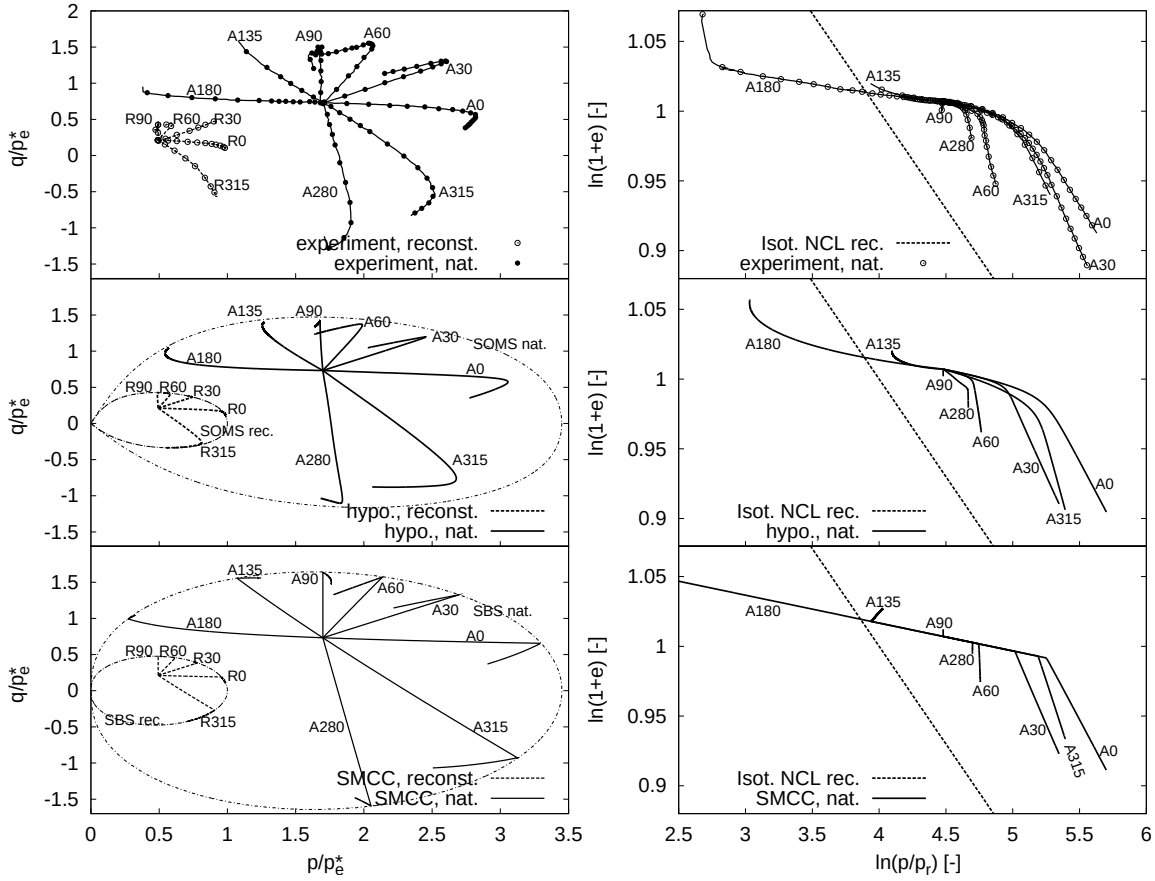

Figure 7.3: (a) normalised stress paths of the natural and reconstituted Pisa clay and (b) experiments on natural Pisa clay plotted in the $\ln(p/p_r)$ vs. $\ln(1+e)$ space. Experimental data and predictions by the hypoplastic and SMCC models.

7.4 Concluding remarks

The presented simulations demonstrate the well-known shortcoming of the SMCC model, the elastic behaviour inside the SBS. Many advanced elasto-plastic constitutive models overcome this problem, for example by introducing a kinematic hardening yield surface (among others see Baudet and Stallebrass [8]). These enhancements, however, often significantly increase complexity of the mathematical formulation of the models and increase the number of parameters, which is a limiting factor for the applicability of the models for practical engineering purposes. The paper aimed to demonstrate that hypoplasticity, which requires only a limited number of material parameters (equivalent to the most simple elasto-plastic models, such as the SMCC model) is a valid alternative to advanced elasto-plastic models for structured clays.

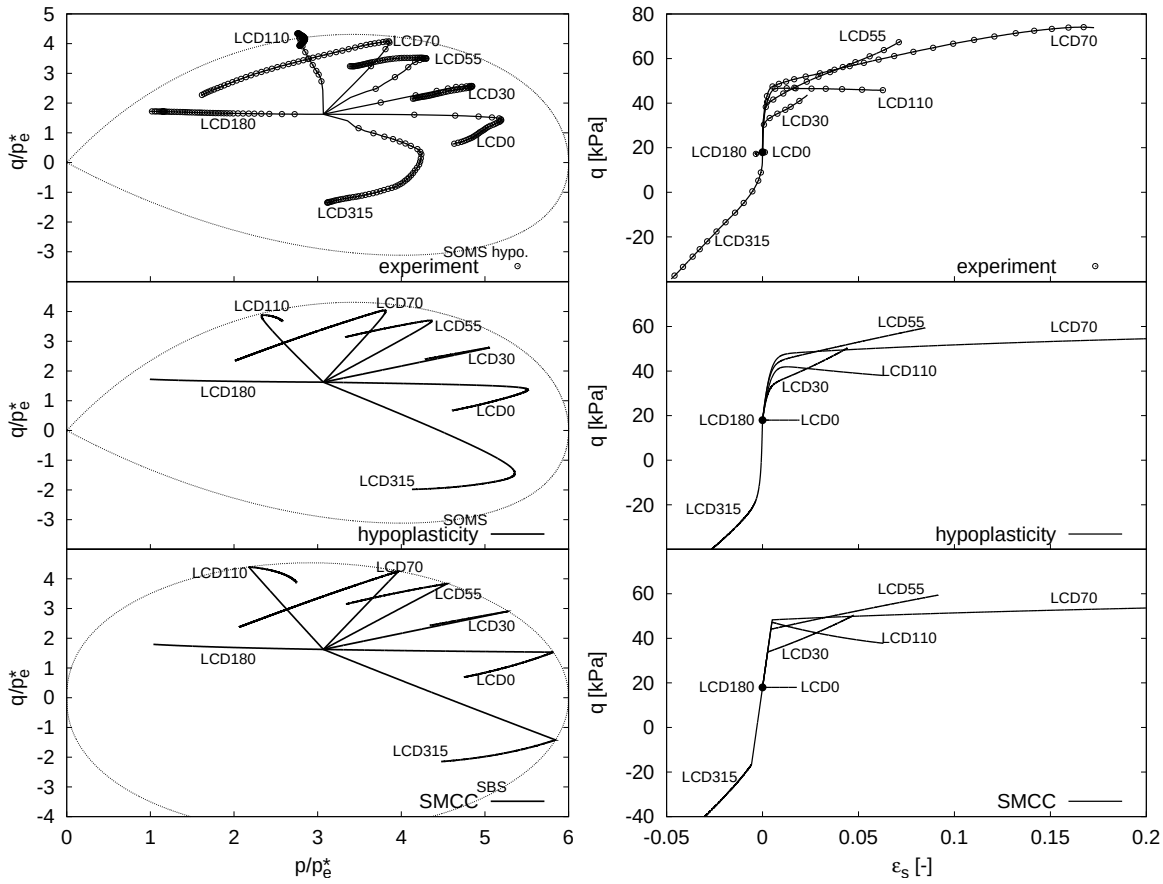

Figure 7.4: (a) normalised stress paths and (b) ϵ_s vs. q curves from experiments on natural Bothkennar clay. Experimental data and predictions by the hypoplastic and SMCC models.

Appendix

The appendix presents a complete mathematical formulation of the Structured Modified Cam clay (SMCC) model. The rate formulation of the model reads

$$\dot{\boldsymbol{\sigma}} = \boldsymbol{\mathcal{D}}^e : (\dot{\boldsymbol{\epsilon}} - \dot{\boldsymbol{\epsilon}}^p) \tag{7.6}$$

The elastic stiffness matrix $\boldsymbol{\mathcal{D}}^e$ is calculated from the shear modulus G (parameter) and bulk modulus K, related to the parameter κ^* via $K = p/\kappa^*$, by

$$\boldsymbol{\mathcal{D}}^e = \left(K - \frac{2}{3}G\right) \mathbf{1} \otimes \mathbf{1} + 2G\,\boldsymbol{\mathcal{I}} \tag{7.7}$$

Yield surface (f) is associated with the plastic potential (g) surface

$$f = g = q^2 + M^2 p\,(p - s^{ep} p_c^*) \tag{7.8}$$

M is the model parameter, s^{ep} (sensitivity) is the state variable and the quantity p_c^* is related to the state variable e (void ratio) through the equation

$$p_c^* = p_r \exp\left(\frac{N - \kappa^* \ln\left(p/p_r\right) - \ln\left(1+e\right)}{\lambda^* - \kappa^*}\right) \tag{7.9}$$

where p_r is the reference stress 1 kPa and N and λ^* are model parameters. Inside the yield surface ($f < 0$), $\dot{\boldsymbol{\epsilon}}^p = \mathbf{0}$. For stress states on the yield surface, the plastic strain rate is given by:

$$\dot{\boldsymbol{\epsilon}}^p = \frac{\langle \mathbf{m} : \boldsymbol{\mathcal{D}}^e : \dot{\boldsymbol{\epsilon}} \rangle}{H + \mathbf{m} : \boldsymbol{\mathcal{D}}^e : \mathbf{m}} \mathbf{m} \tag{7.10}$$

where the operator $\langle x \rangle := (x + |x|)/2$ denotes the positive part of any scalar function x, H is the plastic modulus calculated from the consistency condition

$$H = \frac{M^2 p p_c^*}{\lambda^* - \kappa^*} \left[s^{ep} \operatorname{tr}(\mathbf{m}) - k \left(s^{ep} - s_f^{ep} \right) \sqrt{\operatorname{tr}^2(\mathbf{m}) + \left(\frac{A}{1-A} \right) \frac{2}{3} \operatorname{dev}(\mathbf{m}) : \operatorname{dev}(\mathbf{m})} \right] \tag{7.11}$$

and the tensor $\mathbf{m}$ is calculated by:

$$\mathbf{m} = \frac{\partial f}{\partial \boldsymbol{\sigma}} = \frac{M^2 (2p - s^{ep} p_c^*)}{3} \mathbf{1} + 3 \operatorname{dev}(\boldsymbol{\sigma}) \tag{7.12}$$

s_f^{ep} and k are model parameters. Evolution of state variables is governed by equations:

$$\dot{e} = -\left(1+e\right) \dot{\epsilon}_v \qquad\qquad \dot{s}^{ep} = -\frac{k}{\lambda^* - \kappa^*} (s^{ep} - s_f^{ep}) \sqrt{\left(\dot{\epsilon}_v^p\right)^2 + \frac{A}{1-A} \left(\dot{\epsilon}_s^p\right)^2} \tag{7.13}$$

$\dot{\epsilon}_v^p$ and $\dot{\epsilon}_s^p$ are rates of plastic volumetric and shear strains respectively and A is model parameter.

Chapter 8

Summary and conclusions

The thesis traces the research into the constitutive modelling of fine-grained soils using theory of hypoplasticity. The developed constitutive model is from the practical point of view equivalent to the Modified Cam clay model, since it requires the same number of material parameters with an equivalent physical meaning. However, due to the non-linear character of the hypoplastic formulation, the quality of predictions by the proposed model is at least comparable to more complex advanced elasto-plastic models.

From the mathematical standpoint, the model is positively homogeneous of degree 1 in $\mathbf{D}$ and for a given value of f_d in $\mathbf{T}$. Therefore, the behaviour of the fine-grained soil is assumed to be *rate-independent*. This is clearly a strong assumption that limits the validity of the material parameters only to certain range of loading rates. Positive homogeneity of degree 1 in $\mathbf{T}$ for given f_d implies parallel normal compression lines of the slope λ^* in the $\ln(1+e)$ vs. $\ln p$ space. Also, the behaviour is for a given degree of overconsolidation assumed to be scalable by the mean stress, which is according to experimental evidence a reasonable approximation of the behaviour of clays.

The model requires four other material parameters in addition to λ^*. N determines the position of the isotropic normal compression line, κ^* the slope of the isotropic unloading line in the $\ln(1+e)$ vs. $\ln p$ space. Unlike in the Cam clay-type models, the slope of the unloading branch is exactly equal to the parameter κ^* only for unloading from the isotropic normally consolidated state, at overconsolidated states the slope is higher, due to the non-linear character of the model formulation. The next parameter, φ_c, defines the critical state friction angle at triaxial compression and extension. The model makes use of the Matsuoka-Nakai shape of the critical state locus in the stress space, so for other Lode angles the critical state friction angle is slightly higher than φ_c. This is well in agreement with experimental data. The last parameter, r, controls the shear stiffness, which decreases with increasing r. This parameter is usually calibrated by means of a parametric study.

A shortcoming of hypoplastic models in general is an inevitable "rachetting", i.e. the extensive accumulation of strains during cyclic loading caused by the too soft response upon sharp reversals of the stress/strain paths directions. Niemunis and Herle [108] proposed

a modification of the hypoplastic equation by introducing so-called *intergranular strain concept* that eliminates this shortcoming. The proposed model has been designed to be used with the intergranular strain enhancement by letting the tensor $\boldsymbol{\mathcal{L}}$ to have the form appropriate to predict both the behaviour in the small strain range and upon sharp path reversal (in this case the nonlinear part $\mathbf{N}\|\mathbf{D}\|$ of the hypoplastic equation is ruled out) and for continuing deformation (in limit the model response tends to the basic hypoplastic formulation).

It has been shown that the proposed form of the constitutive tensors $\boldsymbol{\mathcal{L}}$ and $\mathbf{N}$ and the barotropy and pyknotropy factors f_d and f_s allow us to derive a closed-form solution for *swept-out-memory states*, which compose a hypersurface in the stress – void ratio space called *swept-out-memory surface*[1]. This surface is a close approximation of the *state boundary surface*, defined as boundary of all possible states in the stress – void ratio space. Prediction of the state boundary surface is an important property of the proposed model that makes it possible not only to compare the model response with relevant experimental data, but mainly it opens the way for further extensions of the model. The study in Chapter 3 revealed an important shortcoming of the model – the swept-out-memory surface does not have a reasonable shape for too high values of the ratio κ^*/λ^*. However, if κ^*/λ^* is smaller than approx. 1/4, the shape of the state boundary surface compares well with the shape observed experimentally.

Predictions by the proposed model were compared with a number of existing elasto-plastic and hypoplastic models, namely Modified Cam clay model, three surface kinematic hardening (3-SKH) model and a Grenoble-type hypoplastic model (CLoE). With regard to the directional response, the proposed model, together with the 3-SKH model, performed best. As expected, a simple Modified Cam clay model has shown a poor performance for loading paths directed inside the elastic region, while the non-linear character of the hypoplastic model led to at least qualitatively correct predictions for all loading directions. Predictions of stress probes that followed after sharp stress-path reversal were further improved by applying the intergranular strain concept. The 3-SKH model performed similarly to the proposed hypoplastic model. This is a consequence of the fact that although both models are developed using different mathematical concepts, they are both based on the similar physical interpretation of the behaviour of fine-grained soils.

A study of the validity of a single set of material parameters for prediction of behaviour of soils at different overconsolidation ratios (OCR) revealed that if the proposed hypoplastic model is calibrated at higher OCR, it performs well for a broad range of OCRs, both qualitatively and quantitatively. The Modified Cam clay model and the 3-SKH model performed in this case worst than the proposed hypoplastic model.

The last part of the thesis demonstrated a possibility for further extension of the model. In particular, the basic model was modified to predict the behaviour of clays with meta-stable structure. The framework for the mechanical behaviour of natural clays by Cotecchia and Chandler [34], according to which it is possible to relate the behaviour of natural and

[1]This closed-form solution is not available for other hypoplastic models, such as the model by von Wolffersdorff [141]

reconstituted clay through the state variable *sensitivity*, was applied. The sensitivity was incorporated in such a way that the size of the state boundary surface was increased, other material properties were however kept unchanged. A suitable evolution equation for sensitivity then enabled us to predict the behaviour of clays with meta-stable structure. Predictions of the enhanced hypoplastic model were compared with predictions by its elasto-plastic 'equivalent', structured Modified Cam clay model, developed in Chapter 7. It was again clearly demonstrated that with the same number of parameters of equivalent physical interpretation the non-linear hypoplastic model leads to better predictions.

Chapter 9

Outlook

The proposed model is conceptually very simple, and the small number of material parameters obviously does not allow us to tune the model predictions into great detail. Any further modification of the model would, however, require extensive evaluation that would pinpoint systematic differences between model predictions and experiment. In this respect an independent evaluation by different researchers working in the field of constitutive modelling is particularly valuable.

Weifner [143] compared predictions by the proposed model with different hypoplastic models for fine-grained soils [105, 54, 61], based on experimental data on Weald clay by Henkel [59, 60]. The data consist of isotropic loading and unloading tests and drained and undrained triaxial tests starting from isotropic normally consolidated and overconsolidated ($OCR = 24$) states. Weifner observed shortcoming of the model discussed in Chapter 3 – the model does not perform realistically for too high values of the ratio κ^*/λ^*. If κ^* was changed to sufficiently low value the model performed reasonably at normally consolidated states, but the response at isotropic unloading was too stiff. Because the initial state of shear experiments was found by simulating the consolidation stress history, too stiff response in isotropic unloading led to apparently higher overconsolidation and therefore the peak stiffness and dilatancy in tests at $OCR = 24$ was exaggerated.

Huang et al. [63] point out a different shortcoming of the proposed model – the model does not perform correctly under undrained conditions at normally consolidated states. This is an inevitable consequence of a hypoplastic formulation, which is characterised by the translated elliptical response envelope. In order to calibrate the model parameters λ^* and κ^* at isotropic loading and unloading conditions, the response envelope must be shifted in such a way that under constant volume conditions an excessive decrease of the mean stress is predicted. Huang et al. proposed an approach to overcome this shortcoming. Starting from the hypoplastic formulation by Gudehus [53], they produced a hybrid elasto-plastic-hypoplastic model. At isotropic stress states the non-linear part vanishes, the model is incrementally bi-linear, i.e. equivalent to an elasto-plastic model. The predicted initial part of the undrained stress paths is then perpendicular to the p-axis. With higher deviatoric stresses the non-linear part is activated and hybrid elasto-plastic-hypoplastic predictions

are obtained. The formulation by Gudehus [53] is modified in such a way that the model requires parameters equivalent to the model from Chapter 2. The model by Huang et al. does not include pyknotropy, i.e. it can be only used for normally consolidated states and does not predict a unique critical state line in the stress vs. void ratio space. The model is not positively homogeneous of degree 1 in $\mathbf{T}$, so normal compression lines that correspond to higher ratio $\eta = q/p$ do not have a slope of λ^*. However, the directional homogeneity with respect to $\mathbf{T}$ (defined by Niemunis [106]) is satisfied so the model predicts asymptotic states (in the stress space).

A conceptually similar approach to that by Huang et al. [63] to improve response of hypoplastic models to undrained shearing, which is directly applicable to the model from Chapter 2, has been proposed by Niemunis [106]. In this case the linear part $\boldsymbol{\mathcal{L}}$ of the model is kept unchanged, at isotropic state the term $\vec{\mathbf{m}}\|\mathbf{D}\|$ is replaced by $\vec{\mathbf{r}}|\vec{\mathbf{r}} : \mathbf{D}|$, where the unit tensor $\vec{\mathbf{r}}$ is (for any stress state) parallel to $\hat{\mathbf{T}}$. For $\vec{\mathbf{D}} = \pm\vec{\mathbf{r}}$ we have $|\vec{\mathbf{r}} : \mathbf{D}| = \|\mathbf{D}\|$ and since $\vec{\mathbf{r}} = \vec{\mathbf{m}}$ the original hypoplastic response is recovered. For $\mathbf{D} \perp \vec{\mathbf{r}}$, however, $|\vec{\mathbf{r}} : \mathbf{D}| = 0$ and response is hypoelastic and is controlled by the linear term $\boldsymbol{\mathcal{L}} : \mathbf{D}$ only. The hypoelastic response envelope is therefore squeezed in the direction of loading and elongated in the direction of unloading, its shape is equivalent to that proposed by Huang et al. [63] and the model also predicts initial portion of the undrained stress path perpendicular to the p-axis. For anisotropic stress states Niemunis [106] suggests interpolation between $\vec{\mathbf{m}}\|\mathbf{D}\|$ and $\vec{\mathbf{r}}|\vec{\mathbf{r}} : \mathbf{D}|$ such that at the critical state surface (in the stress space) the response is purely hypoplastic.

The next step in the evaluation of predictive capabilities of the model is the comparison of its predictions with measurements on the boundary-value problem scale. The proposed model has been implemented into finite element code via a user-defined subroutine `umat.f` by Tamagnini [129] (direct perturbation method) and Arnold [4] (Fellin and Ostermann algorithm [44]), both with and without intergranular strain concept. Mašín and Herle [94] presented finite element simulations of the Heathrow Express trial tunnel [41] by the proposed model, Mohr-Coulomb model and a Modified Cam clay model. Although the proposed model predicts wider settlement trough than measured in the field, its predictions are significantly more realistic than predictions by the simpler models. Further evaluation of the model with respect to boundary-value problems is needed.

The behaviour of fine-grained soils is markedly rate-dependent, and the assumption of rate-independence is reasonable only for a relatively narrow ranges of loading rates. This fact necessarily complicates any experimental program as in looking for parameters relevant to the given boundary value problem the soil should be tested at the loading rates similar to the field. These rates can only be estimated, often very roughly. Rate effects could be relatively easily incorporated into the proposed model by adopting an approach proposed by Niemunis [106] and further discussed by Gudehus [54]. The stretching rate $\mathbf{D}$ is decomposed into the viscous ($\mathbf{D}^v$) and non-viscous ($\mathbf{D} - \mathbf{D}^v$) part. The viscous part $\mathbf{D}^v$ has the same tensorial direction as the non-linear part of the reference model ($\vec{\mathbf{m}}$), its magnitude is dependent on overconsolidation ratio via two new material parameters. The reference stress p_r is dependent on the stretching rate $\|\mathbf{D}\|$. It has been shown [106, 54] that a hypoplastic model modified in this way can qualitatively correctly predict creep, relaxation

and response to strain rate jumps. A thorough evaluation of this concept when used with the proposed model would, however, be needed.

During the geological history natural soils undergo compression under K_0 conditions, which often leads to one-dimensionally oriented fabric. This fabric implies a textural anisotropy, which may be observed even when the soil is tested from isotropic stress state. The model of Chapter 2 is orthotropic with the planes of symmetry given by eigenvectors of $\mathbf{T}$, at isotropic stress state, however, the response is isotropic [107]. Incorporation of anisotropy into hypoplasticity has been first proposed by Wu [150, 152]. He replaced the non-linear part $\mathbf{N}$ of his early version of hypoplastic model [151] by $\boldsymbol{\mathcal{A}}^a : \mathbf{N}$, where $\boldsymbol{\mathcal{A}}^a$ is a fourth-order transversally isotropic tensor. As discussed by Niemunis [107], shortcoming of this rather simple approach is that the modification of the non-linear part $\mathbf{N}$ only does not provide the desirable independent control over dilatancy, strength and stiffness, as in hypoplasticity these features are implied by a combined effect of $\boldsymbol{\mathcal{L}}$ and $\mathbf{N}$. Niemunis [107] therefore suggested a different modification, which is applied to the formulation from Eq. (2.8) and keeps the critical state locus (incorporated via Y) and a hypoplastic flow rule ($\vec{\mathbf{m}}$) unchanged. Modification of the linear term $\boldsymbol{\mathcal{L}}$ and a pyknotropy factor f_d only enabled him to improve the dilatancy curve and the shape of the undrained stress path produced by the model. Further development would be needed to incorporate most effects of textural anisotropy, such as anisotropic shape of the state boundary surface, stiffness, dilatancy and shape of the undrained stress path.

With regard to the model for structured soils (Chapter 6), more research would be required to incorporate true cohesion caused by interparticle bonding. A simple idea of the replacement of stress tensor $\mathbf{T}$ by a transformed stress tensor $\mathbf{T}^t$ according to equation (6.7) has undesired effects. Namely, the normal compression lines are shifted in the $\ln(1+e)$ vs. $\ln p$ space, they are in this space no-more linear and undefined for $p \to 0$, so the parameter λ^* loses its physical meaning. Also other material properties (e.g. shear and bulk stiffnesses), which are measured with respect to the true stress $\mathbf{T}$, now relate to the transformed stress $\mathbf{T}^t$. The model loses its positive homogeneity of degree one in $\mathbf{T}$ so it does not predict any longer asymptotic (swept-out-memory) states in the true stress space $\mathbf{T}$.

The model for structured clays of Chapter 6 can be straightforwardly applied to double porosity materials. A typical example of these materials are double-porosity clayfills from open-cast coal mines in north Bohemia, which consist of clay lumps up to half meter in size, dumped without any compaction. In addition to the intragranular porosity (porosity of clay lumps) the overall void ratio is increased by the intergranular porosity (voids between clay lumps). Mechanical behaviour of such a composite material is relatively complex. A framework for its description has been put forward by Mašín et al. [93], a similar approach has been suggested by Koliji et al. [74]. The reference constitutive model now describes the behaviour of the material of clay lumps, whereas *sensitivity* s is a measure of additional structure caused by intergranular porosity. The evolution of sensitivity represents degradation of the intergranular porosity, i.e. closing the voids between individual clay lumps. The evolution equation for sensitivity may be calibrated by means of compression experiments on the material of clay lumps and corresponding granulated material. Due to the dimensions of experimental apparatuses the material with reduced granulometry must

often be used.

As the last point, a modification of the proposed model to predict the behaviour of unsaturated soils will be discussed. An attempt to incorporate partial saturation into an existing hypoplastic equation has been proposed by Gudehus [52]. In his work the effective stress principle is applied, i.e. the existing hypoplastic equation is without further modification written in terms of the effective stress in partially saturated soils, starting with the definition by Bishop [15] and continuing with a more complex one. Qualitatively correct predictions for some loading paths are claimed. The model was, primarily from the mathematical point of view, further investigated by Niemunis [106]. However, as discussed by Wheeler and Karube [144], the model does not enable us to represent some of the most fundamental features of unsaturated soil behaviour, most notably the correct pattern of swelling and collapse on wetting. To overcome this problem, a scalar state variable that represents normal forces on grain contacts produced by the menisci of the pore fluid is needed, in addition to the tensorial stress variable that represents the action of external forces. An extensive research in unsaturated soil behaviour did not lead to a unique choice of the two state variables that would be ideal. In general, simple state variables (used, e.g., by Alonso et al. [3]) lead to more complex constitutive models. More complex state variables (advocated, e.g., by Loret and Khalili [83]) simplify the definition of the constitutive models, but complicate description of the stress state in such a way that it may be difficult to devise simple experimental tests to measure relevant soil parameters.

An attempt to develop a hypoplastic model for granular materials considering a scalar state variable that represents the action of capillary mensici has been presented by Bauer et al. [11]. Their model is, however, oversimplified – the only modification of the original equation is that the granulate hardness h_s (an equivalent of a reference pressure p_r of the model of Chapter 2) is made dependent on degree of saturation. In this way different compressibilities of soils with different moisture contents are predicted. However, the model does not predict the behaviour of soils when subjected to changes in degree of saturation.

A more comprehensive modification of the model of Chapter 2 is being developed by Mašín [91]. The approach by Alonso et al. [3] is used, the stress state is characterised by net stress $\boldsymbol{\sigma} = \boldsymbol{\sigma}^t - \mathbf{1}u_a$ and suction $s = u_a - u_w$, where $\boldsymbol{\sigma}^t$ is total stress, u_a and u_w are the pressures of the pore air and water respectively. The influence of suction is treated similarly to the model by Alonso et al. [3]. Equivalent suction s_e^* is introduced as the additional state variable that characterises the previous suction-loading history, the straining due to suction changes at overconsolidated states is controlled by the non-linear hypoplastic equation resembling the basic form of hypoplastic models for saturated soils. A consistency condition for the swept-out-memory surface from Chapter 3 is introduced in order to model wetting induced collapse. The model therefore shares some features with the bounding surface plasticity models [38].

The next step in the development of the hypoplastic model for unsaturated soils will be the application of more complex state variables (such as those discussed by Khalili et al. [72]) and a comparison of the merits and disadvantages of both formulations. Subsequently, the hysteretic soil-water characteristic curve should be incorporated.

References

[1] A. Al Tabbaa and D. M. Wood. An experimentally based "bubble" model for clay. In *Proc. 3^{th} Int. Conf. on Numerical Models in Geomechanics*. Niagara Falls, 1989.

[2] M. A. Allman and J. H. Atkinson. Mechanical properties of reconstituted Bothkennar soil. *Géotechnique*, 42(2):289–301, 1992.

[3] E. Alonso, A. Gens, and A. Josa. A constitutive model for partially saturated soils. *Géotechnique*, 40(3):405–430, 1990.

[4] M. Arnold. Private communication. University of Dresden, 2006.

[5] A. Asaoka. Compaction of sand and consolidation of clay: a super/subloading yield surface approach. In *Proc. 11^{th} Int. Conference IACMAG*, volume 4, pages 121–140. Turin, Italy, 2005.

[6] J. H. Atkinson, D. Richardson, and S. E. Stallebrass. Effects of recent stress history on the stiffness of over–consolidated soil. *Géotechnique*, 40(4):531–540, 1990.

[7] B. A. Baudet. *Modelling effects of structure in soft natural clays*. PhD thesis, City University, London, 2001.

[8] B. A. Baudet and S. E. Stallebrass. A constitutive model for structured clays. *Géotechnique*, 54(4):269–278, 2004.

[9] E. Bauer. Modelling of critical stress in hypoplasticity. In *NUMOG V*, pages 15–20, Davos, 1995. Balkema.

[10] E. Bauer. Calibration of a comprehensive constitutive equation for granular materials. *Soils and Foundations*, 36(1):13–26, 1996.

[11] E. Bauer, W. Cen, Y. Zhu, K. Kast, and S. F. Tantono. Modelling of partly saturated weathered broken rock. In H. F. Schweiger, editor, *Proc. 6th European Conference on Numerical Methods in Geomechanics (NUMGE06), Graz, Austria*, pages 87–92. Taylor & Francis Group, London, 2006.

[12] E. Bauer and W. Wu. A hypoplastic model for granular soils under cyclic loading. In D. Kolymbas, editor, *Modern Approaches to Plasticity*, pages 247–258. Elsevier Science Publishers B.V., 1993.

[13] E. Bauer and W. Wu. Extension of hypoplastic constitutive model with respect to cohesive powders. In Siriwardane and Zeman, editors, *Computer methods and advances in geomechnics*, pages 531–536. A.A.Balkema, Rotterdam, 1994.

[14] A. Beghini and P. Bažant. Discussion of paper "Shear and objective stress rates in hypoplasticity". *International Journal for Numerical and Analytical Methods in Geomechanics*, 28:365–372, 2004.

[15] A. W. Bishop. The principle of effective stress. *Teknisk Ukeblad*, 106(39):859–863, 1959.

[16] R. I. Borja, C.-H. Lin, and F. J. Montans. Cam–clay plasticity, Part IV: Implicit integration of anisotropic bounding surface model with nonlinear hyperelasticity and ellipsoidal loading function. *Comp. Meth. Appl. Mech. Engng.*, 190:3293–3323, 2001.

[17] J. B. Burland. On the compressibility and shear strength of natural clays. *Géotechnique*, 40(3):329–378, 1990.

[18] R. Butterfield. A natural compression law for soils. *Géotechnique*, 29(4):469–480, 1979.

[19] L. Callisto. *Studio sperimentale su un'argilla naturale: il comportamento meccanico dell'argilla di Pisa*. PhD thesis, Universita La Sapienza, Roma, 1996.

[20] L. Callisto and G. Calabresi. Mechanical behaviour of a natural soft clay. *Géotechnique*, 48(4):495–513, 1998.

[21] L. Callisto, A. Gajo, and D. Muir Wood. Simulation of true triaxial tests on natural and reconstituted pisa clay. *Géotechnique*, 52(9):649–666, 2002.

[22] L. Callisto and S. Rampello. Shear strength and small–strain stiffness of a natural clay under general stress conditions. *Géotechnique*, 52(8):547–560, 2002.

[23] L. Callisto and S. Rampello. An interpretation of structural degradation for three natural clays. *Canadian Geotechnical Journal*, 41:392–407, 2004.

[24] F. Calvetti, C. Tamagnini, and G. Viggiani. On the incremental behaviour of granular soils. In *NUMOG VIII*, pages 3–9. Swets & Zeitlinger, 2002.

[25] M. Cecconi, A. DeSimone, C. Tamagnini, and G. M. B. Viggiani. A constitutive model for granular materials with grain crushing and its application to a pyroclastic soil. *International Journal for Numerical and Analytical Methods in Geomechanics*, 26:1531–1560, 2002.

[26] R. Chambon. Une classe de lois de comportement incrémentalement nonlináires pour les sols non visqueux, résolution de quelques problèmes de cohérence. *C. R. Acad. Sci.*, 308(II):1571–1576, 1989.

[27] R. Chambon. Discussion of paper "shear and objective stress rates in hypoplasticity" by d. kolymbas and i. herle. *International Journal for Numerical and Analytical Methods in Geomechanics*, 28:365–372, 2004.

[28] R. Chambon and J. Desrues. Bifurcation par localisation et non linéarité incrémentale: un example heuristique d'analyse complete. In *Plastic Instability*, pages 101–113, Paris, France, 1985. Presses ENPC.

[29] R. Chambon, J. Desrues, W. Hammad, and R. Charlier. CLoE, a new rate–type constitutive model for geomaterials. theoretical basis and implementation. *International Journal for Numerical and Analytical Methods in Geomechanics*, 18:253–278, 1994.

[30] C. R. I. Clayton and G. Heymann. Stiffness of geomaterials at very small strains. *Géotechnique*, 51(3):245–255, 2001.

[31] D. Costanzo, G. Viggiani, and C. Tamagnini. Directional response of a reconstituted fine grained soil. Part I: Experimental investigation. *International Journal for Numerical and Analytical Methods in Geomechanics*, 30(13):1283–1301, 2006.

[32] F. Cotecchia. *The effects of structure on the properties of an Italian Pleistocene clay.* PhD thesis, University of London, 1996.

[33] F. Cotecchia and J. Chandler. The influence of structure on the pre–failure behaviour of a natural clay. *Géotechnique*, 47(3):523–544, 1997.

[34] F. Cotecchia and J. Chandler. A general framework for the mechanical behaviour of clays. *Géotechnique*, 50(4):431–447, 2000.

[35] T. Cuccovillo and M. R. Coop. The measurement of local axial strains in tiaxial tests using LVDT's. *Géotechnique*, 47(1):167–171, 1997.

[36] R. Cudmani and V. A. Osinov. The cavity expansion problem for the interpretation of cone penetration and pressuremeter tests. *Canadian Geotechnical Journal*, 38:622–638, 2001.

[37] M. Cudny and P. A. Vermeer. On the modelling of anisotropy and destruction of soft clays within the multi-laminate framework. *Computers and Geotechnics*, 31(1):1–22, 2004.

[38] Y. F. Daffalias. Bounding surface plasticity. I: Mathematical foundation and hypoplasticity. *Journal of Engineering Mechanics ASCE*, 112(9):966–987, 1986.

[39] F. Darve. The expression of rheological laws in incremental form and the main classes of constitutive equations. In F. Darve, editor, *Geomaterials: Constitutive Equations and Modelling*, pages 123–148. Elsevier, 1990.

[40] R. de Borst and O. Heeres. A unified approach to the implicit integration of standard, non-standard and viscous plasticity models. *International Journal for Numerical and Analytical Methods in Geomechanics*, 26:1059–1070, 2002.

[41] A. P. Deane and R. H. Basset. The heathrow express trial tunnel. *Proc. Instn. Civil Engineers*, 113:144–156, 1995.

[42] J. Desrues. Private communication. Grenoble, 2004.

[43] J. Desrues and R. Chambon. Shear band analysis for granular materials: the question of incremental non–linearity. *Ingenieur–Archiv*, 59:187–196, 1989.

[44] W. Fellin and A. Ostermann. Consistent tangent operators for constitutive rate equations. *International Journal for Numerical and Analytical Methods in Geomechanics*, 26:1213–1233, 2002.

[45] R. J. Finno, I. S. Harahap, and P. J. Sabatini. Analysis of braced excavations with coupled finite element formulations. *Computers and Geotechnics*, 12:91–114, 1989.

[46] A. Gajo and D. Muir Wood. A new approach to anisotropic, bounding surface plasticity: general formulation and simulations of natural and reconstituted clay behaviour. *International Journal for Numerical and Analytical Methods in Geomechanics*, 25:207–241, 2001.

[47] J. Graham and G. T. Houlsby. Anisotropic elasticity of a natural clay. *Géotechnique*, 33(2):165–180, 1983.

[48] J. Graham, M. L. Noonan, and K. V. Lew. Yield stress and strain relationship in a natural plastic clay. *Canadian Geotechnical Journal*, 20:502–516, 1983.

[49] R. J. Grant, S. E. Stallebrass, and R. N. Taylor. Prediction of pre-failure ground movements: Physical and numerical techniques. In *Proc.* 14^{th} *Int. Conf. Soil Mechanics and Foundation Engineering*, pages 663–668. Balkema Rotterdam, 1996.

[50] G. Gudehus. A comparison of some constitutive laws for soils under radially symmetric loading and unloading. In *Proc.* 3^{rd} *Int. Conf. on Numerical Methods in Geomechanics*, pages 1309–1323. Aachen, 1979.

[51] G. Gudehus. Attractors for granular storage and flow. In 3^{rd} *European Symposium – Storage and Flow of Particulate Solids, Paper for the conf. 'Partec 95'*, pages 333–345, 1995.

[52] G. Gudehus. A comprehensive concept for non-saturated granular bodies. In Alonso and Delage, editors, 1^{st} *Int. Conference on Unsaturated Soils, Paris, France*, volume 2, pages 725–737. Balkema, Rotterdam, 1995.

[53] G. Gudehus. A comprehensive constitutive equation for granular materials. *Soils and Foundations*, 36(1):1–12, 1996.

[54] G. Gudehus. A visco-hypoplastic constitutive relation for soft soils. *Soils and Foundations*, 44(4):11–25, 2004.

[55] G. Gudehus, M. Goldscheider, and H. Winter. Mechanical properties of sand and clay and numerical intergration methods: some sources of errors and bounds of accuracy. In G. Gudehus, editor, *Finite Elements in Geomechanics*, pages 121–150. Wiley, 1977.

[56] V. Hájek and D. Mašín. An evaluation of constitutive models to predict the behaviour of fine-grained soils with different degrees of overconsolidation. In H. F. Schweiger, editor, *Proc. 6th European Conference on Numerical Methods in Geomechanics (NUMGE06), Graz, Austria*, pages 49–55. Taylor & Francis Group, London, 2006.

[57] K. Hashiguchi. Two– and three–surface models of plasticity. In *V Int. Conf. Num. Meth. in Geomechanics*, pages 285–292, Nagoya, Japan, 1985. Balkema, Rotterdam.

[58] M. Hattab and P.-Y. Hicher. Dilating behaviour of overconsolidated clay. *Soils and Foundations*, 44(4):27–40, 2004.

[59] D. J. Henkel. The effect of overconsolidation on the behaviour of clays during shear. *Géotechnique*, 6:139–150, 1956.

[60] D. J. Henkel and V. A. Sowa. The influence of stress history on stress paths in undrained triaxial tests on clay. *Laboratory Shear Testing of Soils, ASTM Special Technical Publication*, 361:280–291, 1963.

[61] I. Herle and D. Kolymbas. Hypoplasticity for soils with low friction angles. *Computers and Geotechnics*, 31(5):365–373, 2004.

[62] D. W. Hight, A. J. Bond, and J. D. Legge. Characterisation of the Bothkennar clay: an overview. *Géotechnique*, 42(2):199–217, 1992.

[63] W.-X. Huang, W. Wu, D.-A. Sun, and S. Sloan. A simple hypoplastic model for normally compressed clay. *Acta Geotechnica*, 1(1):15–27, 2006.

[64] M. Hvorslev. Physical components of the shear strength of saturated clays. In *Shear Strength of Cohesive Soils, proc. ASCE Research Conf.* Boulder, Colorado, 1960.

[65] P. J. Ingram. *The applicaton of numerical models to natural stiff clays.* PhD thesis, City University, London, 2000.

[66] J. Jáky. The coefficient of earth pressure at rest. *Journal for Society of Hungarian Architects and Engineers*, pages 355–357, 1944.

[67] R. J. Jardine, M. J. Symes, and J. B. Burland. The measurement of soil stiffness in the triaxial apparatus. *Géotechnique*, 34(3):323–340, 1984.

[68] V. Jovičić. *The measurement and interpretation of small strain stiffness of soil.* PhD thesis, City University, London, 1997.

[69] V. Jovičić and M. R. Coop. The measurement of stiffness anisotropy in clays with bender element tests in the triaxial apparatus. *Geotechnical Testing Journal*, 21(1):3–10, 1998.

[70] C. Karcher. Tagebaubedingte Deformationen im Lockergestein. Veröffentlichungen des Institutes für Bodenmechanik und Felsmechanik der Universität Fridericiana in Karlsruhe, 2003. Heft 160.

[71] M. Kavvadas and A. Amorosi. A constitutive models for structured soils. *Géotechnique*, 50(3):263–273, 2000.

[72] N. Khalili, F. Geiser, and G. E. Blight. Effective stress in unsaturated soils: review with new evidence. *International Journal of Geomechanics*, 4(2):115–126, 2004.

[73] M. M. Kirkgard and P. V. Lade. Anisotropic three–dimmensional behaviour of a normally consolidated clay. *Canadian Geotechnical Journal*, 30:848–858, 1993.

[74] A. Koliji, L. Vulliet, L. Laloui, A. Carminati, A. Kaestner, H. Flühler, P. Lehmann, R. Hassanein, E. Lehmann, and P. Vontobel. Structure degradation of dry aggregated soil: experimental evidence and model formulation. In A. Miller, C. E. Zapata, S. L. Houston, and D. G. Fredlund, editors, 4^{th} *Int. Conference on Unsaturated Soils, Carefree, Arizona*, volume 2, pages 2174–2185. ASCE, USA, 2006.

[75] D. Kolymbas. *Eine konstitutive Theorie für Böden und andere körnige Stoffe*. PhD thesis, Karlsruhe University, Germany, 1978.

[76] D. Kolymbas. Computer-aided design of constitutive laws. *International Journal for Numerical and Analytical Methods in Geomechanics*, 15:593–604, 1991.

[77] D. Kolymbas. An outline of hypoplasticity. *Archive of Applied Mechanics*, 61:143–151, 1991.

[78] D. Kolymbas and I. Herle. Shear and objective stress rates in hypoplasticity. *International Journal for Numerical and Analytical Methods in Geomechanics*, 27:733–744, 2003.

[79] R. Lagioia and R. Nova. An experimental and theoretical study of the behaviour of a calcarenite in triaxial compression. *Géotechnique*, 45(4):633–648, 1995.

[80] J. Lanier, D. Caillerie, R. Chambon, G. Viggiani, P. Bésuelle, and J. Desrues. A general formulation of hypoplasticity. *International Journal for Numerical and Analytical Methods in Geomechanics*, 28:1461–1478, 2004.

[81] P. I. Lewin and J. B. Burland. Stress-probe experiments on saturated normally consolidated clay. *Géotechnique*, 20(1):38–56, 1970.

[82] M. D. Liu and J. P. Carter. A structured Cam Clay model. *Canadian Geotechnical Journal*, 39:1313–1332, 2002.

[83] B. Loret and N. Khalili. An effective stress elastic-plastic model for unsaturated porous media. *Mechanics of Materials*, 34:97–116, 2002.

[84] L. X. Luccioni, J. M. Pestana, and R. L. Taylor. Finite element implementation of non-linear elastoplastic constitutive laws using local and global explicit algorithms with automatic error control. *International Journal for Numerical Methods in Engineering*, 50:1191–1212, 2001.

[85] H. Matsuoka and T. Nakai. Stress–deformation and strength characteristics of soil under three different principal stresses. In *Proc. Japanese Soc. of Civil Engineers*, volume 232, pages 59–70, 1974.

[86] D. Mašín. *Laboratory and Numerical Modelling of Natural Clays*. MPhil Thesis, City University, London, 2004.

[87] D. Mašín. A hypoplastic constitutive model for clays. *International Journal for Numerical and Analytical Methods in Geomechanics*, 29(4):311–336, 2005.

[88] D. Mašín. A hypoplastic constitutive model for clays with meta-stable structure. *Canadian Geotechnical Journal (accepted)*, 2006.

[89] D. Mašín. Incorporation of meta-stable structure into hypoplasticity. In *Proc. Int. Conference on Numerical Simulation of Construction Processes in Geotechnical Engineering for Urban Environment*, pages 283–290. Bochum, Germany, 2006.

[90] D. Mašín. Comparison of elasto-plastic and hypoplastic modelling of structured clays. In *Proc. International Workshop on Constitutive Modelling - Development, Implementation, Evaluation, and Application (in print)*. Hong Kong, China, 2007.

[91] D. Mašín. A hypoplastic model for unsaturated soils based on barcelona basic model. In *Proc. Tenth International Symposium on Numerical Models in Geomechanics (in preparation)*. Rhodes, Greece, 2007.

[92] D. Mašín, R. Chambon, and J. Desrues. CLoE model modified to predict the behaviour of normally compressed clays. In *Proc.* 11^{th} *Int. Conference IACMAG*, volume 2, pages 417–424. Turin, Italy, 2005.

[93] D. Mašín, V. Herbstová, and J. Boháč. Properties of double porosity clayfills and suitable constitutive models. In *Proc.* 16^{th} *Int. Conference ICSMGE*, volume 2, pages 827–830. Osaka, Japan, 2005.

[94] D. Mašín and I. Herle. The influence of a constitutive assumption on the predictions of deformations around a tunnel in fine-grained soils (in czech). In *In Proc.* 33^{rd} *Conf. Zakládání Staveb*. Brno, Czech Republic, 2005.

[95] D. Mašín and I. Herle. Numerical analyses of a tunnel in london clay using different constitutive models. In *In Proc.* 5^{th} *Int. Symposium TC28 Geotechnical Aspects of Underground Construction in Soft Ground*, pages 595–600. Amsterdam, The Netherlands, 2005.

[96] D. Mašín and I. Herle. State boundary surface in hypoplasticity. In W. Wu and H. S. Yu, editors, *Proc. Int. workshop Modern trends in geomechanics, Vienna, Austria*, pages 117–128. Springer, Berlin, 2005.

[97] D. Mašín and I. Herle. State boundary surface of a hypoplastic model for clays. *Computers and Geotechnics*, 32(6):400–410, 2005.

[98] D. Mašín, S. E. Stallebrass, and J. H. Atkinson. Laboratory modelling of natural structured clays. In Wermeer, Schweiger, Karstunen, and Cudny, editors, *In Proc. International Workshop on Geotechnics of Soft Soils – Theory and Practice*, pages 253–263. Noordwijkerhout, Netherlands, 2003.

[99] D. Mašín, C. Tamagnini, G. Viggiani, and D. Costanzo. Directional response of a reconstituted fine grained soil. Part II: performance of different constitutive models. *International Journal for Numerical and Analytical Methods in Geomechanics*, 30(13):1303–1336, 2006.

[100] P.-M. Mayer. Verformungen und Spannungsänderungen im Boden durch Schlitzwandherstellung und Baugrubenaushub. Veröffentlichungen des Institutes für Bodenmechanik und Felsmechanik der Universität Fridericiana in Karlsruhe, 2000. Heft 151.

[101] P. W. Mayne and F. H. Kulhawy. K_0–OCR relationships in soil. In *Proc. ASCE J. Geotech. Eng. Div.*, volume 108, pages 851–872, 1982.

[102] Z. Mroz, V. A. Norris, and O. C. Zienkiewicz. An anisotropic hardening model for soils and its application to cyclic loading. *International Journal for Numerical and Analytical Methods in Geomechanics*, 2:203–221, 1978.

[103] Z. Mróz, V. A. Norris, and O. C. Zienkiewicz. Application of an anisotropic hardening model in the analysis of elasto-plastic deformation of soil. *Géotechnique*, 29(1):1–34, 1979.

[104] D. Muir Wood. *Soil behaviour and critical state soil mechanics*. Cambridge University Press, 1990.

[105] A. Niemunis. A visco-plastic model for clay and its FE implementation. In E. Dembicki, W. Cichy, and L. Balachowski, editors, *Recent results in mechanics of soils and rocks.*, pages 151–162. TU Gdańsk, 1996.

[106] A. Niemunis. *Extended hypoplastic models for soils*. Habilitation thesis, Ruhr-University, Bochum, 2002.

[107] A. Niemunis. Anisotropic effects in hypoplasticity. In Di Benedetto et al., editor, *Deformation Characteristics of Geomaterials*, pages 1211–1217, 2003.

[108] A. Niemunis and I. Herle. Hypoplastic model for cohesionless soils with elastic strain range. *Mechanics of Cohesive-Frictional Materials*, 2:279–299, 1997.

[109] A. Niemunis and S. Krieg. Viscous behaviour of soil under oedometric conditions. *Canadian Geotechnical Journal*, 33:159–168, 1996.

[110] A. Niemunis, K. Nübel, and C. Karcher. The consistency conditions for density limits of hypoplastic constitutive law. *Task Quarterly*, 4(3):412–420, 2000.

[111] R. Nova, R. Castellanza, and C. Tamagnini. A constitutive model for bonded geomaterials subject to mechanical and/or chemical degradation. *International Journal for Numerical and Analytical Methods in Geomechanics*, 27:705–732, 2003.

[112] K. Nübel and R. Cudmani. Examples of finite element calculations with the hypoplastic law. In D. Kolymbas, editor, *Constitutive Modelling of Granular Materials*, pages 523–538. Springer, 2000.

[113] J. H. Prevost. Mathematical modelling of monotonic and cyclic undrained clay behaviour. *International Journal for Numerical and Analytical Methods in Geomechanics*, 1:195–216, 1977.

[114] S. Rampello and L. Callisto. A study on the subsoil of the tower of pisa based on results from standard and high–quality samples. *Canadian Geotechnical Journal*, 35(6):1074–1092, 1998.

[115] J. R. Rice. The localization of plastic deformations. In Koiter, editor, *Theoretical and Applied Mechanics*, pages 207–220. North–Holland, 1976.

[116] G. Rocchi, M. Fontana, and M. Da Prat. Modelling of natural soft clay destruction processes using viscoplasticity theory. *Géotechnique*, 53(8):729–745, 2003.

[117] K. H. Roscoe and J. B. Burland. On the generalised stress-strain behaviour of wet clay. In J. Heyman and F. A. Leckie, editors, *Engineering Plasticity*, pages 535–609. Cambridge: Cambridge Univesrity Press, 1968.

[118] M. Rouainia and D. Muir Wood. A kinematic hardening constitutive model for natural clays with loss of structure. *Géotechnique*, 50(2):153–164, 2000.

[119] M. Rouainia and D. Muir Wood. Implicit numerical integration for a kinematic hardening soil plasticity model. *International Journal for Numerical and Analytical Methods in Geomechanics*, 25:1305–1325, 2001.

[120] P. Royis and T. Doanh. Theoretical analysis of strain response envelopes using incrementally non-linear constitutive equations. *International Journal for Numerical and Analytical Methods in Geomechanics*, 22(2):97–132, 1998.

[121] J. W. Rudnicki and J. R. Rice. Conditions for the localization of deformation in pressure–sensitive dilatant materials. *Journal of the Mechanics and Physics of Solids*, 23:371–394, 1975.

[122] A. N. Schofield and C. P. Wroth. *Critical state soil mechanics*. McGraw-Hill Book Co., London, 1968.

[123] P. R. Smith, R. J. Jardine, and D. W. Hight. The yielding of Bothkennar clay. *Géotechnique*, 42(2):257–274, 1992.

[124] H. D. St. John, D. M. Potts, R. J. Jardine, and K. G. Higgins. Prediction and performance of ground response due to construction of a deep basement at 60 Victoria Embankment. In G. T. Houlsby and A. N. Schofield, editors, *Predictive Soil Mechanics (Wroth Mem. Symp.)*. Thomas Telford, London, 1993.

[125] S. E. Stallebrass. *Modelling the efects of recent stress history on the behaviour of overconsolidated soils*. PhD thesis, City University, London, 1990.

[126] S. E. Stallebrass, J. H. Atkinson, and D. Mašín. Manufacture of samples of overconsolidated clay by laboratory sedimentation. *Géotechnique (accepted)*, 2007.

[127] S. E. Stallebrass and R. N. Taylor. Prediction of ground movements in overconsolidated clay. *Géotechnique*, 47(2):235–253, 1997.

[128] A. Takahashi, D. W. H. Fung, and R. J. Jardine. Swelling effects on mechanical behaviour of natural london clay. In *Proc.* 16^{th} *Int. Conference ICSMGE*, volume 2, pages 443–446. Osaka, Japan, 2005.

[129] C. Tamagnini. Private communication. University of Perugia, 2006.

[130] C. Tamagnini, D. Mašín, D. Costanzo, and G. Viggiani. An evaluation of different constitutive models to predict the directional response of a reconstituted fine-grained soils. In W. Wu and H. S. Yu, editors, *Proc. Int. workshop Modern trends in geomechanics, Vienna, Austria*, pages 143–157. Springer, Berlin, 2005.

[131] C. Tamagnini, D. Mašín, G. Viggiani, and D. Costanzo. An evaluation of different constitutive models to predict the directional response of a reconstituted fine-grained soils. In *Proc. Int. workshop Modern trends in geomechanics (in print)*. Vienna, Austria, 2005.

[132] C. Tamagnini and G. Viggiani. On the incremental non-linearity of soils. Part I: theoretical aspects. *Rivista Italiana di Geotecnica*, 36(1):44–61, 2002.

[133] C. Tamagnini, G. Viggiani, and R. Chambon. A review of two different approaches to hypoplasticity. In D. Kolymbas, editor, *Constitutive modelling of granular materials*, pages 107–144. Springer, 2000, 2000.

[134] C. Tamagnini, G. Viggiani, R. Chambon, and J. Desrues. Evaluation of different strategies for the integration of hypoplastic constitutive equations: Application to the CLoE model. *Mechanics of Cohesive-Frictional Materials*, 5:263–289, 2000.

[135] S. Teachavorasinskun and T. Amornwithayalax. Elastic shear modulus of bangkok clay during undrained triaxial compression. *Géotechnique*, 52(7):537–540, 2002.

[136] J. Tejchman and I. Herle. A "class A" prediction of the bearing capacity of plane strain footings on sand. *Soils and Foundations*, 39(5):47–60, 1999.

[137] C. A. Truesdell. Hypo–elastic shear. *Journal of Applied Physics*, 27:441–447, 1956.

[138] H. A. M. van Eekelen. Isotropic yield surface in three dimensions for use in soil mechanics. *International Journal for Numerical and Analytical Methods in Geomechanics*, 4:89–101, 1980.

[139] G. Viggiani and J. H. Atkinson. Stiffness of fine–grained soil at very small strains. *Géotechnique*, 45(2):245–265, 1995.

[140] G. Viggiani and C. Tamagnini. Ground movements around excavations in granular soils: a few remarks on the influence of the constitutive assumptions on FE predictions. *Mechanics of Cohesive-Frictional Materials*, 5(5):399–423, 2000.

[141] P. A. von Wolffersdorff. A hypoplastic relation for granular materials with a predefined limit state surface. *Mechanics of Cohesive-Frictional Materials*, 1:251–271, 1996.

[142] C. C. Wang. A new representation theorem for isotropic tensor functions. *Archive for Rational Mechanics and Analysis*, 36:166–223, 1970.

[143] T. Weifner. *Review and extension of hypoplastic equations*. PhD thesis, University of Innsbruck, Austria, 2005.

[144] S. Wheeler and D. Karube. State of the art report - constitutive modelling. In 1^{st} *Int. Conference on Unsaturated Soils, Paris, France*, volume 3, pages 1323–1356. Balkema, Rotterdam, 1995.

[145] S. J. Wheeler, A. Näätänen, M. Karstunen, and M. Lojander. An anisotropic elastoplastic model for soft clays. *Canadian Geotechnical Journal*, 40:403–418, 2003.

[146] A. J. Whittle, Y. M. A. Hashash, and R. V. Whitman. Analysis of deep excavation in Boston. *Journal of Geotechnical Engineering ASCE*, 119(1):69–90, 1993.

[147] D. M. Wood. *Some aspects of the Mechanical Behaviour of Kaolin under Truly Triaxial Conditions of Stress and Strain*. PhD thesis, University of Cambridge, 1974.

[148] C. Wroth and G. Houlsby. Soil mechanics - property characterisation, and analysis procedures. In *Proc.* 11^{th} *Conf. Soil. Mech., San Francisco*, volume 1, pages 1–55, 1985.

[149] W. Wu. *Hypoplastizität als mathematisches Modell zum mechanischen Verhalten granularer Stoffe*. PhD thesis, Karlsruhe University, Germany, 1992.

[150] W. Wu. Rational approach to anisotropy of sand. *International Journal for Numerical and Analytical Methods in Geomechanics*, 22:921–940, 1998.

[151] W. Wu and E. Bauer. A simple hypoplastic constitutive model for sand. *International Journal for Numerical and Analytical Methods in Geomechanics*, 18:833–862, 1994.

[152] W. Wu and W. Huang. Rational approach to anisotropy of rocks. In *Proc. EUROCK Symposium*, pages 623–628. Aachen, Germany, 2000.

[153] W. Wu and D. Kolymbas. Hypoplasticity then and now. In D. Kolymbas, editor, *Constitutive Modelling of Granular Materials*. Springer, Berlin, 2000.

[154] W. Wu and A. Niemunis. Beyond failure in granular materials. *International Journal for Numerical and Analytical Methods in Geomechanics*, 21:153–175, 1997.